# Multifunctional UV-C LED

# Virus Inactivation Experimental Platform

Xinyun Xu

**T**U Delft

Delft
University of
Technology
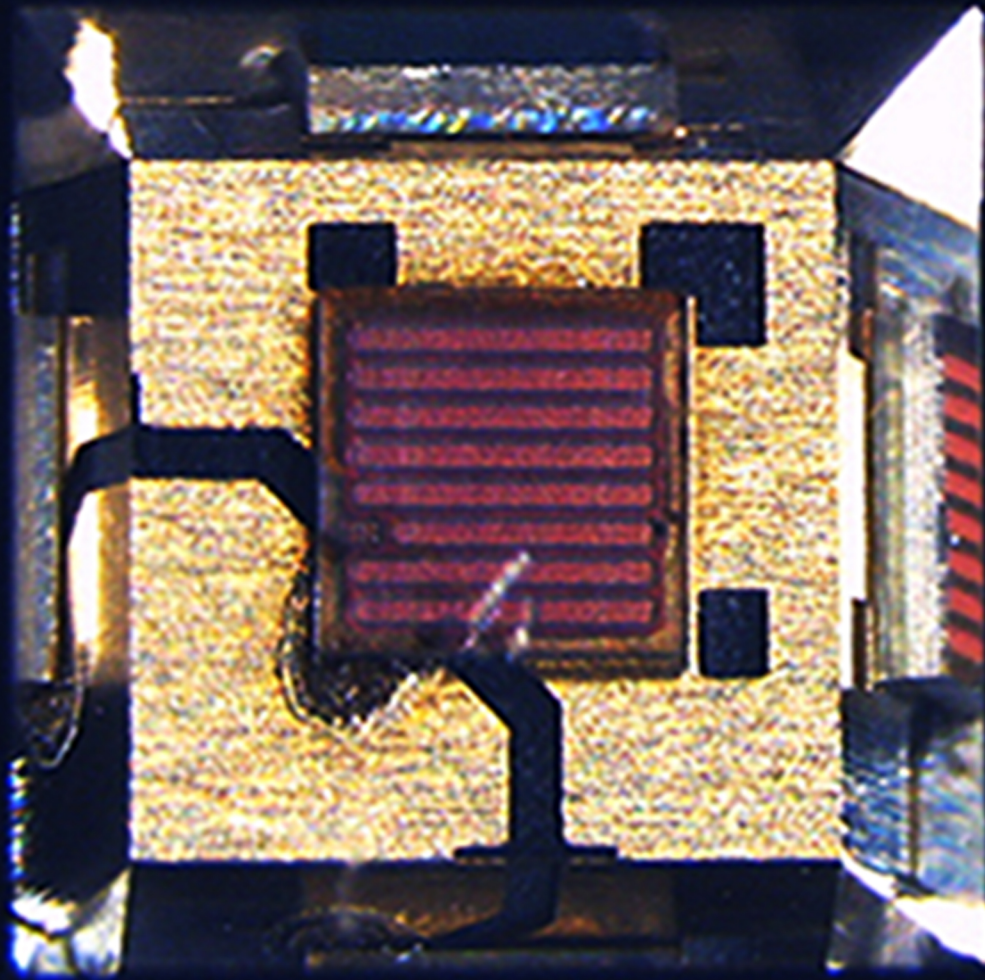
# MULTIFUNCTIONAL UV-C LED VIRUS INACTIVATION EXPERIMENTAL PLATFORM

by

Xinyun Xu

A thesis submitted to the Delft University of Technology in partial fulfillment
of the requirements for the degree of

**Master of Science in Embedded Systems**

Thesis committee:  G. Q. Zhang
W. D. van Driel
Ir. Tianyi Jin

The work in this thesis was made in the:

**TU**Delft

Delft
University of
Technology

Electronic Components, Technology and Materials Group
Department of Microelectronics
Faculty of Electrical Engineering, Mathematics and Computer Science
Delft University of Technology

Supervisors:   G. Q. Zhang
               W. D. van Driel
               Ir. Tianyi Jin

# ABSTRACT

Since the outbreak of SARS-COV-2, various virus inactivation techniques have been applied to suppress the spread of virus. Ultraviolet exposure inactivation is an efficient approach to inactivate virus, within UV band, UV-C with comparatively higher energy. UV-C has been proved to inactivate viruses efficiently, while to figure out efficient inactivation approach, virus reduction rate as a function of UV-C wavelength with different viral sensitivity and quantitative exposure dose should be measured through experiments. On the one hand, miniatured, energy-efficient and fully-customized UV-C light-emitting diodes (LED) offer possibility of switching wavelengths and adjusting quantitative optical properties, on the other hand, UV-C LEDs have been produced with the latest technology based on Aluminium gallium nitride (AlGaN).

Multifunctional UV-C LED Virus Inactivation Experimental Platform is a system designed with replaceable UV-C wavelengths, controllable light intensity and exposure time for quantitative virology experiments. The system has an initial design for standard virology experimental equipment which offers a new and consistent tool for virus researchers. The Inactivation Platform has been assembled and utilized to perform several Influenza A (ssRNA virus) inactivation experiments in order to obtain reduction rate as a function of UV-C wavelength and exposure dose with Germicidal Curve and Inactivation Curve respectively.

After inactivation experiments implementation and result analysis, the inactivation mechanism on the basis of molecular dynamic research theory and simulation is supposed to be figured out. Due to the complexity of proteins in virus, the research focuses on Nucleic Acid Bases (NABs) as target genetic viral material. The absorbed ultraviolet energy results in ultrafast decay, including molecular electronic transition, virus structure variation (Dimerization) theoretically. The absorbed energy along the band is revealed with Absorption Spectrum, and the potential electronic transition depends on the initial structure NABs, together with inside chemical bonds. When absorbed energy populates the molecules to transition state, ultrafast decay takes place because of the existence of Gibbs energy of activation. In the light of molecular dynamic simulation, it proves that compared to ground state, excited state leads to lower standard Gibbs energy of activation, causing higher reaction rate (faster inactivation speed).

Keywords: virus inactivation, UV-C LED, wavelength, light intensity, inactivation mechanism

# ACKNOWLEDGEMENTS

<div align="right">

Xinyun Xu
September 3rd, 2021

</div>

# CONTENTS

# LIST OF FIGURES

# LIST OF TABLES

# ACRONYMS

**SARS-COV-2** Severe acute respiratory syndrome coronavirus 2

**BSL** Biosafety Level

**UV** Ultraviolet

**UV-A** Long Wave ultraviolet light

**UV-B** Middle Waveultraviolet light

**UV-C** Short Wave ultraviolet light

**LED** Light-emitting diode

**AlGaN** Aluminium gallium nitride

**DUV** Deep ultraviolet

**LCD** Liquid Crystal Display

**FFC** Flat flex cable

**IR** Infrared

**PCB** Print circuit board

**SMD** Surface-mounted device

**MCU** Microcontroller unit

**PWM** Plus-width modulation

**CCS** Constant Current Source

**PC** Personal computer

**DoE** Design of Experiments

**PSU** Power supply

**RBCs** Red blood cells

**HAU** Hemagglutination units

**HOMO** Highest occupied molecular orbital

**LUMO** Lowest unoccupied molecular orbital

**HA** Hemagglutinin

**NA** Neuraminidase

**PCR** Polymerase chain reaction

**DRC** DNA repair capacity

**NER** Nucleotide excision repair

**BER** Base excison repair

**MMR** Mismatch repair

**CBPyr** Cyclobutane Pyrimidine Dimers

**CI** Conical Intersection

**NABs** Nucleic Acid Bases

**TA** Transient Absorption

**FU** Fluorescence Upconversion

**ISC** Intersystem Crossing

**TET** Triplet - tripletenergy transfer

**TDDFT** Time-dependent density functional theory

**TST** Transition state theory

**AC** Activated Complex

**Erasmus MC** Erasmus Medical Centre

# 1 | INTRODUCTION

At the end of 2019, the outbreak of Severe acute respiratory syndrome coronavirus 2 (SARS-COV-2) was originally reported in China. It is reported that SARS-COV has caused 126 million infection cases, of which 2.76 million deaths til March 2021, the life-threatening respiratory disease has influence on people's lives significantly worldwide since the outbreak of epidemic. Numerous institutions have been working on virus vaccination research and development, while the growing amount of infected cases cannot be controlled until effective vaccinations are widely applied. Seeking efficient virus inactivation method is one approach to suppress the spread of virus, which is supposed to be put in the first place to prevent more people from being infected. Considering safety requirements, inactivation virology research is supposed to be performed in Biosafety Level (BSL) 2 laboratory or even BSL 3 laboratory.

Traditional widely used virus inactivation processes include solvent inactivation, acidic inactivation, pasteurization and ultraviolet inactivation. SARS-COV belong to enveloped virus, enveloped viruses are typically equipped with lipid and protein coat, as viruses could not live without lipid coating so they would be inactivated with detergent (solvent inactivation). When applied to the treatment, mixture of solvent and detergent irreversibly disrupts the envelope of viruses [1]. In addition, when enveloped viruses are exposed to acidic environment, their protein coating would be vulnerable to low pH, resulting in viral protein denaturation [2]. There are also several physical inactivation means, radiation pasteurization is commonly used method to control the foodborne pathogens effectively with low doses of gamma rays, X-rays and electrons, inactivating food-borne bacteria and parasitic organisms [3]. In addition to the above categories, ultraviolet rays belongs to electromagnetic radiation with wavelength from 100 nm to 400 nm, which exists in sunlight. In Figure 1.1, Ultraviolet (UV) light are composed of Long Wave ultraviolet light (UV-A, 315 nm - 400 nm), Middle Wave ultraviolet light (UV-B, 280 nm -315 nm), Short Wave ultraviolet light (UV-C, 200 nm - 280 nm) and Vacuum UV (100 nm - 200 nm) [4]. UV-C light is almost completely absorbed by ozone layer and atmosphere, and the amount of ultraviolet radiation reaching the surface of earth is mostly UV-A with small amount of UV-B [5]. As for humans, skin exposure to sunlight is the primary environmental cause of sunburn and skin cancer [6]. According to the Planck's Equation 1.1, when particles oscillate with frequency, the energy produced by oscillation is proportional to the frequency, and inversely proportional to wavelength. h is the Planck's constant, f is the frequency of a photon, c is the speed of light, $\lambda$ represents the wavelength of a photon [7]. Therefore, light with shorter wavelength would produce higher energy, in which case, UV-C has the higher energy than UV-A and UV-B.

$$E = hf = hc/\lambda \tag{1.1}$$

The energy of short wave ultraviolet light (UV-C) with the highest energy level would cause damage to DNA and RNA structures. When it comes to virus, UV-C exposure results in adjacent cross-links between nucleic acids on the nucleotide chain to form dimers and destroy the function of virus genes, in which case, viruses lose the ability to infect others [8]. Among all the above inactivation approaches, solvent and acidic inactivation depends much on biology and chemical laboratory environment, radiation pasteurization requires professional equipment and maintenance. With regard to Ultraviolet rays, some traditional equipment have been produced and taken into inactivation experiments. Considering the virus inactivation approaches, ultraviolet inactivation is comparatively feasible, portable and user-friendly.
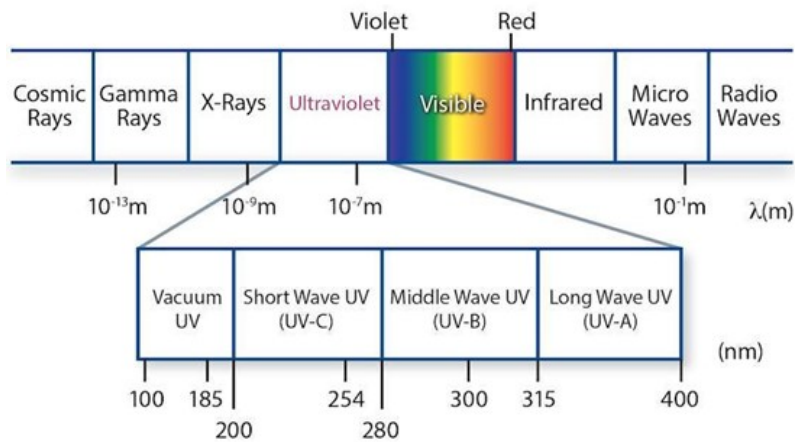
**Figure 1.1:** Ultraviolet in Electromagnetic spectrum

## 1.1 BACKGROUND KNOWLEDGE

During the past years, especially because of the outbreak of the epidemic, numerous institutions put their effort to ultraviolet inactivation experiment.There are a number of UV devices on the market, black light, tanning lamp, mercury-vapor lamp, germicidal lamp and UV Light-emitting diode (LED). However, there are limitations of some traditional ultraviolet light sources, which would be illustrated in the chapter. Applying various ultraviolet light sources, a large amount of inactivation experiments have been implemented on various microorganisms. The experiments based on typical conditions would be discussed in the chapter, the conditions consist of light sources, temperature, exposure distance, inactivation doses, interference factors and etc. The ultraviolet light sources and inactivation experiments research in the chapter are the guidance of the thesis project.

### 1.1.1 Ultraviolet Devices

Ultraviolet radiation is not only present in sunlight, it could also produced by ultraviolet equipment, for example, mercury-vapor lamp, tanning lamps and black lights. The black light lamp applies phosphor on inter tube which emits almost UV-A radiation, ranges from 300 nm to 425 nm [9]. Tanning lamps also produce UV-A and UV-B radiation. There are various traditional UV-C light sources on the market, the most common devices are mercury-vapor lamps as Figure 1.2a, they apply an electric arc through vaporized mercury to produce light. Low pressure mercury-vapor lamps utilizes fluorescent lamp tube and lamp envelope. There are two distinct emitting wavelengths, 185 nm and 254 nm because of mercury within the lamp, the designed lamp envelope is applied to attenuate 184 nm, suppressing the generation of ozone efficiently. Soft glass technology referred in Figure 1.2b absorb wavelengths under 240 nm, preventing the escape of 184 nm emission completely [10].

**Figure 1.2:** (a) Mercury-vapor Lamp (b) Soft Glass UV-C Lamp

The envelope of higher power low pressure mercury lamps is made from fused quartz, such envelope could not completely block the transmission of 184 nm radiation. On the contrary, it creates ozone with certain efficiency because of the existence of 254 nm, which is able to destroy ozone. However, titanium doped quartz would not generate detectable ozone, hence there exists ozone-free low pressure mercury lamp [10; 11].

When it comes to traditional mercury-vapor lamps, within range from 200 nm to 400 nm, the spectrum is shown in Figure 1.3a. There are several peak wavelengths distribute within the range, including not only UV-C wavelengths. Traditional UV-C light source mercury-vapor lamps have several peak UV wavelengths, covers a fixed and wide wavelength range. This reduces the efficiency and cost excess energy, and lacks of the possibility in switching from different wavelengths. Furthermore, there exist not a purely UV-C light source that can be fit into the standard virology experimental equipment. In addition, mercury-vapor lamps have obvious disadvantages during operations in standard virology experimental condition, bulky size, the mercury supplement is a known hazardous material [12], debatable mercury exposure harm [13], and short guaranteed lifespan. The lifespan of mercury-vapor lamps ranges from 600 hours to 2000 hours [14].
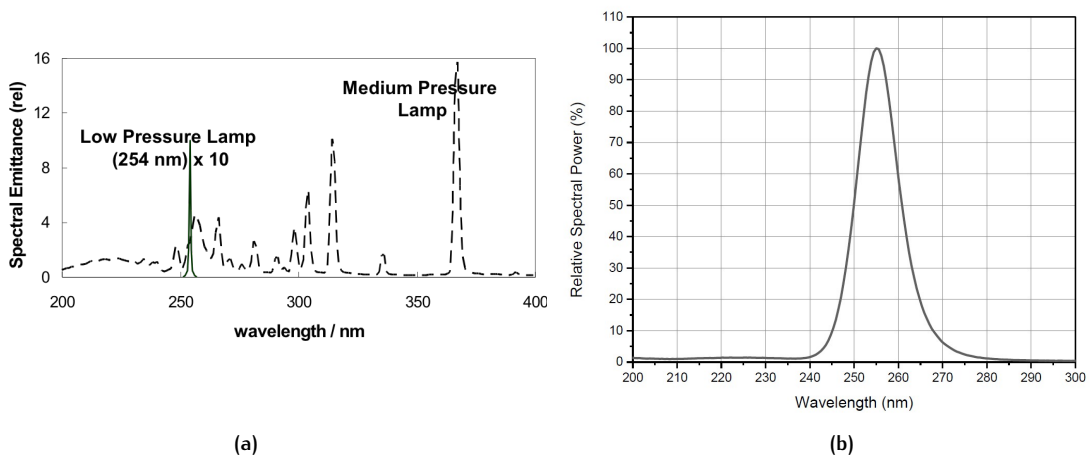


**Figure 1.3:** Power Distribution of (a) Tradition Mercury-vapor lamp spectrum (b) UV- LED spectrum

There have been Light-emitting diodes (LEDs) manufactured to emit radiation in the ultraviolet

range. Originally, produced ultraviolet LEDs are within UV-A spectrum, but UV-C LEDs have been manufactured currently. UV-C LED emits light in a narrow spectrum with single peak wavelength as Figure 1.3, there are several produced peak wavelength on the market, for example, 255 nm, 275 nm and 280 nm, which would be discussed in the next chapter.



(a)

(b)
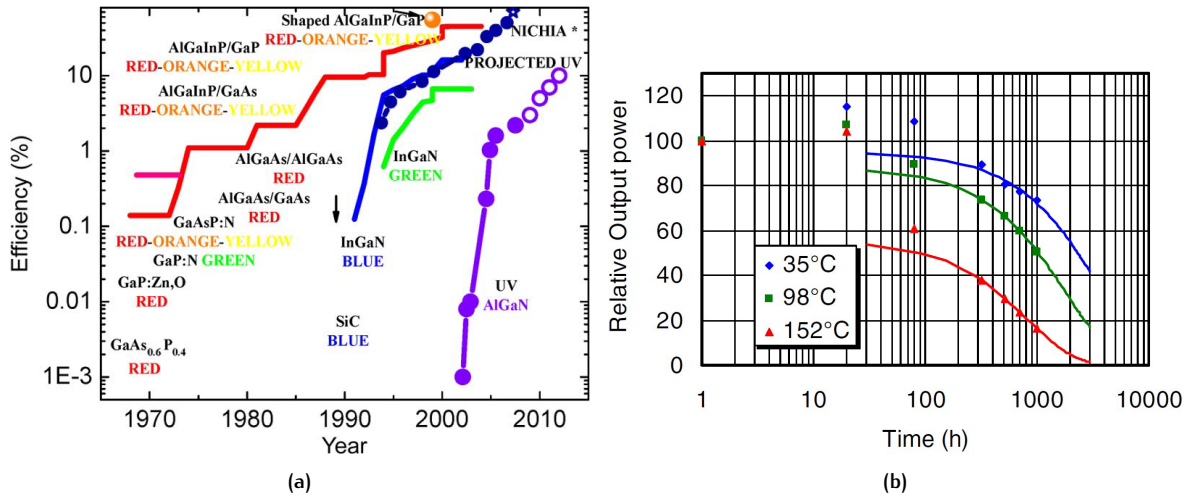
**Figure 1.4:** (a) DUV LEDs performance (b) Decay of output power of 280 nm LEDs during aging tests for varying junction temperatures

**Table 1.1:** Details of UV-C LED Light Sources

| Peak Wavelength (nm) | Optical Output Power | Base | Lifespan (h) | |
|---|---|---|---|---|
| 255 | 45.2 mW @ 350 mA | AlGaN | | |
| 280 | 93.3 mW @ 350 mA | AlGaN | 3000 h @ junction temperature 30°C | [16] |
| 310 | 65.8 mW @ 350 mA | AlGaN | | |
| 257 | photon fluence $2 * 10^{12} p/cm^2$ | AlGaN | 19000 h in gaseous nitrogen | [17] |
| 237 | 2.2 mW @ 100 mA | AlGaN | | |
| 235 | 1.9 mW @ 100 mA | AlGaN | 3600 h of lifetime operating at 20 mA | [18] |
| 233 | 1.5 mW @ 100 mA | AlGaN | | |
| 230 | 1.2 mW @ 100 mA | AlGaN | | |

The development of miniature solid-state UV light sources has made the surface sterilization possible. The development progress and performance of LEDs are shown as Figure 1.4a, DUV LEDs belong to latest technology based on Aluminium gallium nitride (AlGaN), and the efficiency rises to some extent, however, the external quantum efficiency of Deep ultraviolet (DUV) LEDs is below 2%, and the low efficiency cannot be solved in a short time [15]. In addition, lead-free, mercury-free UV LEDs are environment friendly RoHS compliant products compared to mercury-vapor lamps. Table 1.1 lists optical output power, LED base material and lifespan of UV-C LED light sources, the 50% lifetime of the LED die is estimated to be 3000 hours at a junction temperature of 30°C. According to Figure 1.4b, at varying junction temperatures, the decay curves of LEDs are different completely, while the performance at 35°C is better than higher temperatures [16]. The operational lifetime of UV-C LEDs varies a lot, also depends much on the working surroundings, the lifetime test in nitrogen reaches more than 19000 hours, and more than 8000 hours in vacuum, hence UV LED is qualified as high reliability products in space environment [17]. Therefore, the operational temperature and surroundings are supposed to be paid attention to. Referring to Table 1.1, the estimated lifespan is within the range of 3000 hours to 19000 hour, much longer than the lifespan of mercury-vapor lamps in Table Table 1.2. The miniatured, energy-efficient and fully-customized UV-C LEDs, which offers possibility of switching wavelengths and adjusting other optical properties.

Table 1.2: Details of Mercury-vapor Lamp [14]

| Light Source | Wavelength | Guaranteed Lifespan (h) |
|---|---|---|
| Low-pressure mercury lamp | 185 and 254 | 2000 |
| Medium-pressure mercury lamp | 200-600 | 800-1000 |
| High-pressure mercury lamp | 300-600 | 600 |

Table 1.3: Reduction Calculation based on $log_{10}$

| Reduction N | Reduction Percentage (%) |
|---|---|
| 1 - $log_{10}$ | 90% |
| 2 - $log_{10}$ | 99% |
| 3 - $log_{10}$ | 99.9% |
| 4 - $log_{10}$ | 99.99% |
| 5 - $log_{10}$ | 99.999% |

### 1.1.2 Inactivation Experiments

Microorganisms consist of bacteria, fungi, archaea, protists and viruses [19]. The experiments mentioned in the chapter are not limited on viruses, but also cover some of other microorganism types. When the UV-C light source (254 nm) emitted dose 4.016 $mW/cm^2$ (measure by radiometric analysis), the UV-C light inactivate SARS-CoV within 15 minutes, at a distance of 3 cm from the bottom of the well to the light source. The inactivation ability is discussed in the research, UV-A is barely absorbed by DNA and RNA, UV-B is able to produce dimers, and could potentially cause genetic damage by producing reactive oxygen species, resulting in oxidization of bases and strand breaks. Compared to UV-A and UV-B, UV-C is the most effective wavelength range to be absorbed by RNA and DNA bases, causing photochemical fusion of two adjacent pyrimidines, making them non-pairing bases [20]. Applying UV-C illumination device (Maco-Tronic, Macopharma), when irradiated with 0.15 $J/cm^2$ UV-C light at a wavelength of 254 nm, the virus reduction factors is greater than 4.5 for Ebola virus, and is greater than 3.7 for Middle East respiratory syndrome coronavirus [21]. The Ebola virus belongs to extremely dangerous Filoviruses, experiments with the virus have to be performed in BSL-4 laboratories [22], the highest biosafety level.

Certain dose of UV radiation would have a lethal effect on microorganisms, in the following research, the log reduction tendency with increase UV dose could be found. As Equation 1.2, $N_0$ is the number of viable microorganisms before treatment, N is the number of viable microorganisms after treatment [23], and log reduction is calculated as Table 1.3.

In Figure 1.5, with the rise of exposure UV dose, the log inactivation increases accordingly for E.coli, MS2 Coliphage and Adenoviruses. There are five categories of light sources, 260 nm LED, 280 nm LED, 260|280 nm combination, Medium pressure lamp and Low pressure lamp. For E.coli and MS2 Coliphage, the inactivation performance does not varies a lot between different light sources. The Medium pressure lamp has 2-log reduction more than remaining light sources when exposed to Adenoviruses. When the log reduction percentage reaches 99.99% (4 - log), it is considered to be highly inactivated, while to reach the same 4-log reduction, exposure UV dose varies to different microorganisms [24].

$$LogReduction = log_{10}(\frac{N_0}{N})$$

(1.2)

As Table 1.4, different UV doses are shown to reach certain log reduction. There are also a quantity of experiment conditions, different UV-C light sources, virus types, disinfection surfaces would influence the final log reduction value. Among the experiments, the types of UV-C light sources
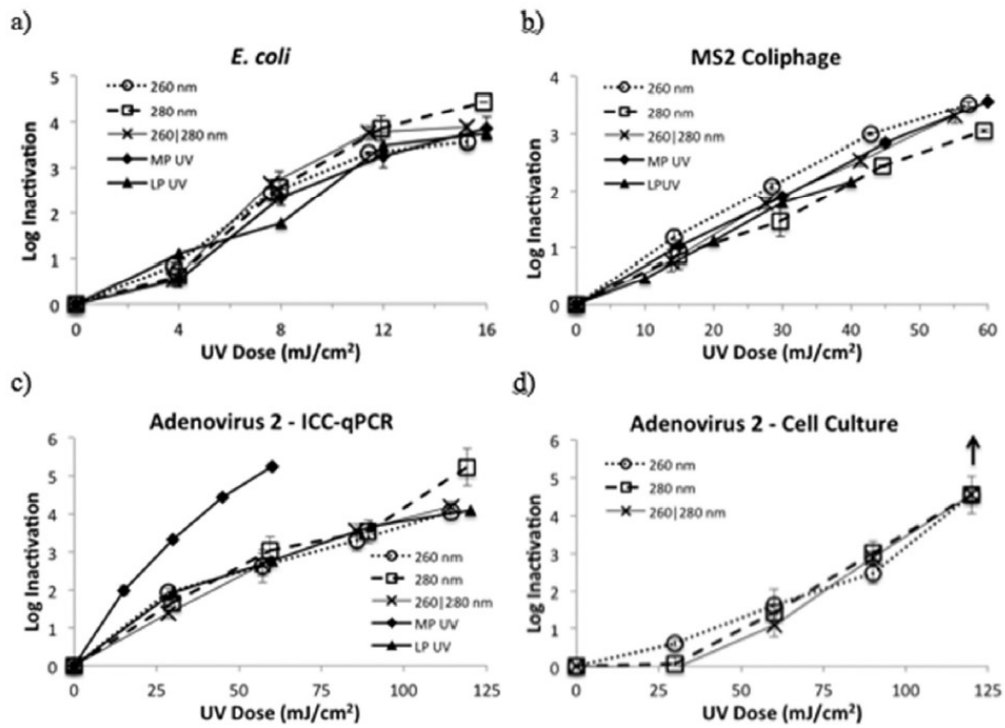
**Figure 1.5:** UV dose response of a) E. coli, b) MS2 coliphage, c) HAdV2 as measured by ICC-qPCR, d) HAdV2 as measured by cell culture

are mostly tubes and traditional lamps, hence the exposure UV dose could result from several peak wavelengths.

**Table 1.4:** Inactivation details of UV-C LED Light Sources

| UV-C Type | Virus | Dose ($mJ/cm^2$) | Reduction | Year | Experiment Condition | |
|---|---|---|---|---|---|---|
| Tube | SARS | 50 | 3.1 | 2020 | Platelet disinfection | |
| Tube | SARS | 100 | 3.4 | 2020 | Platelet disinfection | [25] |
| Tube | SARS | 25 | 6.8 | 2007 | Platelet disinfection | [26] |
| Lamp | Phi 6 corona | 8.5 | 1.7 | 2020 | Surface | |
| Lamp | Phi 6 corona | 17 | 3.7 | 2020 | Surface | |
| Lamp | Phi 6 corona | 25.5 | 4.2 | 2020 | Surface | [27] |
| LP lamp | SARS | 0.7 | 1 | 2020 | Mask disinfection | [28] |
| Signify's UV-C light source | SARS CoV-2 | 5 | 2 | 2020 | | |
| Signify's UV-C light source | SARS CoV-2 | 22 | 6 | 2020 | | |

According to Figure 1.6, Germicidal curve, Ultraviolet Absorption of DNA as a function of wavelength is plotted, which reflects the potential inactivation ability of single UV-C wavelength, and the inactivation trendline through ultraviolet range. As far as is been concerned, within ultraviolet range 100 nm - 400 nm, UV-C band holds the highest absorbance, which would be taken into subsequent inactivation experiment and analysis. The germicidal peak settles at 264 nm, in between UV-C band. Above 264 nm, the absorbance diminishes with wavelength, while below 264 nm, the absorbance drops with wavelength and continues with a turning point nearly 230 nm.
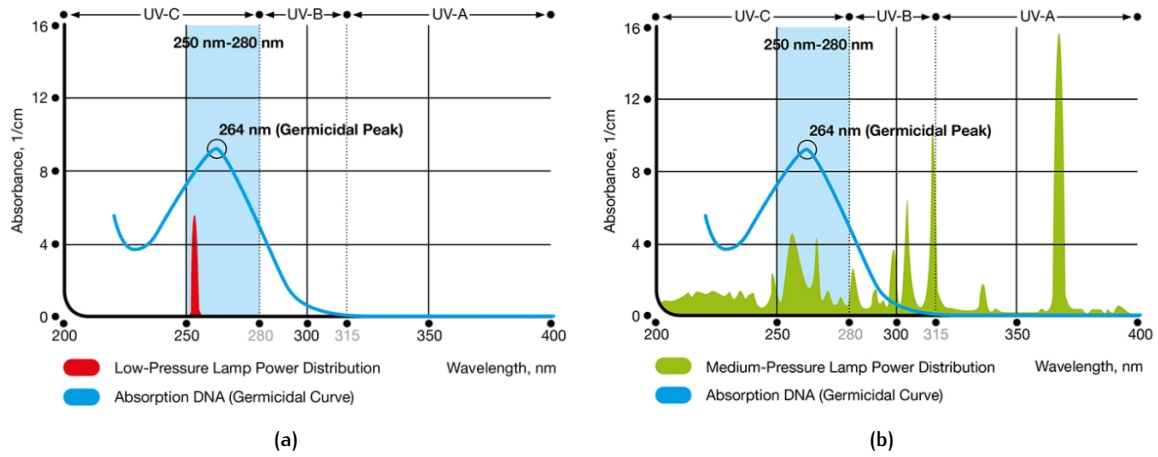
**Figure 1.6:** Low Pressure/Medium Pressure lamp power as a comparison with Absorption DNA (Germicidal Curve)
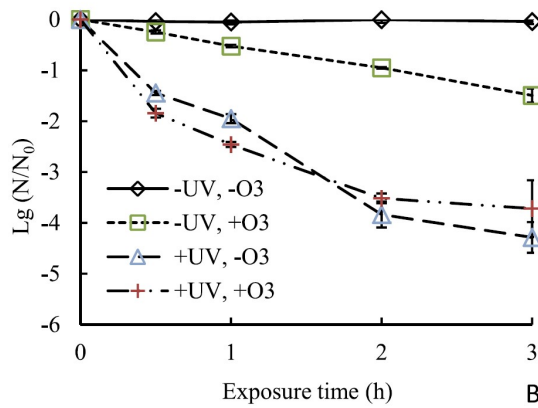


**Figure 1.7:** Inactivation of MUT1

Theoretically, UV light ranges from 240 nm to 315 nm wavelength would convert ozone to oxygen, while UV light near 185 nm would produce ozone from oxygen. Therefore, in UV-C LED production, doped quartz glass will be used as a low pass filter to block short spectrum, including ozone-generating 185 nm light. However, ozone is proven to be effective to microorganism inactivation. As Figure 1.7, with or without the presence of UV exposure, the condition with ozone has 1-$log_{10}$ reduction more than the condition without ozone to MUT1 inactivation [29]. In addition, 10 to 20 ppm doses of ozone are recommended to inactivate the coronavirus with 3.5-$log_{10}$ reduction in 10-15 minutes [30]. Because of the limited inactivation space, it is possible that amount of ozone would accumulate during the experiment, resulting in inactivation due to ozone other than UV light. Therefore, when applying UV inactivation, it is necessary to prove whether there is ozone exist by either gas measuring or a ozone control group in the experiment.

When it comes to the working condition of UV instrument, continuous-wave and pulsed-wave modes are implemented. Disinfection efficiency of pulsed and continuous-wave are compared through experiments. In the research, the pulsed UV system emitting wavelengths ranges from 200 nm to 500 nm, the pulse lasted microseconds and was manually triggered every 10s, which has been proved to be effective to E.coli, the leading cause could be the 6MW peak UVC power per pulse. As Figure 1.8a, the normalized spectra of pulsed UV lamp has especially concentrated high power within 200 nm -280 nm and 490 nm - 500 nm, hence it could be the high power within the range per pulse

disinfect E.coli. It could be figured out from Figure 1.8b that, Pulsed UV is 2 times more effective than medium pressure UV to E.coli, and 2 times more effective for phage. Under the same dose $4\ mJ/cm^2$, medium pressure UV leads to 2.5-log reduction, and pulsed UV causes 5-log reduction. The potential inactivation reason is the effect of high-intensity light on cell enzymes. Moreover, the damage could not only resulted from UV-C light, but also can be caused by light other than UV-C wavelength bands [31].

Daryany et al. revealed that when pulsed UV light presents more energy than continuous wave, it has potential to penetrate into solutions and attain better inactivation performance, reducing the inactivation period. The titer of $4.3\text{-}log_{10}$ BVDV was totally inactivated with $3.2\ J/cm^2$. Since the experiments were implemented with BVD virus suspended in FBS, the effect of solutions has to be taken into consideration. In addition, the study illustrates in viruses, genetic materials have better absorbance at UV-C wavelengths, while proteins have greater absorbance at UV wavelengths of more than 300 nm [32].

According to the above researches, pulsed UV with high energy could be an effective inactivation approach. Also, the pulsed wave light sources mentioned includes not not UV-C wavelengths, hence it is hard to tell which wavelength has the leading inactivation ability. Last but not least, the inactivation condition, suspended in PBS and dried virus are absolutely different, rich protein solution and virus leads to less UV radiation transmission in solution.

To sum up, when it comes to the feasibility of ultraviolet inactivation experiments, the conditions mentioned above are supposed to be taken into consideration. Above all, the Ultraviolet devices are the most significant, the characterization of wavelength with relative optical power is necessary before the inactivation experiments. Also, before the experiments, the influence of ozone is supposed to be ruled out. Pulsed UV light sources with high energy have some potential advantages, while the energy level should probably reach megawatt level. Moreover, virus type, virus status, exposure dose, exposure distance, and virus container are all significant factors to be taken into consideration.
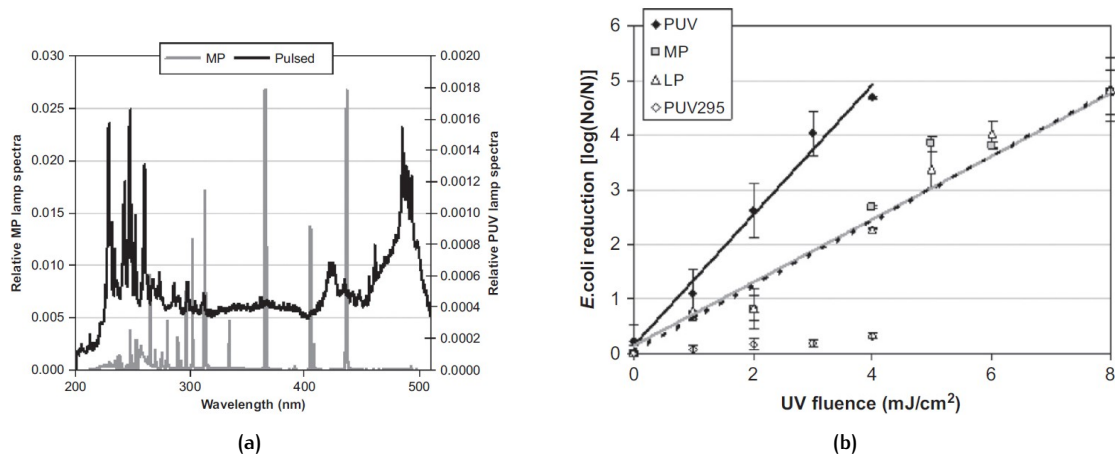


**Figure 1.8:** (a) Normalized MP and PUV lamp spectra in the 200 nm – 500 nm range (b)E. coli inactivation PUV

## 1.2 MOTIVATION AND OBJECTIVE

Due to the severe influence of SARS-COV, it is significant to figure out an efficient inactivation recipe utilizing quantitative ultraviolet equipment. According the previous research, a quantitative ultraviolet virus inactivation platform is supposed to be designed for the research. Above all, an

appropriate UV-C light source is supposed to be chosen, compared to traditional bulky, hazardous and wide wavelength band mercury lamps, UV-C LEDs mentioned in the last section with single peak wavelength based on AlGaN are customized for biomedical usage.

In order to attain an energy-efficient inactivation UV-C wavelength recipe, namely figure out the germicidal curve and the most effective UV-C single-wavelength or dual-wavelength, inactivation experiments are expected with the customized inactivation experimental platform. Therefore, the platform modeling would depend on the standard virology experimental apparatus, meeting the standard laboratory inactivation requirement. The light source module would fit the exposure requirement of inactivation, maintaining designed exposure distance, exposure dose and illumination area. With characterized UV-C light source, the quantitative exposure UV-C wavelength doses are suppose to be applied on the same quantity of viruses, and the reduction rate of virus would tell which recipe is the most effective one.

With the reference of germicidal curve derived from standard inactivation experiment, an inactivation mechanism research based on molecular dynamic level is expected to explain the tendency of germicidal curve. It might be the UV inactivation to genetic materials, proteins or cell enzymes that cause a lethal effect on viruses. Take DNA virus as example, the lethal effect results from thymine dimers, and the secondary damage is produced by cytosine dimers, which leads to mutations or cell death [33]. The details of research would be illustrated in Chapter 4.

In conclusion, the thesis project is to build a quantitative UV-C inactivation platform to inactivate target virus and monitor inactivation conditions. And, the platform could be applied to figure out an efficient Ultraviolet-C virus inactivation recipe and the inactivation tendency with UV-C wavelength. Inactivation mechanism research is expected to give an explanation of the effectiveness of the ultraviolet inactivation recipe.

## 1.3 OUTLINE

The thesis project presents the UV-C inactivation platform modeling and design, standard Virology Inactivation Experiments and genomes research on inactivation mechanism. The content introduction of the chapters are shown as follows:

Chapter 2 introduces the requirement of the UV-C LED Virus Inactivation Experimental Platform, platform modeling and design. The platform diagram would be applied to introduce platform modules, the platform model and module design would be mentioned with the functions in detail . The introduction would focus on platform LED module and Driver module.

Chapter 3 shows the design of inactivation experiments. The inactivation experiment would be designed for target virus, the factors and levels of the experiment are supposed to be designed according to the research on previous experiments in order to obtain expected response. The germicidal curve or the best inactivation recipe is expected after experiment.

Chapter 4 illustrates the inactivation mechanism research on molecular dynamic level. The genomes research with theory and related simulation on inactivation mechanism would give an explanation to the germicidal curve.

Chapter 5 summarizes the report, and provides the proposal of future work.

## 1.4 CONCLUSION

Ultraviolet inactivation is chosen as the inactivation method of the research. Ultraviolet light sources are compared in the chapter in terms of size, energy efficiency and wavelength band. Traditional mercury vapor lamp could not satisfy the requirement of current thesis project, hence ultraviolet inactivation experimental platform would be designed in the project. A large quantity of inactivation experiment researches are mentioned in the chapter, which would be considered as reference of inactivation experiments in Chapter 3. The inactivation experiment result would be analyzed on the basis of molecular dynamic theory.

# 2 | PLATFORM MODELING AND DESIGN

This chapter would introduce the design requirement of the virus inactivation platform, platform modeling and design. The platform has an initial design for standard virology experimental equipment which offers a new and consistent tool for virus researchers. Generally speaking, the inactivation platform is designed for all UV-C LEDs with the same packaging size. In addition, the platform is a system designed with multiple controllable factors for virus inactivation experiments. To satisfy the experiment demand, all the factors of inactivation are supposed to be adjustable in the platform.

## 2.1 PLATFORM REQUIREMENT

Since the platform is designed for standard virology experiments, the UV-C LED array has to fit the standard virology experimental utensils. Erasmus medical center provided the Commercial Eppendorf 6-well Cell Culture Plate as Figure 2.1, dried virus is supposed to be placed in each well during inactivation, hence 6 groups of LEDs are designed for the UV-C LED array corresponding, each group of LEDs is exposed to a single well of the cell culture plate in terms of certain exposure dose and exposure distance. The Cell Culture Plates have been widely used in standard biology researches, which results in the designed inactivation platform a consistent tool for virus inactivation researches.
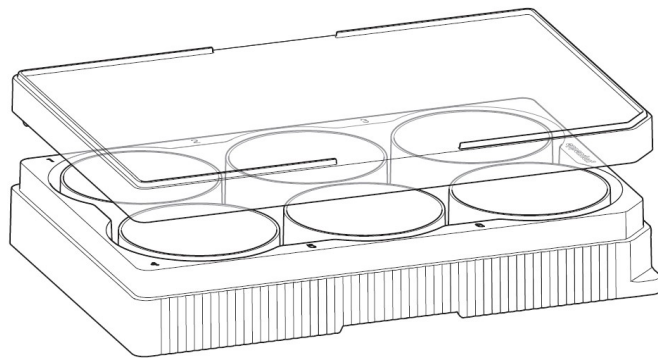
Figure 2.1: Commercial Eppendorf 6-well Cell Culture Plate

The 6 groups of LEDs are controlled by a Driver module, which is able to drive each individual LED with quantitative exposure time and power. Also, considering the diminished LED performance under relative high temperature as Figure 2.2, which reveals optical output power and wavelength shift with temperature rise under the test of 100mA forward current. The LED heat dissipation Therefore, a cooling module is designed for the platform to maintain steady performance.

Overall, the system diagram is shown in Figure 2.3, the platform consists of Driver module, UV-C LED array and Cooling module. The driver module is the key component of the platform, on the
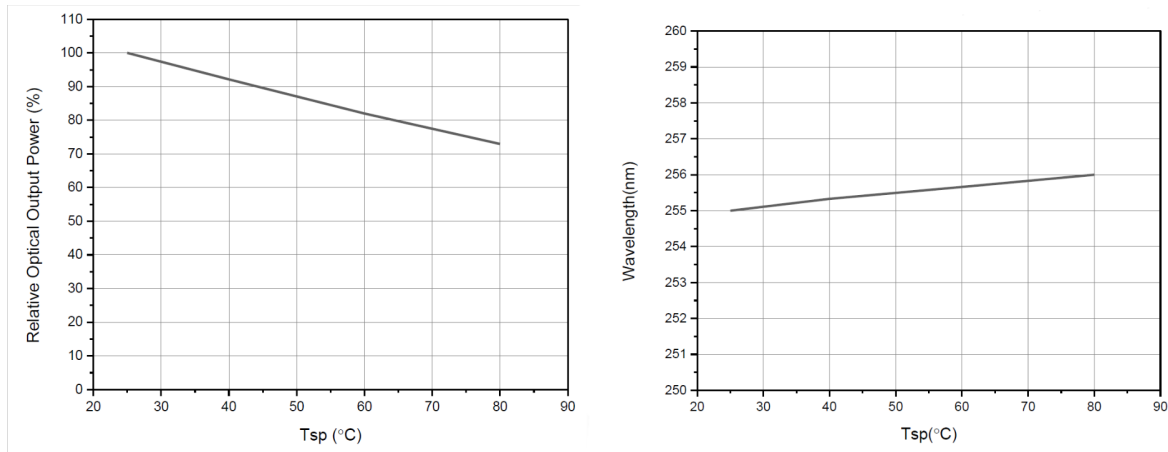
**Figure 2.2:** Relative Optical Output Power vs. Solder Point Temperature, IF=100 mA (left), and Peak Wavelength vs. Solder Point Temperature, IF=100 mA (right)

one hand, it processes interactive signals from PC, keypad and Liquid Crystal Display (LCD) monitor, on the other hand, driver module provides real-time driving signals to each LED of the LED array. Moreover, driver module provides power administration and communication ports. On the UV-C LED array, Flat flex cable (FFC) connectors would transfer temperature and driving signals. Temperature sensors are embedded in the center of each UV-C LED group in order to monitor the real-time on-board temperature. The performance of cooling module could be assessed by temperature monitor at the same time.
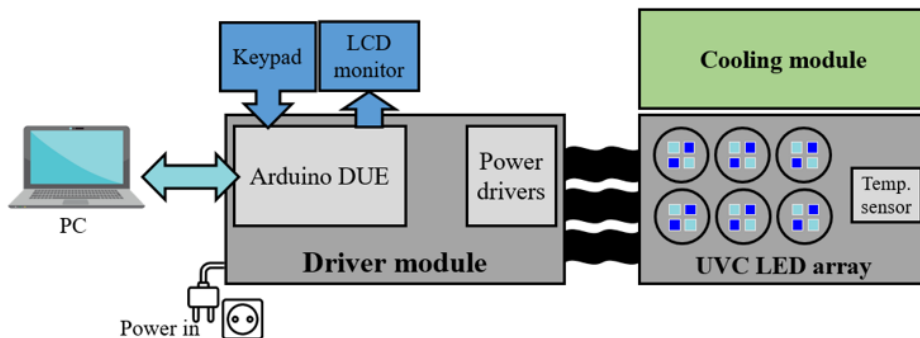


**Figure 2.3:** System Diagram of UV-C LED Virus Inactivation Experimental Platform

The LED spectrum on datasheet usually has a peak wavelength and a half-width smaller than 10 nm. The peak wavelength and optical power could not be identical but vary with chip difference and relative experimental temperature, in which case, an optical characterization is necessary to quantitatively evaluate the performance of LED chips. The characterization could also be allied to calculate the exposure UV dose of each well of the 6-well Cell Culture Plate.

Considering the efficient inactivation probability of single-wavelength or dual-wavelength, LED arrangement in the same well is designed for both approaches. As is shown in the UV-C LED array of Figure 2.3, LEDs of different wavelengths are placed adjacently, and LEDs of same wavelength are settled diagonally.
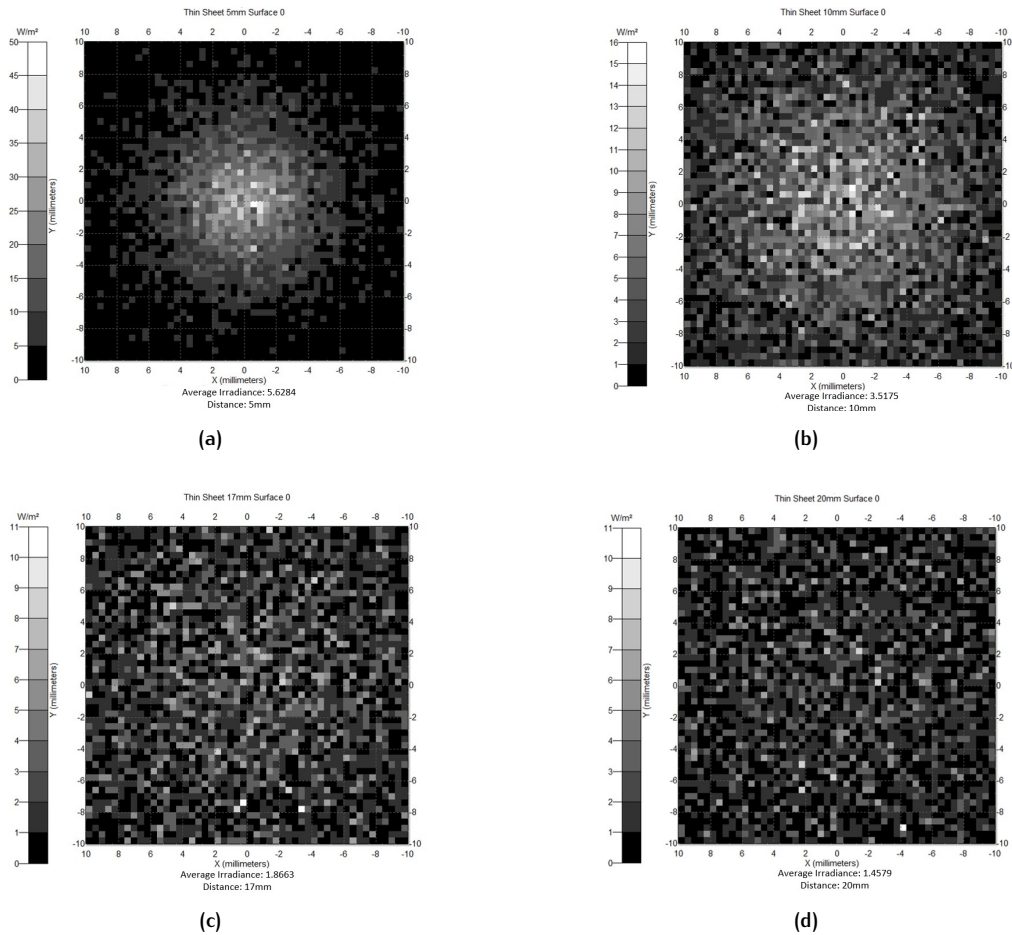
**Figure 2.4:** Irradiance Simulation of single ultraviolet LED a) 5 mm, b) 10 mm, c) 17 mm, d) 20 mm exposure distance

## 2.2 MODELING SIMULATION

The simulation consists of Irradiance Simulation and Thermal Simulation, irradiance simulation is for ensuring the relationship between illumination area and irradiance power, and anticipate the inactivation exposure time of certain virus. In the last section, the temperature rise would result in optical output power attenuation and peak wavelength shift. Moreover, heating inactivation is one of the inactivation approaches, hence thermal simulation is necessary.

### 2.2.1 Irradiance Simulation

The exposure time of each well depends on the irradiance, namely radiant flux emitted, reflected, transmitted or received by a surface per unit projected area. In the research, with 110 $J/m^2$ UV fluence, the surviving fraction of lethal virus Ebola is under 0.01% [34]. In TracePro radiance simulation, single LED is applied as an alternative of UV-C LED, with 8.5 mW radiometric power and 115°typical viewing angle model, which is similar to UV-C LED applied in the platform. The LED package in simulation has almost the same typical 3535 mechanical dimensions.

The irradiance simulation is performed at a distance of 5 mm, 10 mm, 17 mm and 20 mm respectively from the light source, and the irradiance map is shown as Figure 2.4. Take Ebola inactivation as example, when exposed to 1,8663 $W/m^2$ UV fluence at a distance of 17 mm, it would take 59 seconds to reach 110 $J/m^2$. If the surface is exposed to shorter distance, average irradiance is larger,

reaching 5.6284 $W/m^2$ at a distance of 5mm, 3 times of the irradiance at a distance of 17 mm, while the illumination area is smaller. Therefore, the exposure distance and relevant illumination area are supposed to be paid attention to before the experiment. The radiance power could be characterized at a certain distance, and the actual power could be derived accordingly.

## 2.2.2 Thermal Simulation

As is mentioned in the last section, temperature rise would affect the performance of UV-C LEDs, the heat dissipation of LEDs also has the possibility to interfere virus inactivation. As illustrated in the research, two LEDs are placed in series as Figure 2.5a, the steady state temperature captured by Infrared (IR) camera, the average temperature of FR4 circuit board is 76°C, and drops to 55°C for metal core board. As is shown in Figure 2.5b and Figure 2.5c, when LED encapsulation material has lower thermal conductivity than Print circuit board (PCB) underneath, hence thermal energy dissipates mostly through the PCB material underneath. In addition, the temperature of high power LED mounted on FR4 based PCB is higher than the one mounted in aluminum based PCB [35]. Also, Table 2.1 lists the thermal conductivity properties of general material from manufacture, thermal conductivity represents the ability to conduct heat. FR4 is the most common PCB base material with lowest thermal conductivity, and copper turns out to have the highest thermal conductivity. Copper shows twice the thermal conductivity of aluminum, while copper based PCB has five times the price compared to the one based on aluminum. Therefore, aluminum is chosen as the base material of UV-C LED array board, which has better thermal dissipation ability and appropriate price.

**Table 2.1:** Material Thermal Conductivity Properties

| Material | Thermal conductivity $\lambda[W/mk]$ |
| --- | --- |
| Copper | 300 |
| Aluminum | 150 |
| FR4 | 0.25 |
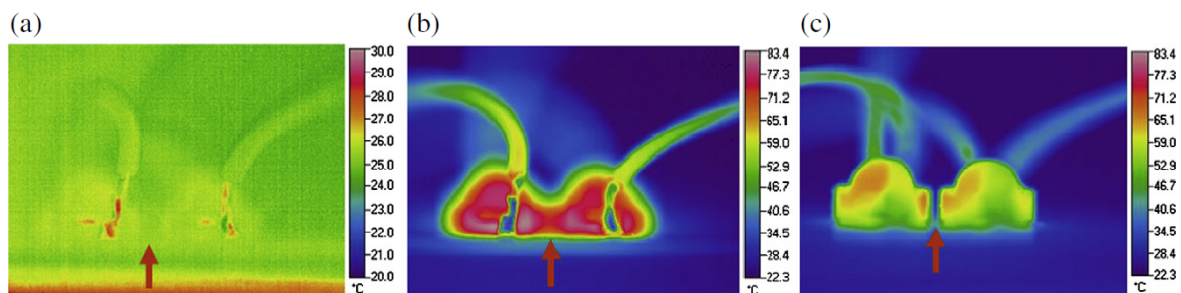


**Figure 2.5:** Effect of the PCB material on the heat dissipation of LEDs at 0.3 A. (a) LEDs held in series on a PCB at room temperature without current supply initially, (b) LEDs on a FR4 PCB, and (c) LEDs on a metal core PCB

Although equipped with aluminum based PCB, in case the thermal dissipation cannot meet the requirement, a cooling module could decrease the temperature furthermore. In the COMSOL simulation, the heat source was originally set to the solid silicon base of LED, the temperature of LED is 80°C and aluminum based PCB would dissipate the heat immediately, hence on-board temperature is around 68°C. In Figure 2.6, the cooling module and Aluminum base are connected through thermal contact in simulation and could result in another 5°C temperature drop, accelerating on board heat dissipation.
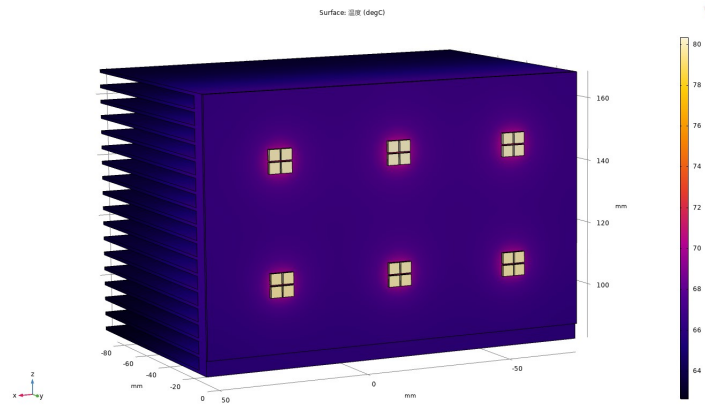
**Figure 2.6:** Thermal Simulation of UV-C LED Array with Cooling module

## 2.3 MECHANICAL STRUCTURE DESIGN

The Mechanical Structure is composed of exposure structure design and cooling structure design. Since the inactivation platform is especially designed for standard virology experiments with Commercial Eppendorf 6-well Cell Culture Plate. To satisfy the platform requirement, adjustable exposure distance and heat dissipation of LED array, the section would introduce the corresponding mechanical structure design.

### 2.3.1 Exposure Structure Design

Due to the exposure dose and exposure distance requirement of the inactivation, a mechanical structure of UV exposure is supposed to be designed as Figure 2.7. The cell culture plate is fixed at the bottom of metal consumables, and the UV-C LED array should be fixed at a certain exposure distance from the light source to the bottom of cell culture plate. Each UV-C LED group is regulated directly above corresponding well, ensuring enough illumination area to corresponding well and no influence to adjacent wells. Several copper pillars are used to fix the cell culture plate, the exposure distance can also be adjusted by the length and amount of copper pillars. Cooling module is supposed to be fixed at the back of UV-C LED array.



**(a)**



**(b)**
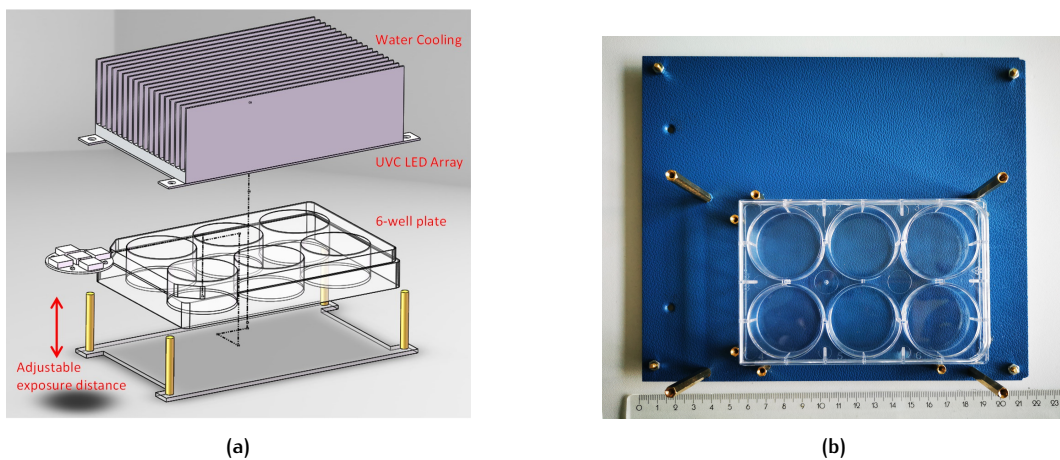
**Figure 2.7:** Structure of (a) UV-C LED array and Cooling module (b) Alternative Cell Culture Plate

The UV-C exposure area of each well depends on the exposure angle of each LED, arrangement of LEDs in each well and exposure distance from the light source to the bottom of each well in the cell culture plate. The radiant power at a certain distance would be characterized, the actual radiant power in experiment would depend on adjustable exposure distance and corresponding power calculation.

### 2.3.2 Cooling Structure Design

Two cooling approaches are designed for the platform, one is air cooling scheme, the other one is liquid cooling scheme. Adding cooling fins to the surface of object by attaching them tightly to surface with thermal grease, total cooling surface is expanded for faster heat dissipation. Liquid cooling is usually more effective than air cooling with heat transfer liquid in cooling blocks. The advantage over air cooling mainly result from heat capacity and thermal conductivity of water. Since liquid leakage of liquid cooling module would do harm to electronic components, the connecting operations are supposed to be paid attention to.

In Figure 2.8, the water pump is the power source of liquid circulation, two liquid blocks are attached at the back of aluminum base of UV-C LED array. Thermal grease is smeared on aluminum base as thermal contact material to liquid blocks. There are two connectors of the water pump, one for Liquid input, another one for Liquid output. The Liquid input pipe of water pump is supposed to be stretched into a water container to introduce liquid into water cooling blocks by connecting water pump Liquid output connector to Liquid blocks Liquid input connector. Liquid in liquid blocks is exported out through Liquid blocks Liquid output connector. The other two connectors of Liquid blocks are linked through a short pipe for internal liquid circulation.
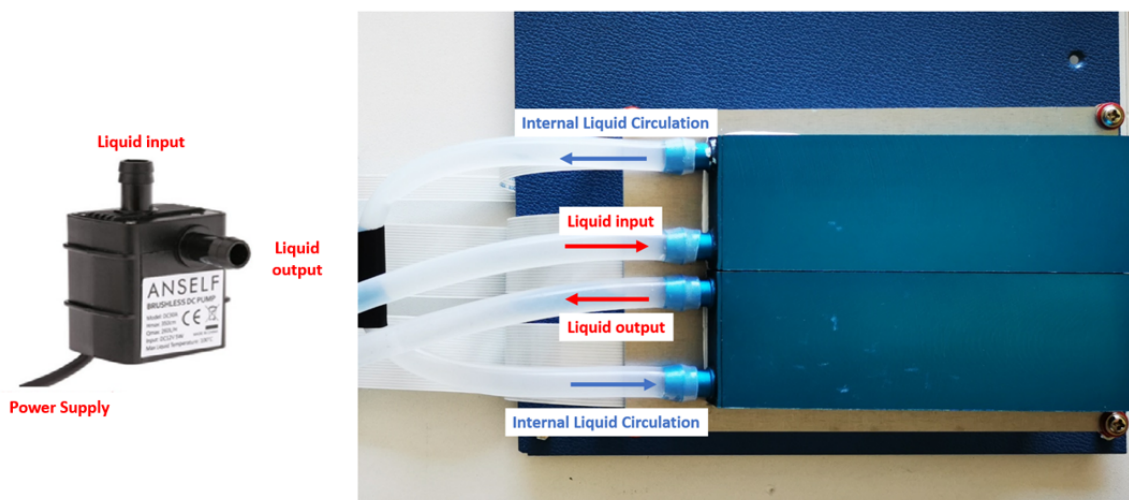


**Figure 2.8:** Water Circulation of Cooling module

## 2.4 SYSTEM COMPONENTS DESIGN

This section would introduce the PCB design of UV-C LED Array Design and Driver Module Design. UV-C LED Array is the UV-C illumination light source, and it is powered by the Driver module with FFC connection between them. Since the platform was a collaborate project at the beginning, the Driver Module is designed by Shanliang, this chapter would give a brief introduction to Driver Module functions. Software design of the platform would take control of the exposure power and exposure light of each LED through PC or keypad. The platform was tested after system assembly to ensure the robustness of platform.

### 2.4.1 UV-C LED Array Design

The PCB design of UV-C LED Array is shown in Figure 2.9, there are six group of LEDs, each group corresponds to a well in the 6-well Cell Culture Plate. Each group is equipped with four UV-C LEDs, there are two reasons for the design. Firstly, it is intended to figure out the most effective single-wavelength or dual-wavelength inactivation recipe, hence four consistent UV-C LEDs or dual-wavelength combination consists of two different wavelength LEDs is designed to be integrated in a LED group. In addition, the TracePro irradiance simulation reveals that single LED would take around one minute to reach $110J/m^2$, inactivating Ebola virus. When four LEDs are exposed to each well of the plate, the inactivation period would be shorten drastically with higher exposure power at the same time. According to the design exposure dose of each group, the amount of LEDs could change flexibly.

At the center of each group, each LED group is equipped with a thermistor, in which case, the real-time temperature of each LED group could be monitored. To readout the data signal of the temperature sensor, a DC Current is added, the sensor would translate the signal and transfer it to the micro-controller. On the right edge of array, the Flexible Flat Cable (FFC) connectors are designed to transfer LED drive current and temperature signals, and test points are left as Surface mounted device (SMD) solder joint.
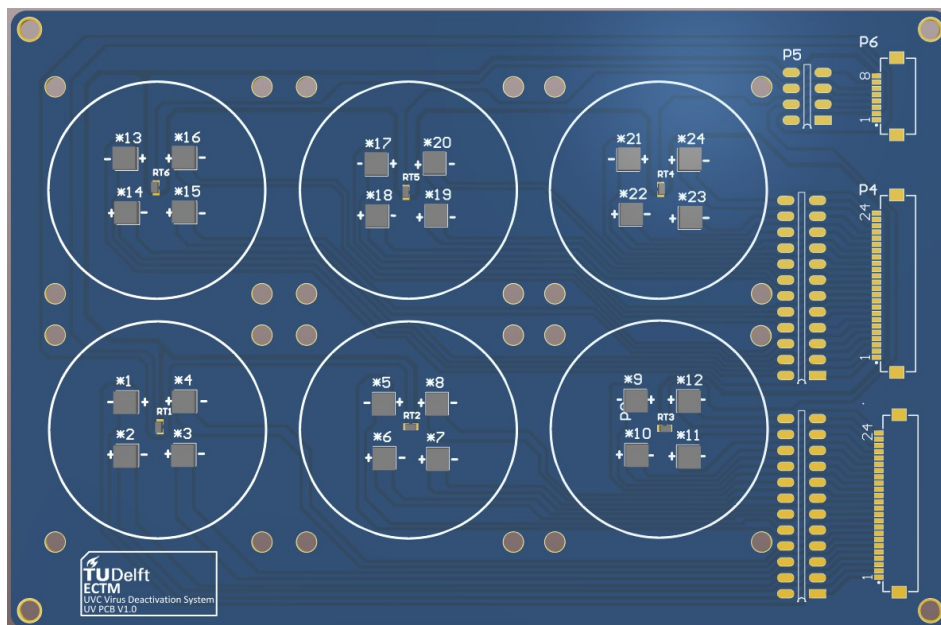


Figure 2.9: UV-C LED Array

### 2.4.2 Driver Module Design

The Driver module is composed of Power Management, Arduino DUE as Microcontroller unit (MCU), PWM Generator, LED controllers, communication ports and input / output ports as Figure 2.10. The section would focus on the introduction of PWM Generator, LED controller and ports design.

The Pulse-width modulation (PWM) generator produce the the power signal of LEDs, the programmable frequency of the PWM generator ranges from 24Hz to 1526Hz. Each PWM LED output signal has 12-bit resolution, namely 4096 power steps with programmable 0% - 100% duty cycle of individual LED brightness control.

$$R_s\left(\Omega\right) = \frac{0.2\left(V\right)}{I_{LED}}\left(A\right) \tag{2.1}$$
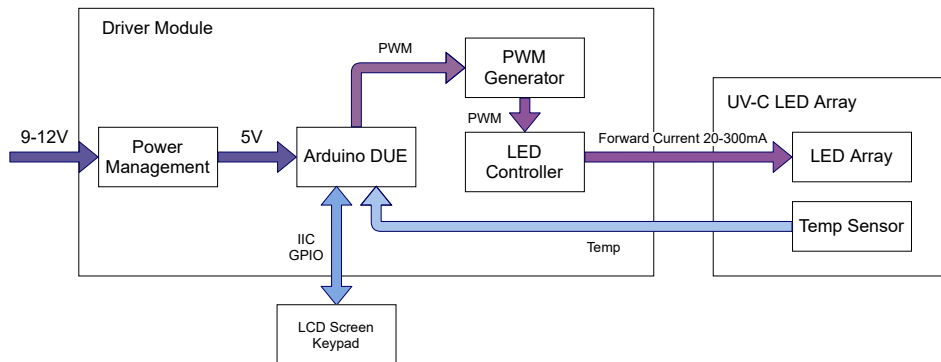


**Figure 2.10:** Driver Module Composition

Besides the PWM generator, Constant Current LED Driver with PWM control is applied for LED controller. With PWM power step control, Constant Current Source (CCS) is constructed as Figure 2.11. When the PWM signals enable the current source, the output current $I_{LED}$ depends on the value of current sense resistor $R_s$ as Equation 2.1, 0.2V is the reference voltage of the amplifier. The output current $I_{LED}$ of selected driver ranges from 20mA to 300mA, and output current accuracy reaches $\pm 1.5\%$.
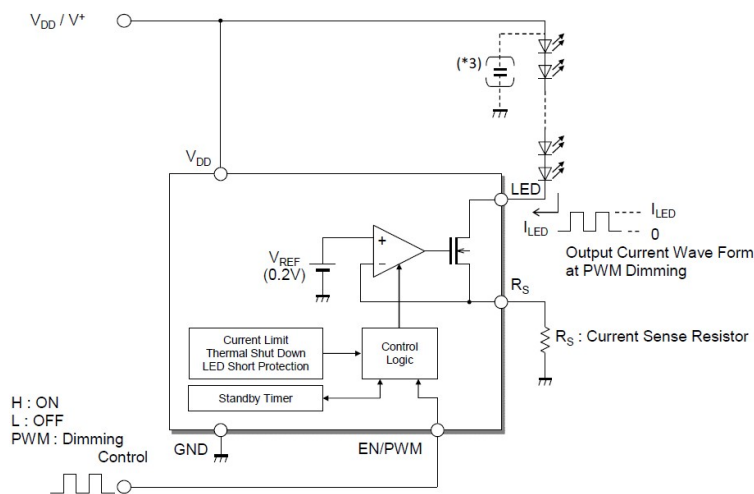


**Figure 2.11:** Constant Current Source

The output ports are designed for transferring LED control signals to UV-C LED Array, and the communication ports serve peripherals. The peripherals are composed of user interactive PC, keypad, LCD, and temperature sensors. PC would transfer exposure power and time parameter to each LED through serial port, keypad transfers input signals, and LCD reveals read-time operations on screen.

### 2.4.3 Software Functions Design

The software functions design of the platform aims to set inactivation experiments parameters with programmable Arduino. PWM controller is applied to take control of the exposure power of each LED, as is discussed in Driver module design, LED brightness is programmable with 0% to 100% duty cycle. In order to obtain a precise value of exposure dose, exposure time is supposed to be paid attention to. In addition, the experiment parameter could be set with keypad input while it takes up too much time, hence PC serial port is applied for parameter transfer before each experiment. This section would focus on the operations flow applied in inactivation experiments and three main. functions as follows.
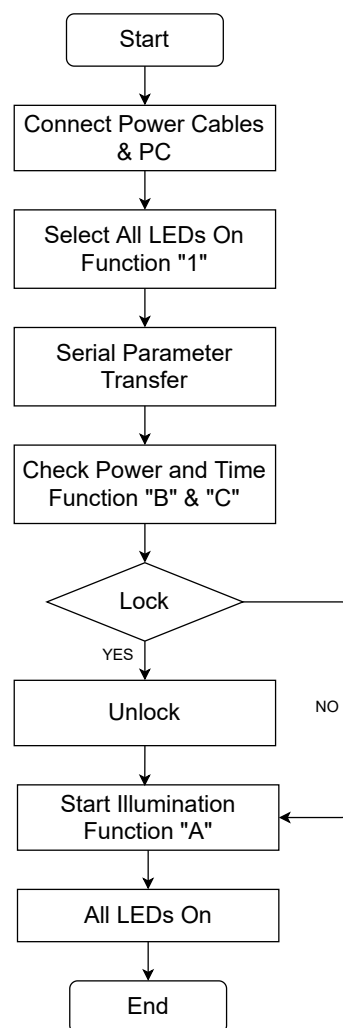


**Figure** 2.12: Operation Flow of Inactivation

Since multiple experiments are done at the same time, one of the four operations is employed in the inactivation experimets and would be introduced. As Figure 2.12, Function 1 is selected and all LEDs

would illumination as programmed exposure power and exposure time. As mentioned, parameter can be transferred through serial port for each recipe, after transferring, check the correctness of each parameter in serial monitor and LCD monitor, if there are some mistaken parameters, re-transferring would resolve the problem. Due to safety concerns, there is also a kill switch designed and utilized as lock of LEDs illumination, hence LEDs unlock is necessary before pressing Function A, resulting in illumination of all LEDs.

1) PWM Controller
   The default PWM frequency is 200Hz, and it supports frequency ranges from 24Hz to 1526Hz. In the final version, the PWM frequency was close to 1000Hz, and duty cycle was 100% in order to obtain continuous wave UV-C exposure with highest exposure brightness.

2) Exposure timer
   The timer resolution is millisecond, and three timers are called for interruptions. The first one is called for screen update every 50ms, the second timer is called for exposure time counter and called each millisecond. The last timer is called for exposure parameter serial transfer before experiments every 100ms, since the transfer is before experiments, there is no strict requirement of interruption intervals, past time period of experiment is shown on top of the LCD monitor.
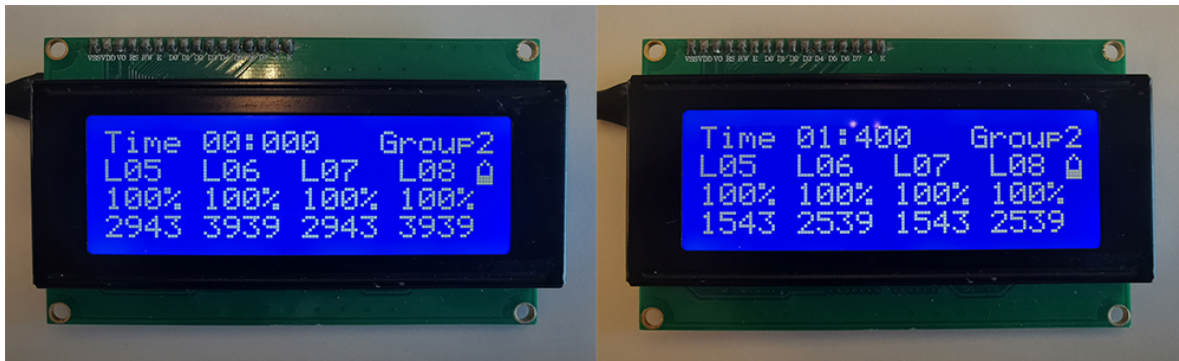


Figure 2.13: LCD Display

According to Figure 2.13, four of all 24 LEDs are shown at a time. On top of screen, past time and group number are shown, LED number and corresponding remaining exposure time are shown in 2nd and 4th rows. The left figure illustrates the original state before inactivation, 1 minute and 400 milliseconds later, past time accumulated, and remaining exposure time counted down during exposure. The lock symbol on the right edge represents the protection lock of all LEDs, unlock symbol would show after pressing the kill switch, in which case, when switch on function A, illumination of all LEDs start up.

3) Serial Transfer
   Connecting Arduino DUE to Personal computer (PC), embedded Serial Monitor would be applied to transfer exposure power duty cycle and exposure time to the platform storage from PC. When choosing correct serial port and corresponding baud rate, the Serial Monitor is prepared for input parameters. Transferring baud rate is 115200, ensuring highest transmission speed. All the parameters are packaged into String, and each String would be divided into exposure power and time value of corresponding LED. After division, each experiment parameter would show up in the monitor for double-check before the experiments. At the same time, all the values are written into storage of Arduino DUE. There is possibility that correct input values would mess up in the monitor, hence re-transfer and check each value on LCD monitor are necessary.

### 2.4.4 Platform Assembling

The assembling of Driver module and UV-C LED Array are completed with re-flow technique, guaranteeing heating temperature, heating uniformity and robustness. The platform prototype is shown, Figure 2.14 (a) is the Air Cooling version platform, and Figure 2.14 (b) is Liquid Cooling version. The air cooling version is suitable for short period inactivation, the temperature rise would reach 30°Cwithin several minutes. Attached cooling fan, the cooling performance could be better while air flow in fume hood could be disturbed. In order to avoid disturbing air flow and obtain temperature rise suppression, Liquid Cooling version is constructed. The Liquid Cooling connection has been discussed in the last section. Within a one hour testing, the temperature rise is completely suppressed, hence Liquid cooling is suitable approach no matter how long the inactivation experiment.



(a)                                                          (b)
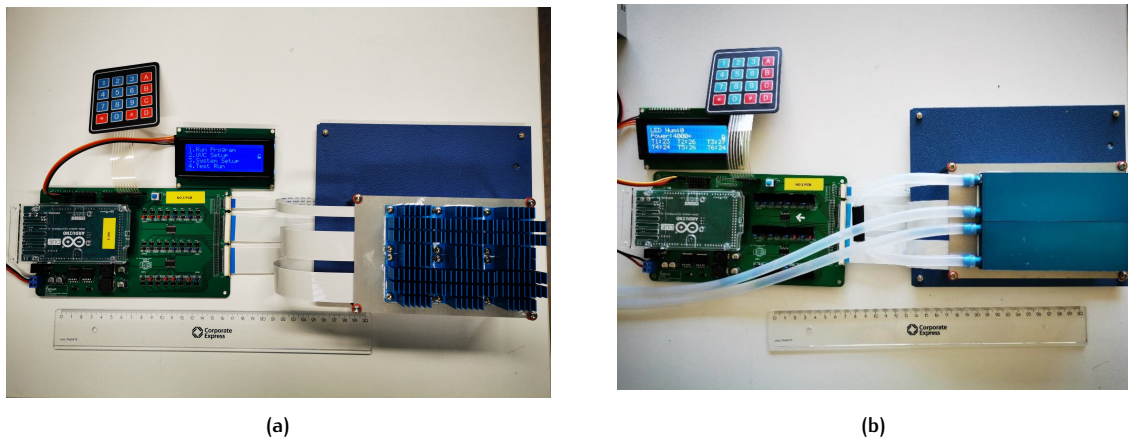
Figure 2.14: UV-C LED Platform (a) Air Cooling version (b) Liquid Cooling version

The UV-C LED Array is fixed as Figure 2.15, each LED is able to be powered with each power step and designed exposure time. In addition, 6-well cell culture plate could be fixed below the array with fixed copper pillars, making sure each LED group directly exposed to each well of the cell culture plate, which could be observed through reflection of LEDs in each well.
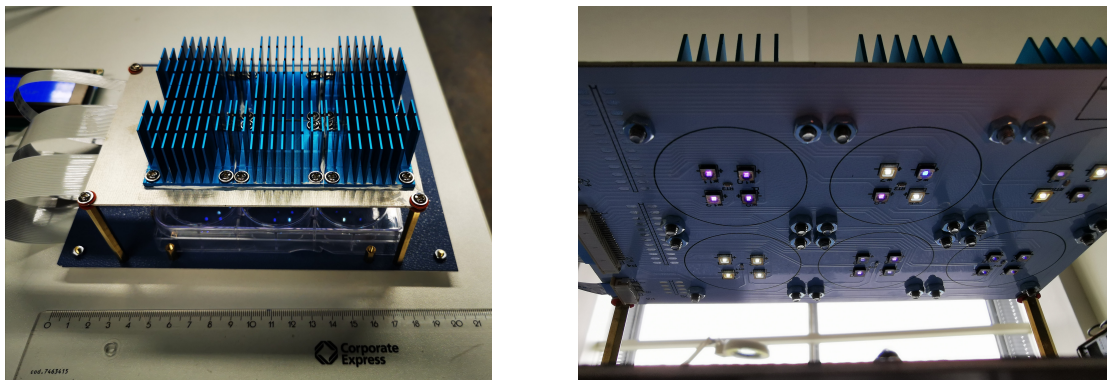


Figure 2.15: UV-C LED Array Structure

## 2.5 UV–C LED CHARACTERIZATION

The purpose of light source characterization is to test LED radiant power and peak wavelength of each LED when it is driven by preset forward current. There could be peak wavelength and radiance variance between data-sheet and characterized result. Therefore, characterization is necessary for LEDs embedded in the inactivation platform. In addition, the exposure doses designed for the inactivation experiments are supposed to be derived from characterized light intensity. This section is composed of brief UV-C LED Description, characterization approach, result, exposure distance and corresponding power analysis.

### 2.5.1 UV-C LED Description

The original parameters of each LED is obtained from datasheet provided by each manufacturer as Table 2.2, in the table, LEDs are from different manufacturers, their peak wavelength and optical power output are measured under preset forward current. However, chips from different batches would vary a lot when applying different dies for batch production. The variances between LEDs could result in uncertain errors when directing using consistent parameters in the datasheet. Moreover, the actual forward current of LED can also be different from the preset values in the datasheet but within absolute maximum forward current value. Therefore, the characterization is to measure the peak wavelength and optical output power under different forward current condition in order to obtain precise values for inactivation experiment design.

In the characterization, the measurement is aim to obtain reliable optical power with stepped driving current, peak wavelength with stepped driving current and whether there is a linear relationship between stepped driving current and radiance of each LED.

Table 2.2: Manufacture LED Description

| Peak Wavelength(nm) | Optical Power Output | Spectrum Half Width | Manufacturer |
|---|---|---|---|
| 255 nm @ 100 mA | 3.5 mW @ 100 mA | 11 | SeoulViosys |
| 255 @ 20 mA | 0.5 mW @ 20 mA | 11 | SeoulViosys |
| 265 @ 500 mA | 60 mW @ 500 mA | 11.2 | UVSIS Technology |
| 278 @ 100 mA | 15 mW @ 100 mA | 10 | Vishay Semiconductors |
| 285 @ 100 mA | 10 mW @ 100 mA | 11 | SeoulViosys |

### 2.5.2 Characterization Approach

The designed characterization is implemented in Signify. UVC LED array was installed on the test platform at a distance of 6.5cm from the surface of the LED quartz window package to the receiver plain of the detector as Figure 2.16 shown. The LEDs to be characterized were fixed and aligned to the center of the detector during each characterization. During each test, UVC LED array was driven by Driver Module operated by loaded program, leading to 25%, 50%, 75% and 100% of maximum driving current. Driver Module is powered by a 9-12 V DC power supply during the testing.

As is mentioned, LED radiant power variance and peak wavelength shift would result from batch variance and individual variance. For each characterized LED, radiant power and peak wavelength values at each programmable power step are measured during the testing, several LEDs with the same nominal wavelength are characterized to verify consistence and exclude outlier, which would be discussed in Characterization Result.
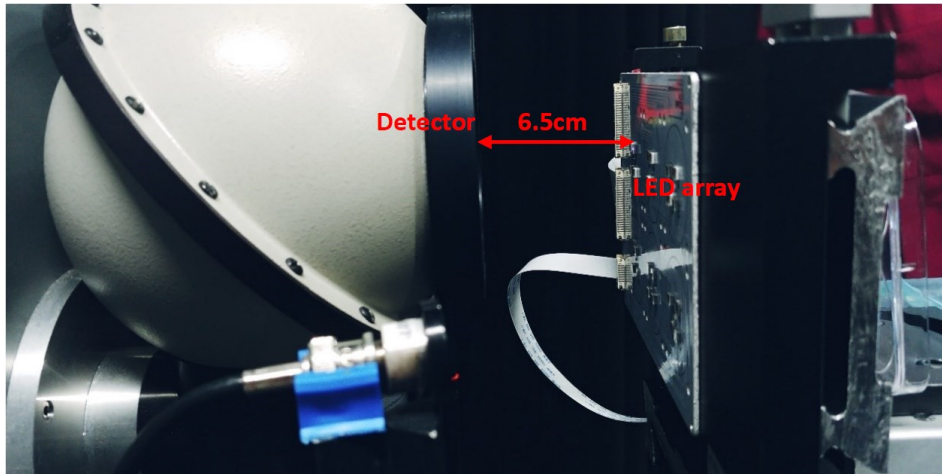
Figure 2.16: Characterization Platform

### 2.5.3 Characterization Result

Totally, five LED chips are chosen for characterization, 255 nm with maximum current 200 mA, 255 nm with maximum current 30 mA, 265 nm, 278 nm and 285 nm. The characterization Result is shown in Figure 2.17a, it reveals the spectra distribution of each LED and Radiance result at maximum power step at a measure distance of 65 mm. As a result, characterized peak wavelengths are 259.4 nm, 260.3 nm, 269.1 nm, 273.9 nm and 283.8 nm for five LED chips respectively. Each LED has a peak wavelength shift from the nominal value more or less.

Besides, take nominal 255 nm as example, Figure 2.17b illustrates radiance power and peak wavelength of five LED models. The radiance values plotted are measured at the maximum power duty cycle, wavelength shift could be seen. The peak wavelength of most nominal 255 nm LEDs characterized to shift close to 259 nm, one of LED shifts to more than 260 nm and reveals comparatively low radiance power.
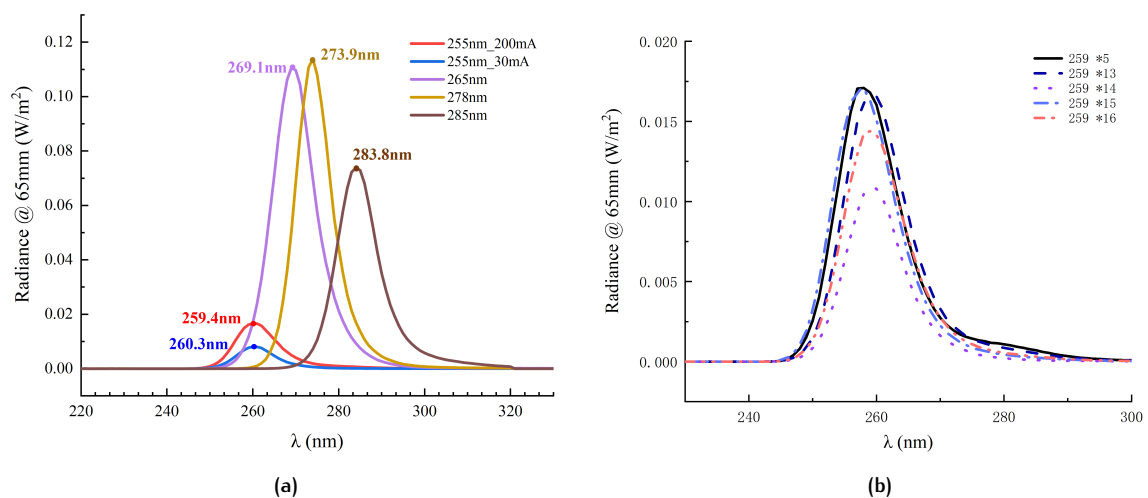


Figure 2.17: Characterization of (a) Overall Radiance Power and Peak wavelength measured at maximum power step (b) Radiance Power variance and Peak wavelength shift of nominal 255 nm LED

Ideally, the radiance power is linear with stepped driving current, in which case, all of the radiance power points could be derived from the linear relationship rather than characterize each power point used for experimental radiation. So, in the actual characterization, linear radiance curve is expected for further experiment. As is shown in Figure 2.18, regardless of radiance power variance of nominal consistent LEDs, with the increase of power step, radiance curve rises almost linearly. The label reveals the characterized LED wavelength and followed LED number to show the difference.

There is also some possibility could result in the tilting curve, each LED is manually aligned to the center of detector, hence slight fluctuation or nonuniform of radiance power is probable. Therefore, with reasonable characterized radiance curve, the designed radiance power parameter of experiment could be directly derived from the linear relationship.
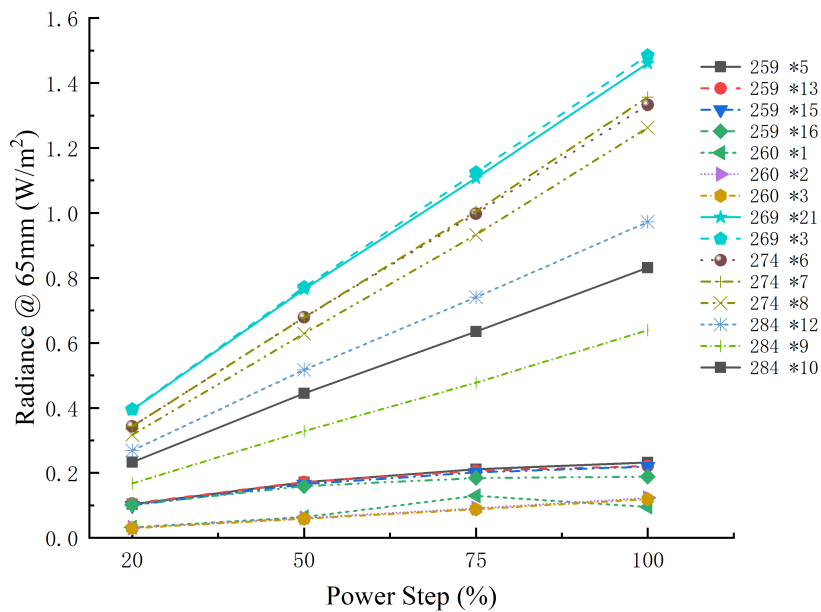


**Figure 2.18:** Linearity of Radiance

The Table 2.3 illustrates the wavelength and optical power on data-sheet and characterized radiant power and wavelength. Characterized radiant power is measured at four power steps 1000, 2000, 3000, 4096, with maximum resolution reaches 4096 power steps, namely four duty cycles 25%, 50%, 75% and 100% are preset, presenting corresponding brightness. Characterized peak wavelength list in the table are also tested with four power steps but averaged values are taken in the table.

During following experiment parameter design, the 100% (power step 4096) is always regarded as calculation reference of radiance power. For example, if 60% of full power is needed in experiments, the value could be derived from the multiplication of full radiance power and selected percentage according to sound linearity of characterization,

### 2.5.4 Exposure distance and Radiant power

In order to ensure enough illumination area in single well and avoid light interference from adjacent well at the same time, Solidworks simulation is applied for verification. The illumination model is

Table 2.3: Characterization Measurement of characterized Radiance Power and Peak Wavelength

| Datasheet Peak Wavelength (nm) | Power step | Characterized Radiance Power ($W/m^2$) | Characterized Peak Wavelength (nm) |
|---|---|---|---|
| 255 nm (200 mA) | 1000 | 0.1206 | 259.4 |
| | 2000 | 0.2035 | |
| | 3000 | 0.2546 | |
| | 4096 | 1.4228 | |
| 255 (30 mA) | 1000 | 0.0306 | 260.3 |
| | 2000 | 0.0602 | |
| | 3000 | 0.0895 | |
| | 4096 | 0.1210 | |
| 265 | 1000 | 0.3957 | 269.1 |
| | 2000 | 0.7715 | |
| | 3000 | 1.1247 | |
| | 4096 | 1.4851 | |
| 278 | 1000 | 0.3432 | 273.9 |
| | 2000 | 0.6785 | |
| | 3000 | 1.0017 | |
| | 4096 | 1.3448 | |
| 285 | 1000 | 0.2002 | 283.8 |
| | 2000 | 0.3869 | |
| | 3000 | 0.5564 | |
| | 4096 | 0.7354 | |

shown as Figure 2.19, the cylinder in the centre stands for a single well of the well plate, the actual height the well is 17 mm. Four UV-C LEDs are fixed at certain height, four cones in the figure used to represent illumination condition.
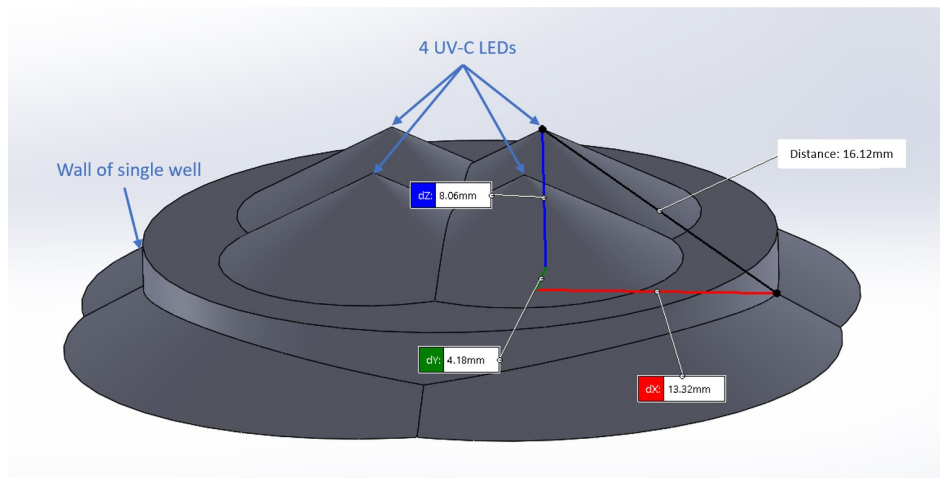


Figure 2.19: 3D illumination model of single well

When LEDs are placed at least 8 mm above the bottom of well, illumination area is guaranteed to fully cover the bottom of well. With any larger distance, the illumination area is always satisfied, namely the full well surface can be illuminated no matter which height (>8 mm) the LED Array is placed. In the model, several trials with different exposure distance are attempted, placement of LED Array outside the well is preferred to avoiding collision of LEDs and cell culture plate. Assuming LEDs are placed at a distance of 20mm from the bottom of well, LEDs are placed above the cell culture plate, preventing collision with the plate and light interference from adjacent well.

Table 2.4: Light Intensity Calculation

| Light source wavelength(nm) | Light Intensity@6.5cm($mW/cm^2$) | Light Intensity@2cm($mW/cm^2$) |
| --- | --- | --- |
| 259.4 | 0.02150 | 0.2270 |
| 260.3 | 0.01065 | 0.1125 |
| 269.1 | 0.14705 | 1.5528 |
| 273.9 | 0.13015 | 1.2744 |
| 283.8 | 0.09015 | 0.9520 |

Assuming that the LED array is placed 20 mm above the bottom of the plate, calculate the maximum light intensity at a distance of 2 cm as Table 2.4 based on characterization result from Signify. Taking the research mentioned as example, 110 $J/m^2$ UV fluence is applied to inactivate Ebola. When applying the lowest light intensity 0.1125 $mW/cm^2$ of 260.3 nm LED, it takes almost 98 seconds to reach the target inactivation dose. In conclusion, with the illumination model of a single well, four UV-C LEDs at a exposure distance of 2 cm, it is possible to inactivate Ebola Virus within one and a half minutes.

## 2.6 CONCLUSION

In the chapter, requirement of the UV-C LED Inactivation Platform is clarified firstly, the platform modeling includes Driver module, UV-C LED Array and Cooling module. Irradiance simulation and thermal simulation are implemented before the design of platform. Irradiance simulation reveals the relationship between exposure distance and average irradiance of certain illumination area. Referring to the COMSOL heat dissipation model of LED Array, the influence of base material and cooling module design is estimated and taken into further design. The design of platform is composed of Mechanical Structure Design and System Components Design. Mechanical Structure Design proposes feasible structural assembling approaches. After the design of each module and software Design, the platform assembling is ultimately completed. For the purpose of preparing reliable exposure parameter for experiments, LEDs are characterized in Signify. Referring to characterization result, exposure distance is designed for experiments, inactivation exposure time within 2 minutes is expected in the next chapter.

# 3 | STANDARD VIROLOGY INACTIVATION EXPERIMENTS

Applying the platform designed in Chapter 2, Standard Virology Inactivation Experiments are performed. The experiment purpose, preparation, components, design scheme and result analysis are introduced in this chapter. The experiment purpose is clarified beforehand, and experiment preparation and design would obey the purpose. Taking multiple components into account, experiments are able to be designed as Design of Experiments (DoE) in order to obtain corresponding response, experiments have been improved during several attempts. After inactivation and back titration, experiment data would be collected and analyzed.

## 3.1 PURPOSE OF EXPERIMENTATION

The purpose of virus inactivation experiments is to obtain the optimal recipe for efficient target virus inactivation with platform in last chapter. Apart from the recipe obtained with present preform, an assumption of better scheme could be put forward base on current inactivation result. The evaluation criteria of the optimal recipe is log reduction rate of target virus under the same exposure dose of different wavelength. Owing to different virus is probable to have variable effective inactivation dose and wavelength as is mention in Chapter 1, one target virus is chosen for experiment in the project as reference. Moreover, the inactivation result could be more than an optimal recipe, law of inactivation is also expected, the inactivation performance could follow the regularity, changing with factors accordingly.

Considering the variance of virus, the inactivation method varies accordingly. The optional scheme would be a combination of all the factors and levels, resulting in corresponding response. Levels are variables cannot change during the experiment, they could depend on experiment fume hood condition setting or preset parameters before experiments. Factors are variables change with design of experiments, exploiting control variates method, one factor varies when others factors maintaining the same. To reduce variability of experiments, levels of experiments are supposed to be designed before inactivation experiments, and explore the possible influence of all the factors according to literature and multiple attempts at the same time. Based on literature review, design of factor values would obtain original range. After trial experiments, factor range would shrink, and designed to be more reasonable in the following experiments.

All the factors are composed of wavelength, exposure dose and ozone concentration. The existence of ozone concentration is to be confirmed or to be ruled out, hence ozone sensor testing scheme, an experimental group and a control group are supposed to implement together. The single-wavelength and dual-wavelength recipes are designed during LED Array assembly, single-wavelength inactivation experiments are designed to obtain the optimal single-wavelength recipe, whereas dual-wavelength inactivation experiments are planned to figure out a better recipe, and whether dual-wavelength inactivation is superior to single-wavelength inactivation.

## 3.2 PREPARATION OF EXPERIMENT

This section would introduce preparation before each experiment, including Platform connection, arrangement, Dried virus preparation and Safety measures. Preparation of Experiment would ensure smooth progress of inactivation, LED illumination, LCD monitor display and water circulation are supposed to be guaranteed.

### 3.2.1 Preparation of Inactivation

The platform is fully prepared as Figure 3.1 Before inactivation, the power supply would be connected to Driver Module and water pumps with cables, and UV-C LED Array is connected to Driver Module through FFCs. Driver Module and power supply (PSU) are placed on experiment cart, keypad connected to Driver Module is fixed on the cart for convenience of operations. The UV-C LED Array structure is supposed to be placed inside the fume hood during inactivation. Water pipes connected to the cooling module are fixed on cart and reached into water container. Water circulation testing is required before the experiments, making sure water circulates smoothly through all pipes, hence heat dissipation requirement of LEDs could be satisfied. Experiment note and PC serial transfer parameters are prepared beforehand, before inactivation of each recipe, parameters are transferred through serial port and checked on LCD display with keypad.
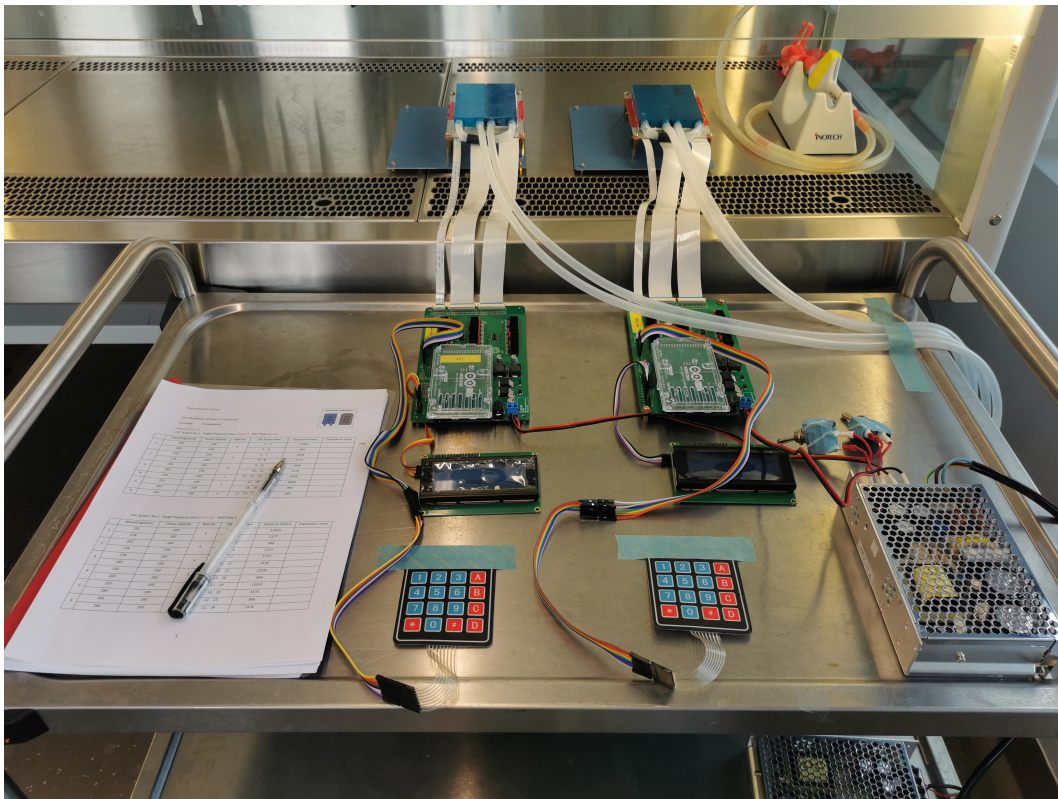


Figure 3.1: Experiment Platform

Virus chosen for inactivation experiment is Influenza A PR8 (A/Puerto Rico/8/1934), it belongs to single-stranded RNA virus. In the experiment, dried virus are laid as a dot at the centre of each well as Figure 3.2a, and will be exposed to UV-C light. The 6-well cell culture plates for virus storage are on the right of Figure 3.2b, 96-well cell culture plates on the left with EMEM Eagle/EBSS solutions inside are used for back titration after inactivation. Each container is labeled before use for further operations and data track.
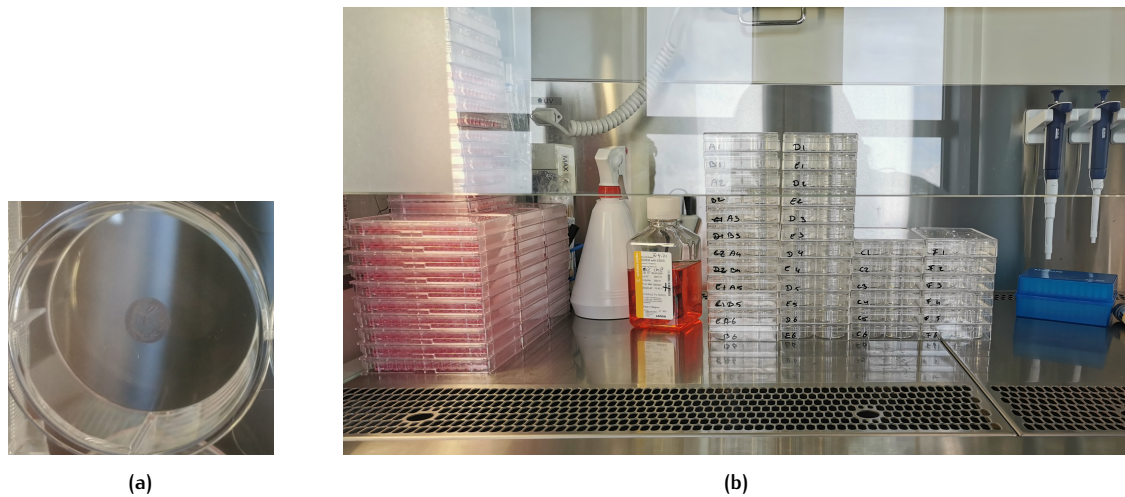
**Figure 3.2:** Preparations for the inactivation experiments (a) Dried Virus at the center of each single well (b) Cell Culture Plates for Inactivation and post-experiment Back Titration

### 3.2.2 Safety Measures

As platform testing and experiments are implemented with UV-C light source, there are several protection measures should be paid attention to according to ISO 15858:2016 [36]. As exposure to invisible UV-C radiation could have effect on health, resulting in ocular damage (photokeratitis) and cutaneous damage (erythema). Although UV-C radiation would not lead to erythema at the wavelength of 254 nm, skin protections and eye protections are both necessary, the personal protective equipment is composed of:

1) Eye protection gear: UV glasses, face shield, or safety glasses complying with EN 170.

2) Clothing covering all exposed skin with direct UV expose.

The inactivation experiment is supposed to be done in Biological Safety Level (BSL) 2 laboratory. Therefore, we have to follow corresponding guidelines, wear laboratory coats upon entry, wear safety goggles or safety glass especially when exposed to UV-C light and wear gloves when handling microorganisms. As for standard laboratory practices, washing hands after entering and before existing is a must, only platform and necessary tools could be taken in laboratory. Also, the bench we used for inactivation has to be disinfected before and after laboratory session [37]

## 3.3 COMPONENTS OF EXPERIMENT

Considering all the input factors of the virus inactivation process, UV-C Wavelength, Exposure Dose of each LED and the probable ozone release are significant to the response of experiments. Wavelength and Exposure Dose are controllable factors, while ozone concentration is uncontrollable, causing possible unknown influence. Among them, exposure dose is composed of exposure power of each wavelength and exposure time, All of experiment levels exposure distance, humidity and temperature are designed and maintained during experiments based on exposure coverage calculation, laboratory condition and platform cooling testing, and responses are listed as expected results to be analyzed after experiments.

### 3.3.1 Factors

1) Wavelength

Table 3.1: Peak Wavelength and corresponding Light Intensity

| Light source peak wavelength (nm) | Light Intensity @ 2 cm ($mW/cm^2$) |
| --- | --- |
| 259.4 | 0.2270 |
| 260.3 | 0.1125 |
| 269.1 | 1.5528 |
| 273.9 | 1.2744 |
| 283.8 | 0.9520 |

According to the characterization in signify, the actual peak wavelength of each LED and radiance are measured as Table 3.1. In total, three UV-C LED arrays are designed for the platform, four LEDs are embedded in a group, single-wavelength and dual-wavelength groups are designed as Table 3.2, Table 3.3 and Table 3.4, each LED is labelled with LED number, wavelength and driving current. Comparisons between single-wavelength groups and dual-wavelength groups are implemented to evaluate inactivation performance, the group with the highest inactivation reduction would be figured out as the best recipe.

Table 3.2: UV-C LED Array No.1

| UV-C LED Array no.1 | | | | | | | |
| --- | --- | --- | --- | --- | --- | --- | --- |
| LED no. | 1 | 2 | 3 | 4 | 5 | 6 | 7 | 8 |
| $\lambda$ (nm) | 260 | 269 | 260 | 269 | 259 | 274 | 259 | 274 |
| Max. Id (mA) | 30 | 200 | 30 | 200 | 200 | 150 | 200 | 150 |
| LED no. | 9 | 10 | 11 | 12 | 13 | 14 | 15 | 16 |
| $\lambda$ (nm) | 259 | 284 | 259 | 284 | 259 | 259 | 259 | 259 |
| Max. Id (mA) | 200 | 200 | 200 | 200 | 200 | 200 | 200 | 200 |
| LED no. | 17 | 18 | 19 | 20 | 21 | 22 | 23 | 24 |
| $\lambda$ (nm) | 259 | 269 | 259 | 269 | 269 | 269 | 269 | 269 |
| Max. Id (mA) | 200 | 200 | 200 | 200 | 200 | 200 | 200 | 200 |

Table 3.3: UV-C LED Array No.2

| UV-C LED Array no.2 | | | | | | | |
| --- | --- | --- | --- | --- | --- | --- | --- |
| LED no. | 1 | 2 | 3 | 4 | 5 | 6 | 7 | 8 |
| $\lambda$ (nm) | 260 | 274 | 260 | 274 | 269 | 274 | 269 | 274 |
| Max. Id (mA) | 30 | 150 | 30 | 150 | 200 | 150 | 200 | 150 |
| LED no. | 9 | 10 | 11 | 12 | 13 | 14 | 15 | 16 |
| $\lambda$ (nm) | 274 | 284 | 274 | 284 | 260 | 269 | 260 | 269 |
| Max. Id (mA) | 150 | 200 | 150 | 200 | 30 | 200 | 30 | 200 |
| LED no. | 17 | 18 | 19 | 20 | 21 | 22 | 23 | 24 |
| $\lambda$ (nm) | 260 | 284 | 260 | 284 | 269 | 284 | 269 | 284 |
| Max. Id (mA) | 30 | 200 | 30 | 200 | 200 | 200 | 200 | 200 |

Some researches state the most effective virus inactivation wavelength is around 253.7 nm because the wavelength is the main target which is absorbed by nucleic acids dominantly, leading to

Table 3.4: UV-C LED Array No.3

| UV-C LED Array no.3 | | | | | | | |
|---|---|---|---|---|---|---|---|
| LED no. | 1 | 2 | 3 | 4 | 5 | 6 | 7 | 8 |
| $\lambda$ (nm) | 260 | 274 | 260 | 274 | 274 | 284 | 274 | 284 |
| Max. Id (mA) | 30 | 150 | 30 | 150 | 150 | 200 | 150 | 200 |
| LED no. | 9 | 10 | 11 | 12 | 13 | 14 | 15 | 16 |
| $\lambda$ (nm) | 284 | 284 | 284 | 284 | 260 | 260 | 260 | 260 |
| Max. Id (mA) | 200 | 200 | 200 | 200 | 30 | 30 | 30 | 30 |
| LED no. | 17 | 18 | 19 | 20 | 21 | 22 | 23 | 24 |
| $\lambda$ (nm) | 260 | 284 | 260 | 284 | 274 | 274 | 274 | 274 |
| Max. Id (mA) | 30 | 200 | 30 | 200 | 150 | 150 | 150 | 150 |

formation of photo-products as structure damage, among them, dimers of thymine are prominent [38], in which case, the closest characterized wavelength 259 nm should be paid attention to.

2) Exposure Dose

The target exposure dose is designed for each LED group, corresponding to each well of cell culture plate. Take measured UV fluence to inactivate Adenoviridae as example, 220 $J/m^2$ is necessary [39]. Assuming array is fixed at a distance of 2 cm, only 3.5-4.3 seconds illumination is enough for 269 nm or 274 nm LEDs single-wavelength groups with highest light intensity. For each 284 nm LEDs single-wavelength group, 5.7 seconds also enough to reach 110 $J/cm^2$ UV dose. As for each 259 nm LED and 260 nm LED single-wavelength groups with the lowest power, 24.2 seconds and 48.8 seconds (almost one minute) are necessary for inactivation respectively. Considering all the combination, the exposure time took for inactivation ranges from 3 seconds to one minute. The evaluation of inactivation performance not only depends on the estimated exposure time, but also wavelength sensitivity. Under the same exposure dose of different wavelength, there could be performance differences in between.

As Exposure dose is designed for each LEDs group, the dual-wavelength group divides the dose of two wavelengths equally. For example, 30 $J/m^2$ is supposed to be cast on virus, dual-wavelength group 259|269 would divide 15 $J/m^2$ to 259 nm LEDs, and 15 $J/m^2$ to 269 nm LEDs. If reduction rate of dual-wavelength group 259|269 is higher than single-wavelength group 259 nm and group 269 nm, the dual-wavelength group could be regarded as more efficient recipe.

3) Ozone concentration

It is stated in Section 1.1.2, ozone is probable to be significant factor of inactivation other than ultraviolet exposure. Under direct UV radiation of 107.1 $\mu W/cm^2$ UV dose rate for one hour, the ozone concentration is 4.64ppm, survival rate of CON1 is $10^{-1}$, survival rate of MUT1 is $10^{-2.5}$ [29]. It is recommended to apply 10-20 ppm ozone for 10-15 minutes to inactivate CoVs at $3.5 \log_{10}$ reductions [30]. For pure ozone virus inactivation, standard ozone concentration 20 ppm was taken into experiment, the effective inactivation of influenza virus took 18min to 90min exposure [40]. As for UV-C lamp and 5ppm ozone concentration, survival rate of niger spores on bare chip for one hour is $10^{-3}$ [41]. According to the above experiments, effective ozone inactivation usually takes 5-20 ppm ozone for one hour, while UV inactivation with designed platform can be done in minutes. Therefore, to rule out the influence of ozone inactivation, corresponding approach is shown in design of experiments.

As for UV-C LED Array No.2, probable ozone inactivation has to be taken into consideration. To block the ozone interference, reference groups should be set, one is directly exposed to UV exposure and probable ozone. In the other group , a layer of black polyethylene plastic or metal

stripe would be applied to shield samples against UV light while probable ozone could leak inside, in which case, virus sample could only be influenced by ozone concentration.

### 3.3.2 Levels

1) Exposure Distance
   According to the characterization, at a distance of 6.5 cm from LED Array, the light intensity at a distance of 2 cm is calculated in Chapter 2. The 2 cm distance setting ensures full well illumination area and avoid the light interference from adjacent LED groups.

2) Humidity
   The experiment executed under the condition of 80% relative humidity at room temperature to maintain effective inactivation, otherwise, the disinfection period would become more variable [40]. In addition, the required ozone concentration at 85% RH was lower than at 55% RH to inactivation [42]. Therefore, the relative humidity is better to reach 80%-85% for steady virus inactivation rate, while it depends on real fume hood condition.

3) Temperature
   Experiments are supposed to be done at room temperature. When platform is equipped with liquid cooling, temperature of LED array can maintain 25°C. As for platform equipped with air cooling module, it could keep the LED array around 30°C. The temperature in each well of plate could be monitored with on board temperature sensors.

### 3.3.3 Response

1) Virus Log Reduction - UV Dose
   The UV dose is the product of UV intensity (expressed as energy per unit surface area) and residence time. With fixed illumination distance, when dose rises, reduction is expected to increase accordingly, forming **Inactivation Curve**.

2) Virus Log Reduction - Wavelength
   Applying the same UV dose but different wavelength to inactivate same amount of virus, it is expected to obtain the most effective wavelength and corresponding **Germicidal Curve**.

3) Virus Log Reduction - Ozone concentration
   With or without a layer of black polyethylene plastic or metal strip, a reference group would be set. In addition, the existence of ozone resultd from LEDs not equipped with doped quartz glass, which is characterized as 269 nm LEDs in LED arrays. If ozone is proven to exist, the log reduction would increase with ozone concentration.

## 3.4 DESIGN OF EXPERIMENT

All of experiment components and their variantion have been described in above section, this section would bring in precise design parameters of each experiment. Some hypothetical conditions are stated in this section with corresponding experiment expectation. Each level has been confirmed, with a exposure distance of 2 cm, fume hood humidity 38% RH, experiments could be implemented. All platform applied liquid cooling scheme, maintaining stable temperature 25°C. To maintain simplest condition, the experiments aim at forecasting consequence by introducing one factor into consideration as prerequisite. As stated in Section 3.3, each factor stands for an independent predictor variable. Wavelengths has been designed and equipped with platform, hence this section would concentrate on Exposure Dose design, Exposure wavelength design and Ozone and Control Group.

### 3.4.1 Order of log magnitude

Usually, the logarithm base 10 is applied in most inactivation experiments. As the readout limitation with base 10 was 4.17, which is far lower than experiments in researches. Therefore, in the following experiments, the logarithm base drops to 5 by making smaller dilution steps with the back titration, so as to lead the readout become more accurate. The log reduction with base 5 could be calculated according to Equation 3.1, with $N_0$ is the number of viable microorganisms before treatment, N is the number of viable microorganisms after treatment.

$$LogReduction = log_5(\frac{N_0}{N})$$ (3.1)

Table 3.5: Reduction Calculation based on $log_{10}$

| Reduction N | Reduction Percentage(%) |
|---|---|
| 1 - $log_5$ | 80 |
| 2 - $log_5$ | 96 |
| 3 - $log_5$ | 99.2 |
| 4 - $log_5$ | 99.84 |
| 5 - $log_5$ | 99.968 |
| 6 - $log_5$ | 99.9936 |
| 7 - $log_5$ | 99.99872 |

The reduction N with 5 based logarithm is translated into reduction percentage in Table 3.5, in which case, the log reduction would be compared to literature virus inactivation results. When N reaches 6-7, the inactivation percentage reaches 99.99%, representing high inactivation level.

### 3.4.2 Exposure Dose Design

The Design of Exposure Dose is to explore effective inactivation dose range, discovering the relationship between dose and log reduction. At the beginning, effective inactivation dose ranges were obtained from previous researches in Chapter 1, a brief list of dose statistics is shown as Table 3.6. Since efficient dose in the table ranges from 5 to 100 $mJ/cm^2$ to various categories of viruses, in the beginning experiment, designed doses were briefly sketched as 30, 65, 100 $mJ/cm^2$ to ensure efficient inactivation, in case original dose is too weak to inactivate Influenza A PR8. However, during first experiment, most of the experiments are too effective to inactivate target virus. The full reduction value was 4.17 according to the negative control limitation, only the reduction of group with 30 $mJ/cm^2$ exposure dose turns out to be smaller than 4.17, which means under this dose, there is virus remaining without being inactivated. Therefore, 30 $mJ/cm^2$ is chosen as upper bound for inactivation in the following experiments.

Table 3.6: Dose statistics of UV-C Light Source Inactivation

| UV-C Type | Virus | Dose ($mJ/cm^2$) | Reduction | Year | Experiment Condition |
|---|---|---|---|---|---|
| Tube | SARS | 100 | 3.4 | 2020 | Platelet disinfection |
| Tube | SARS | 25 | 6.8 | 2007 | Platelet disinfection |
| Lamp | Phi 6 corona | 25.5 | 4.2 | 2020 | Surface |
| Signify's UV-C light source | SARS CoV-2 | 5 | 2 | 2020 | |
| Signify's UV-C light source | SARS CoV-2 | 22 | 6 | 2020 | |

In order to keep the same dose of different wavelength LEDs, a trade-off between radiant power and exposure time has to be achieved. In optical characterization of the UV-C LEDs (by Signify), it is proven that the current-irradiance curve remains sound linearity within characterized range, hence corresponding light intensity of each power step can be derived. For each LED group, under 15 $mJ/cm^2$, LEDs share target dose uniformly in single wave-wavelength group, while dual-wavelength group divides the dose between two wavelengths equally as Table 3.7. In accordance with rule of **Inactivation Curve**, doses are sketched increasing gradually but below the upper bound 30 $mJ/cm^2$, so doses for experiment are delineated as 1, 3, 6, 10, 15, 20, 25 $mJ/cm^2$ with repetition of 4 (N = 4).

Linearity or Smoothness of curve is a standard to tell whether the repetition of same experiment is sufficient to derive inactivation regular pattern, sufficient datapoints is the key prerequisite to keep the property. N = 4 was design for **Inactivation Curve**, and repetition time increases to 6 (N = 6) to obtain more reliable **Germicidal Curve**. The selectable doses for current experiment are 6 and 15 $mJ/cm^2$. To achieve better dose precision, the exposure time precision was upgraded to millisecond, hence power duty cycle could all be set to 100% as characterization. Although the linearity of radiance has been proven, applying characterized power step is closer to real light intensity, it also ensures a continuous-wave UV exposure because of 100% duty cycle at 1kHz driving frequency.

Table 3.7: Dose Design of Single wave-wavelength and Dual-wavelength Groups

| Wavelength (nm) | Light Intensity (mW/cm2) | Exposure Time(s) | Estimated dose(mJ/cm2) | |
| --- | --- | --- | --- | --- |
| 259 | 0.2270 | 16.520 | 15 | |
| 259 | 0.2270 | 16.520 | 7.5 | 15 |
| 269 | 1.5528 | 2.415 | 7.5 | |

### 3.4.3 Exposure Wavelength design

Apart from the influence of total exposure dose, as an ingredient, wavelength is the key factor of inactivation performance. The variety of virus sensitivity to different wavelength is supposed to be figured out through experiments within UV-C band. Exposure single-wavelength and dual-wavelength groups are illustrated as Table 3.8. Five characterized single peak wavelength LEDs are implemented in the platform.

Table 3.8: Exposure wavelength design for each LED array group

| UV-C LED Array No.1 | | | | | |
| --- | --- | --- | --- | --- | --- |
| Well no. | 1 | 2 | 3 | 4 | 5 | 6 |
| $\lambda$ (nm) | 260\|269 | 259\|274 | 259\|284 | 259 | 259\|269 | 269 |
| UV-C LED Array No.2 | | | | | |
| Well no. | 1 | 2 | 3 | 4 | 5 | 6 |
| $\lambda$ (nm) | 260\|274 | 269\|274 | 274\|284 | 260\|269 | 260\|284 | 269\|284 |
| UV-C LED Array No.3 | | | | | |
| Well no. | 1 | 2 | 3 | 4 | 5 | 6 |
| $\lambda$ (nm) | 260\|274 | 274\|284 | 284 | 260 | 260\|284 | 274 |

### 3.4.4 Ozone Control Group

Employing the platform, Ozone is a potential factor of inactivation experiment, as the existence of ozone os to be proven through experiments. Theoretically, in UV-C LED manufacture, doped quartz glass will be used as a low pass filter to block short spectrum, including ozone-generating 185 nm light. All UV-C LEDs implemented in this platform come with doped quartz glass, except the one in 269 nm wavelength. In characterization, it is hard to find any 185 nm UV light, but it is necessary to prove whether there is ozone exist by either gas measuring or a ozone control group in the experiment. On the one hand, ozone sensor is utilized to measure the concentration of ozone, on the other hand, experimental and control groups are implemented as powerful evidence.

Experiments as prerequisite reveals half of the full scale reduction value of ozone reference group, which is doubted because it is probable that the blinding tape could not block all UV-C light, causing UV-C light leakage through side walls of opening from current well and adjacent wells. The penetration ability of UV-C is weak, making it cannot penetrate most transparent glass and plastic. To dissolve the UV-C blocking issue, wells are better to be mostly covered with metal strips during the experiment, and metal is proved to block ultraviolet rays.

As is shown in Figure 3.3, half of the amount of wells are blocked with metal strips indicated with yellow tape, while remaining wells are exposed to LEDs. 260|269 dual-wavelength group is chosen as inactivation light source, two wells of dried virus are exposed directly an experimental group and control group. The ozone control group will be treated as irradiance of 25 $mJ/cm^2$ with metal strip blocking the UV-C light but allow any potentially ozone leakage into the well. The virus reduction read-out of the ozone control group should be a strong evidence to prove whether the virus inactivation observed in other groups attribute to UV-C light or ozone, or even combined effort.
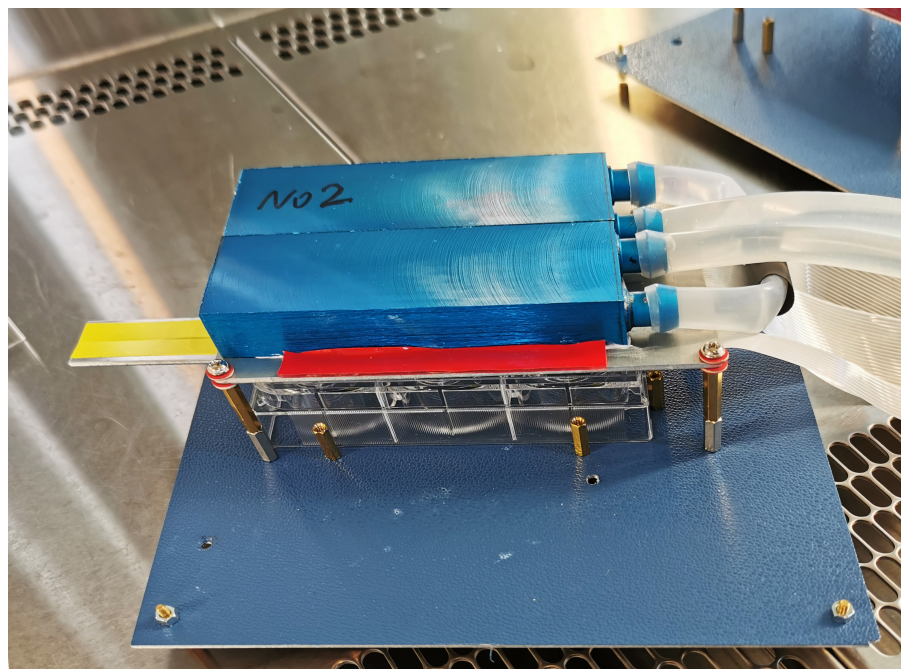


**Figure 3.3:** Ozone reference group

### 3.4.5 Hemagglutination

Hemagglutination is a method often used for quantification of viruses, and it is commonly used for the diagnosis of some enveloped viruses such as influenza viruses, so it is applied to our inactivation experiment. This method works depend on the characteristic of some enveloped viruses that can adsorb to Red blood cells (RBCs). If there is no virus particles, RBCs would land to the bottom of a well, forming a red-colored dot. In the presence of virus particles, RBCs dispersed, a red dot is not formed [43]. During back titration of each virus sample, each dilution is diagnosed with hemagglutination to judge whether there are virus particles.

As is shown as side view of Figure 3.4, two cone shaped wells are placed, the left one is full of virus particles, while the right one is stuffed with red blood cells. During a hemagglutination assay, with existence of virus particles, the well turns out to be transparent, without the existence of virus particles, there are still red blood cells in the well, forming a red dot as top view.
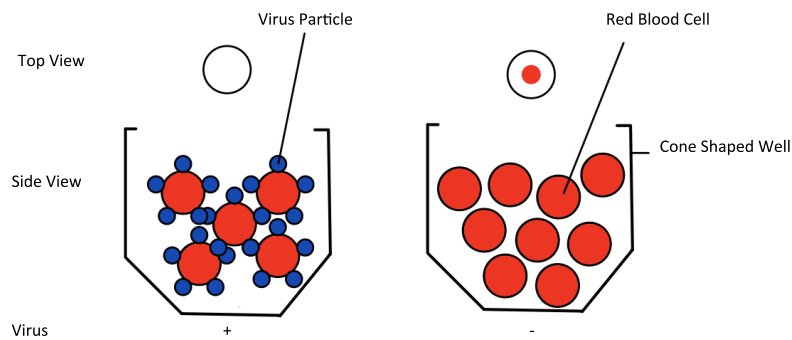


**Figure** 3.4: Hemagglutination Diagram

Figure 3.5 is a Hemagglutination Assay result after virus dilution, it could be observed that most of wells are stuffed with a red dot, representing inactivation of virus in these wells, other wells are transparent, meaning there are remaining virus particles. With a detection limit of 7.2 hemagglutination units (HAU), dried Influenza Virus A are prepared for inactivation experiments in advance, and the log reduction is supposed to be subtracted from the detection limitation.
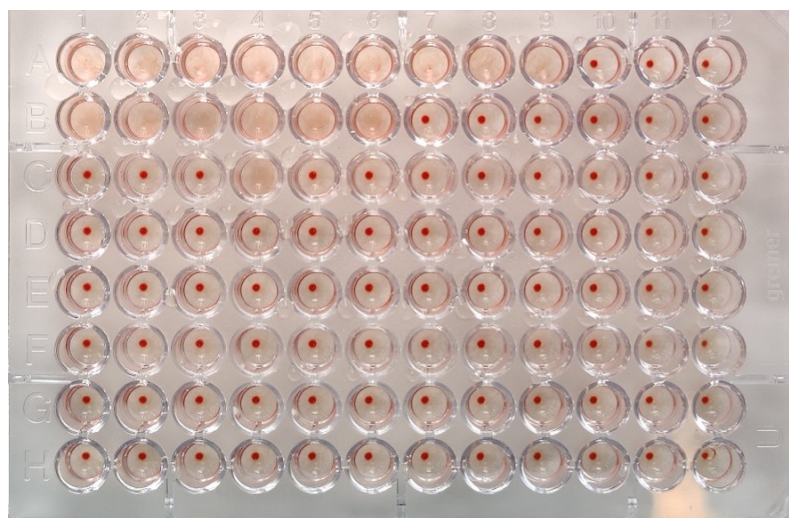


**Figure** 3.5: Hemagglutination Assay

## 3.5 EXPERIMENT RESULT

Several experiments are done step by step, all of results are concluded in this section. Resulting from the possible variance of viruses, inactivation results are all extracted from experiments with same detection limit of 7.2 hemagglutination units (HAU), in which case, log reduction has consistent benchmark. First of all, the section would introduce inactivation performance of ozone control group in case ozone plays the role of potential powerful inactivation factor. If the influence of ozone inactivation could be ruled out, the platform inactivation would only take ultraviolet light into consideration. As the inactivation performance regarding exposure dose, **Inactivation Curve** is anticipated. With respect to the disinfection influence of UV-C wavelength, **Germicidal Curves** are plot consequently, both single-wavelength and dual-wavelength disinfection results would be discussed in the section. With the influence of Exposure Time under the same dose, the relationship between Log Reduction and Exposure Time is anticipated at last.

### 3.5.1 Ozone Control Group

As is measured by the ozone sensor, the concentration is close to zero, which reveals the ozone concentration could barely inactivate the virus effectively. To confirm the impossibility of inactivation, two ozone control groups are designed as Figure 3.6, and four adjacent wells are left for leakage check. During the experiment, two ozone control groups are blocked with metal strips, UV light are completely shielded physically, while potential ozone could leak into the well through gaps between well edge and metal strips. Both of ozone control groups apply dual-wavelength 260|269, which has been proven to be the one effective combination. The left four adjacent wells were utilized for leakage check. During the testing, two of six LED groups are exposed to wells, the other LEDs are turned off, in which case, if there is UV leakage, it could be figured out through reduction of viruses in adjacent wells.
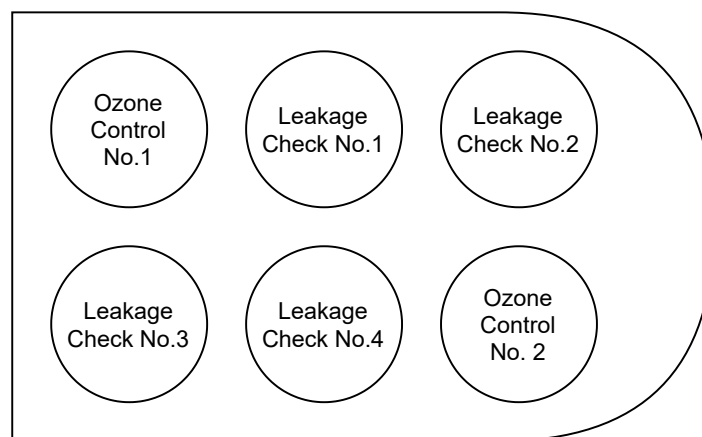


**Figure 3.6:** Ozone Control Well Distribution

The Ozone Control is done under the exposure dose of 25 $mJ/cm^2$, which is verified in Section 3.5.2 as an effective inactivation dose. An reference negative control group of dried virus is done before all inactivation experiments as Table 3.9 shown. As is mentioned, the detection limitation of prepared dried Influenza A/Puerto Rico/34 virus is 7.2 hemagglutination units (HAU). Reaching the detection limit stands for viruses are not inactivated at all, so do the two Ozone Control Groups, in which case ozone could be completely ruled out from the significant factors of the inactivation with designed platform. Moreover, when it comes to the leakage check groups of adjacent wells, if there is UV light leakage or ozone leakage from adjacent illuminating LED groups, reduction could be observed from their negative control results, whereas four leakage check groups reveals no log reduction as table shown.

**Table 3.9**: Negative Control Results of Ozone Control Group

| Ozone Control | | Leakage Check | | | | Reference Dried Virus |
|---|---|---|---|---|---|---|
| No.1 | No.2 | No.1 | No.2 | No.3 | No.4 | Negative Control |
| 7.20 | 7.20 | 7.55 | 7.20 | 7.20 | 7.20 | 7.20 |

According to the above discussion, it could be concluded that under the maximum exposure dose setting 25 $mJ/cm^2$ of all designed experiments, there is no released ozone, or the release amount of ozone could be completely ignored from the influence of disinfection. Therefore, only UV-related factors influence would be taken into consideration in the following argument.

### 3.5.2 Inactivation Curve

To explore the reduction tendency with the increase of exposure dose, and discover an appropriate dose for Germicidal Curve. Suitable dose range is a prerequisite of effective inactivation, obvious disinfection 3-4 log reduction is expected to be observed. At the same time, viruses cannot be completely inactivated during the dose range. For the dose of Germicidal Curve dose, the divergence between LED groups under the exposure dose is better to be differentiated, regardless of single-wavelength groups or dual-wavelength groups.
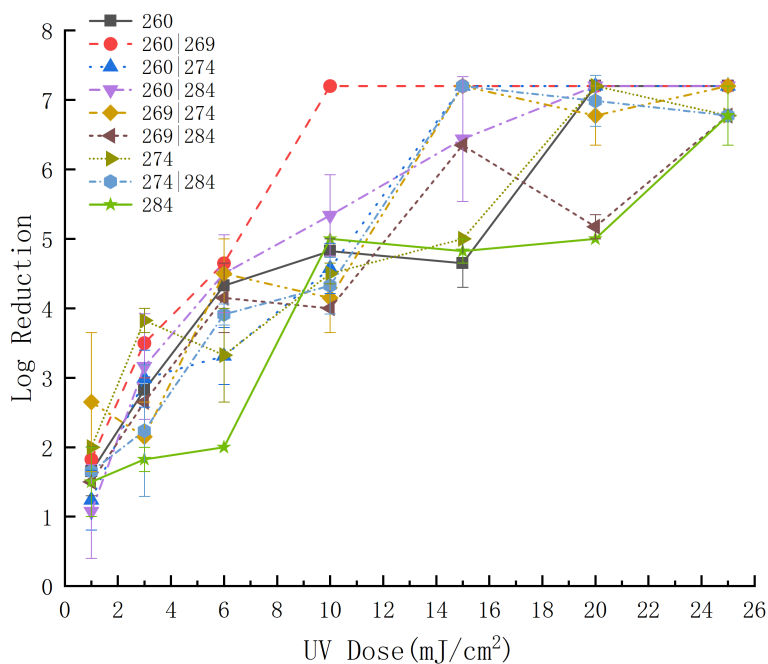


**Figure 3.7**: Inactivation Curve

As is shown in Figure 3.7, generally speaking, the log reduction of each LED group increases with the rise of UV dose until a plateau, in spite of fluctuations in between. Among all the groups, 260|269 is the most efficient combination, the log reduction attains detect limitation 7.2 when dose reaches 10 $mJ/cm^2$, at least 2-log superior to other groups. As for 15 $mJ/cm^2$, 260|269, 269|274, 260|274, 274|284 groups all attain the detect limitation, and reduction divergence between groups are the most discrete.

The disinfection performance of single-wavelength groups are not distinct among all samples, 260 nm and 274 nm single-wavelength UV light source leads to 7.2 log reduction under the dose of 20 $mJ/cm^2$. Since there are five wavelengths in characterization, but two of them have not been taken into account till the experiment of Inactivation Curve. The promising single-wavelength 259 nm and 269 nm are included in Germicidal Curve, and the comparison of their inactivation performance would be performed within single wavelength groups.

Since there is a rising plateau, which is not suitable for inactivation performance between single-wavelength and dual-wavelength groups, exposure dose below 20 $mJ/cm^2$ is supposed to be taken into account for divergence observation. The difference between groups are mixed in Inactivation Curve while effective dose has been figured out accordingly, hence experiments for a Germicidal Curve is design at exposure dose 6 $mJ/cm^2$ and 15 $mJ/cm^2$.

### 3.5.3 Germicidal curve

The designed doses for current experiment are 6, 15 $mJ/cm^2$, each dose is applied to each setup with 6 times of repetition to obtain more reliable Germicidal Curve. With negative control, the dried virus without UV-C threat could not be readout after 7.2log$_5$ titer, namely 7.2 HAUs. Taking the single-wavelength result of previous experiment into account and removing the outliners, the **Germicidal Curve** trend-line of five single-wavelength groups is plotted as Figure 3.8. Trendline is applied to sketch the mediums of each single-wavelength reduction value, attached with error bars.
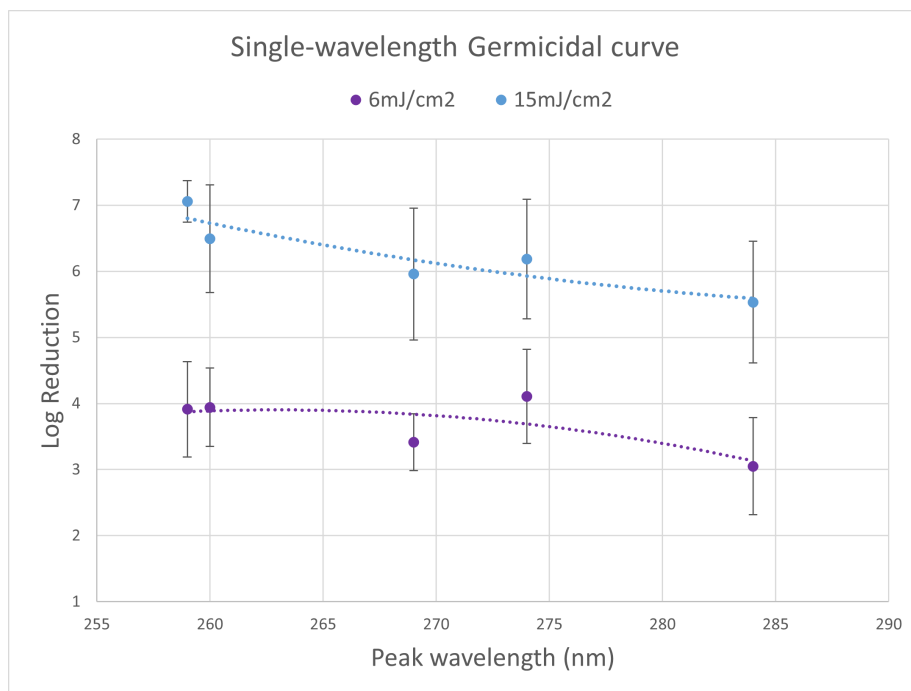


**Figure 3.8:** Single-wavelength Germicidal curve

The tendency of both 6 $mJ/cm^2$ and 15 $mJ/cm^2$ are similar, with the rise of peak wavelength between 259 nm and 284 nm, the log reduction decreases gradually. Under the dose of 15 $mJ/cm^2$, 259 nm single-wavelength group turns out to be the most effective one. In addition, between the same peak wavelength under two exposure doses, there is a 2-3 log difference. Take 259 nm group as example, there is 7-log reduction when exposed to 15 $mJ/cm^2$, and 4-log reduction when exposed to 6 $mJ/cm^2$, 3-log divergence between two doses.

When it comes to dual-wavelength groups, since each group separate exposure dose between two wavelengths equally, the average value of two wavelengths is taken as comparable benchmark and plot, the log reduction tendency of two doses is similar to single-wavelength result. Log reduction drops with the rising of wavelength.
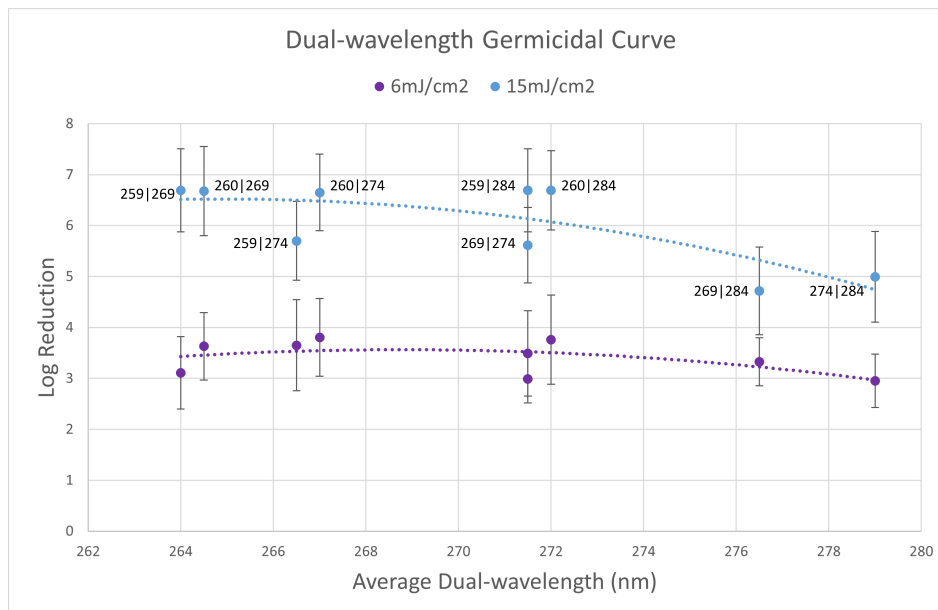


**Figure 3.9:** Dual-wavelength Germicidal curve

Referred to the result of single-wavelength and dual-wavelength, the optimal single-wavelength 259 nm group obtained 7.06-log reduction, which is higher than the optimal dual-wavelength group 259|269 group 6.69-log reduction. Therefore, single-wavelength 259 nm group tends to obtain the best inactivation performance among all the wavelength recipes with the testing platform.

## 3.6 CONCLUSION

The purpose of Standard Virology Inactivation Experiments are stated at the beginning of the chapter. Before the experiments, preparation and safety measures are supposed to be put in the first place. According to the purpose of experiments, all of influence factors and levels are discussed, as a result, responses are expected to obtain after inactivation. Based on the analysis of experiment components, experiment parameters are sketched, ozone control group is especially designed, remaining experiments are done with dose and wavelength setting. To analyze the inactivation performance, Hemagglutination principle and corresponding cell culture plate are illustrated. Finally, Inactivation results are plotted, manifesting performance of specific wavelength and exposure dose, the performance are discussed according to inactivation plots.

# 4 | MOLECULAR DYNAMIC RESEARCH ON INACTIVATION MECHANISM

The inactivation performance under specific UV-C wavelength and exposure dose have been illustrated in Chapter 3. In the current chapter, the molecular dynamic research reveals inactivation mechanism during the UV inactivation process would be analyzed and interpreted. The chapter consists of introduction of background knowledge, molecular dynamics research on various viruses and molecular dynamics simulations on nucleic acid bases of RNA viruses.

## 4.1 BACKGROUND KNOWLEDGE

During the inactivation experiments, UV LEDs emits quantitative dose, and dried Influenza A sample serves as the absorption sample. The absorption of UV energy has an influence on the inactivation of virus sample theoretically, which would be verified in the chapter in terms of molecular dynamics perspective. This section is composed of Absorption Spectroscopy and Molecular Electronic Transition.

### 4.1.1 Absorption Spectroscopy

Each sample or material has its absorption spectrum, which is fragment of sample's absorbed radiation over a number of frequencies. The absorption spectrum essentially depends on the atomic and molecular ingredient of the sample [43; 44; 45]. Visible light is taken into the principle discussion of the electromagnetic radiation overview as an example. Assume a beam source is irradiating the sample in Figure 4.1, it emits multiple wavelengths at the same time. In the graph, green light is absorbed by the sample, while remaining wavelengths are transmitted to the detection, attenuating the emmission light. On the molecules level, photons satisfy the energy gap of molecules, energy is absorbed during the process, driving molecules to excited state. Upon detection, transmission spectra is plot, while absorption spectra is the attenuation from the emission spectra, which is plot as absorption intensity varies along with frequency. The spectroscopic techniques applied to delineate the sample absorption of radiance concerns the frequency or wavelength of a sample, called an **Absorption Spectrum**.
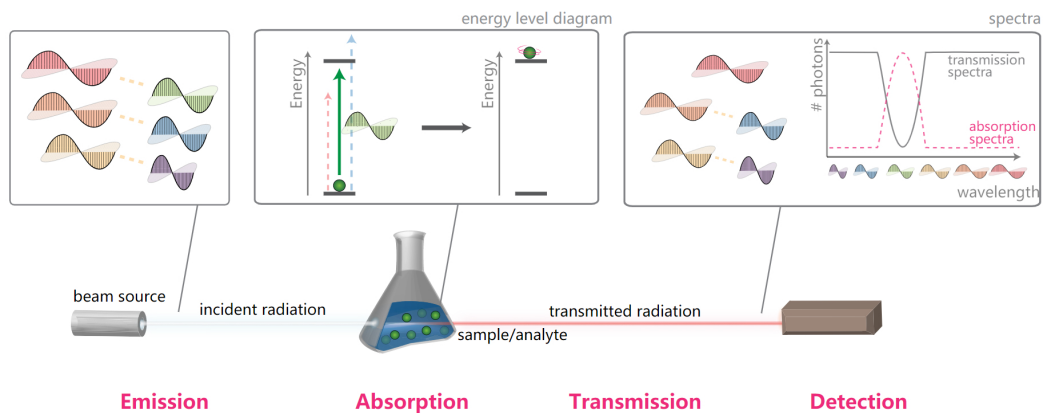


Figure 4.1: Spectroscopy Overview

If a photon has an interaction with an atom or a molecule, radiance absorption occurs when photon energy matches the energy gap between the discrete quantum states of the atom or molecule as Equation 4.1, in which E is photon energy (Joules), h is the Planck constant - $6.62606957 * 10^{-34}$ $(m^2 kgs^{-1})$, the $\nu$ is the photon's frequency.

$$E = h\nu \tag{4.1}$$

The photon flux is expressed as Equation 4.2 the number of photons absorbed per second per unit area could be delineated by the multiplication of fluence rate H $(photons/cm^2/s)$ and linear absorption coefficient $\mu_a$ $(cm^{-1})$.

$$\phi = \#photons/s/cm^2 = H\mu_a \tag{4.2}$$

The variable power density of photons at specific wavelength would be derived as Equation 4.3, where $\phi$ is the photon flux and q is the value of the electronic charge $1.6 * 10^{-19}$. Also, the product of photon flux and the energy of a solitary photon could represent power intensity, in which case, the photon wavelength and energy at a given wavelength could be utilized to derive photon power intensity [46].

$$H(\frac{W}{m^2}) = \phi * \frac{hc}{\lambda} = \phi * qE(eV) \tag{4.3}$$

description sketches how radiance absorption takes place when there is an interaction between photon and atom/molecule, the absorption of photons depends in wavelength, energy and absorption coefficient. In the ultraviolet (UV) and visible (VIS) regions, which ranges from 190nm to 800nm, on the basis of electromagnetic radiation, Molecular absorption spectroscopy is generally applied to biological measurements, leading to the discussion of **Absorbance**. The extent of light absorption is determined by the number of molecules' absorbance capability at certain wavelength, and the molecule's absorbance efficiency at a specific wavelength, which is concluded and known as **Beer–Lambert Law**.

$$A = -logT = log(\frac{P_0}{P}) = log(\frac{I_0}{I}) = \epsilon cl \tag{4.4}$$

According to Equation 4.4, A represented by $log(\frac{I_0}{I})$ is known as **Absorbance**, which is determined by **Molar absorptivity, concentration and length of sample**, remaining variables of equation are illustrated in Table 4.1. The Molar absorptivity, namely molar extinction coefficient is one characteristic of molecule experiencing an electronic transition, it depends on the dimension of absorbing system and the possibility of electronic transition [47; 48].

Table 4.1: Variables of Beer–Lambert Law [47]

| Term and Symbol | Definition |
|---|---|
| A | Absorbance |
| T | Transmittance |
| $P_0$ | Radiant power of light incident upon sample cell |
| I | Radiant power of light leaving sample cell |
| $I_0$ | Intensity of light incident upon sample cell |
| I | Intensity of light leaving sample cell |
| $\epsilon$ | Molar absorptivity |
| c | Molar concentration of solute |
| l | Length of sample cell (cm) |

### 4.1.2 Molecular Electronic Transition

Given that transitions in ultraviolet (UV) and visible (VIS) region of electromagnetic spectrum takes place for some organic compound, electronic transitions of the compounds could be diagnosed through ultraviolet-visible spectroscopy [49]. As is mentioned in measurement of Absorption Spectrum, the spectra attenuation results from energy absorption, in which case, atoms or molecules transfers from ground (lowest energy state) to excited state (higher energy state) as Figure 4.2. The **absorbed energy** of electromagnetic radiance is identical to the **energy difference between excited state and ground state**.



$$\Delta E = [E(excited) - E(ground)]$$
$$= h\upsilon$$
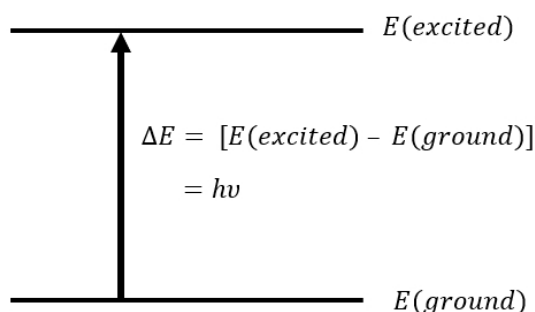
**Figure 4.2:** The Excitation Process [52]

As claimed by **Frontier Orbital Theory**, once a molecule absorbs energy, an electron would jump from its original orbital to a more energetic orbital, which has greater potential energy. The highest occupied molecular orbital (HOMO)/the lowest unoccupied molecular orbital (LUMO) interaction is nothing but the most considerable of a quantity of small interactions. Therefore, generally speaking transitions tend to take place from the HOMO to the LUMO. Within a organic molecule, there are mainly three types of orbitals with corresponding bonds, which can introduce five typical electronic transitions as Figure 4.3. The occupied molecular orbitals with the lowest energy are called $\sigma$, similar bonding orbitals but lying at relatively higher energy levels called $\pi$, the non-bonding orbitals with rather higher energy level is n orbital, holding un-shared pair, and the orbitals with the highest energy is anti-bonding $\sigma^\star$ and $\pi^\star$.
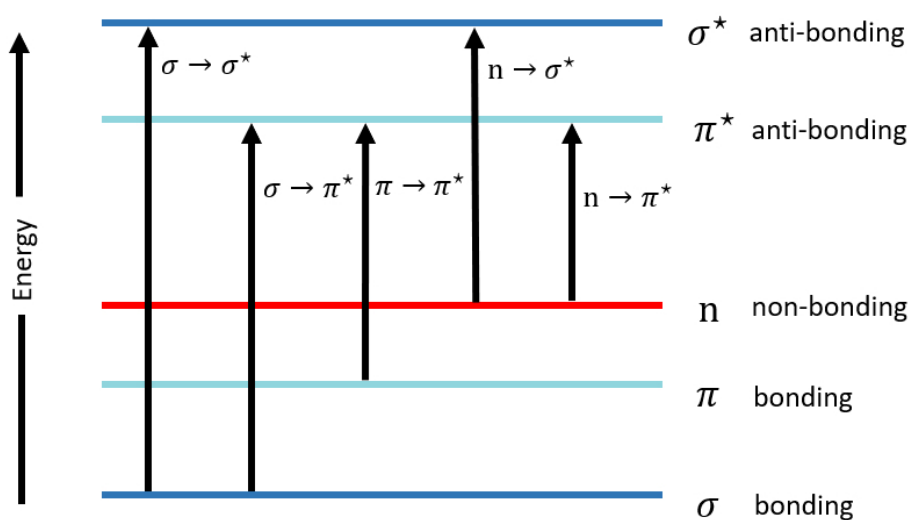


**Figure 4.3:** Electronic Energy Levels and Transitions Diagram [52]

Disregarding complicated aromatic compounds, the plausible and important transitions in ultraviolet and visible region are:

– $\sigma \longrightarrow \sigma^\star$   In alkanes

– $\sigma \longrightarrow \pi^\star$   In carbonyl compounds

– $\pi \longrightarrow \pi^\star$   In alkenes, carbonyl compounds, alkynes, azo compounds, and so on

– $n \longrightarrow \sigma^\star$   In oxygen, nitrogen, sulfur, and halogen compounds

– $n \longrightarrow \pi^\star$   In carbonyl compounds

According to the molecular orbital approach, the absorbed energy of radiance is applied to transfer an electron from a bonding or non-bonding molecular orbital to an anti-bonding molecular orbital in Figure 4.3. The energy required for the transition is determined by the energy gap between two orbitals, it could be figured out that the $\sigma \longrightarrow \sigma^\star$ transition requires the largest energy gap, namely it requires the highest energy because $\sigma$ electrons are held very tightly, whereas $n \longrightarrow \pi^\star$ transition owns the smallest energy gap, so the transition need the least energy. Among which, $\sigma \longrightarrow \sigma^\star$ and $n \longrightarrow \sigma^\star$ transitions require high energy and absorb energy within the Vacuum UV region of less than 200nm, while $\pi \longrightarrow \pi^\star$ and $n \longrightarrow \pi^\star$ transitions are mainly responsible for the absorption within UV and visible region, ranging from 200nm to 800nm [50; 51].

Taking acetone as example, as is shown in Figure 4.4, all of single bonds are $\sigma$, while the double bond belongs to $\pi$. Also, free electron pairs denoted as n are the non-bonding electrons with oxygen. Therefore, three types of transitions are plausible to take place on Acetone, including $\sigma \longrightarrow \sigma^\star$, $n \longrightarrow \pi^\star$ and $\pi \longrightarrow \pi^\star$.
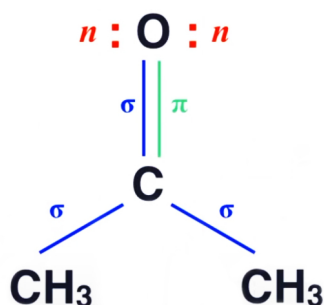


Figure 4.4: Acetone Structural

The bond types of each organic compound could be observed from their structure of chemical bonds as Table 4.2. Typically there is a $\sigma$-Bond between C——H, C——C and C——O bonds, the existence of $\pi$-Bond between C——O bond could result from double bond. Moreover, there are n electrons of oxygen, on the non-bonding orbital, which indicates plausible $n \longrightarrow \sigma^\star$ transition in Ethanol.

Table 4.2: Chemical Bonds and Plausible Transitions

| Chemical Bonds | Bond Type | Organic Compound | Chemical Formula | Plausible Transition |
|---|---|---|---|---|
| C——H | $\sigma - Bond$ | Methane | $CH_4$ | $\sigma \longrightarrow \sigma^\star$ |
| C——C | $\sigma - Bond$ | Ethane | $C_2H_6$ | $\sigma \longrightarrow \sigma^\star$ |
| C——O | $\sigma - Bond, n - electrons$ | Ethanol | $C_2H_5OH$ | $\sigma \longrightarrow \sigma^\star, n \longrightarrow \sigma^\star$ |
| C══C | $\pi - Bond$ | Ethylene | $C_2H_4$ | $\pi \longrightarrow \pi^\star$ |
| C══O | $\pi - Bond, n - electrons$ | Acetone | $(CH_3)_2CO$ | $\pi \longrightarrow \pi^\star, n \longrightarrow \pi^\star$ |

Although the above discussion illustrates the mechanism of absorption of radiance, which is attributed to the transition of electrons from ground states to excited states, the decisive factor of which wavelengths the radiation would absorb is the nuclei. The bounded strength or tightness of electrons are determined by the nuclei, having significant influence on energy spacing between ground states to excited states. Therefore, considering the characteristic energy of a transition, instead of the property of electrons themselves, the wavelength of absorption is feature of a group of atoms. The absorption generated by group of atoms is entitled as **Chromophore**. The actual energy and intensity of absorption are considered to change according to the structure changes take place in a chromophore. As is usual the case, the prediction of absorption with the structure modification of chromophore is too difficult to implement, hence empirical guidelines are becessary to be taken into the prediction of relationship.

Table 4.3: Typical Absorption of Isolated Chromophore [52]

| Class | Transition | $\lambda_{max}(nm)$ | log | Class | Transition | $\lambda_{max}(nm)$ | log |
|---|---|---|---|---|---|---|---|
| R——OH | $n \longrightarrow \sigma^\star$ | 180 | 2.5 | R——$NO_2$ | $n \longrightarrow \pi^\star$ | 271 | <1.0 |
| R——O——R | $n \longrightarrow \sigma^\star$ | 180 | 3.5 | R——CHO | $\pi \longrightarrow \pi^\star$ | 190 | 2.0 |
| R——$NH_2$ | $n \longrightarrow \sigma^\star$ | 190 | 3.5 | | $n \longrightarrow \pi^\star$ | 290 | 1.0 |
| R——SH | $n \longrightarrow \sigma^\star$ | 210 | 3.0 | $R_2CO$ | $\pi \longrightarrow \pi^\star$ | 180 | 3.0 |
| $R_2C$══$CR_2$ | $\pi \longrightarrow \pi^\star$ | 175 | 3.0 | | $n \longrightarrow \pi^\star$ | 280 | 1.5 |
| R——C≡≡C——R | $\pi \longrightarrow \pi^\star$ | 170 | 3.0 | RCOOH | $n \longrightarrow \pi^\star$ | 205 | 1.5 |
| R——C≡≡N | $n \longrightarrow \pi^\star$ | 160 | <1.0 | RCOOR$'$ | $n \longrightarrow \pi^\star$ | 205 | 1.5 |
| R——N══N——R | $n \longrightarrow \pi^\star$ | 340 | <1.0 | $RCONH_2$ | $n \longrightarrow \pi^\star$ | 210 | 1.5 |

Typical absorption class and peak wavelength of isolated chromophores are illustrated in Table 4.3. It could be observed that, with alternative attachment of substituent groups lead to the position shift and intensity variation of the absorption band of the chromophore. The change does not result from the substituent groups themselves, but the modification due to their presence. The substituent call **Auxochromes** tends to raise the intensity of absorption, and probably the wavelength. There are four categories of influence on absorption due to existence of substituent:

– Bathochromic shift (red shift)   —   a shift to lower energy or longer wavelength.

– Hypsochromic shift (blue shift)   —   a shift to higher energy or shorter wavelength.

– Hyperchromic effect   —   an increase in intensity.

– Hyperchromic effect   —   an increase in intensity [52; 53].

Taking Bathochromic shift for example, increasing the extent of conjugation in a double-bonded system is the suitable approach to the red shift. The chemical compound to be tested is Dimethylpolyenes $(CH_3 - (CH = CH)_n - CH_3)$, with n = 2 plotted as curve A, n = 3 plotted as curve B, and n = 4 plotted as curve C. With the increase length of the conjugated chain, the bathochromic shift could be observed in a series of conjugated polyenes as Figure 4.5. The influence of two chromophores is not only the bathochromic shift, but also lead to the intensity increase of the absorption. Because of the selective light absorption of isolated chromophores resulted from bathochromic shift, the effects are supposed to be put in the prime place [54].
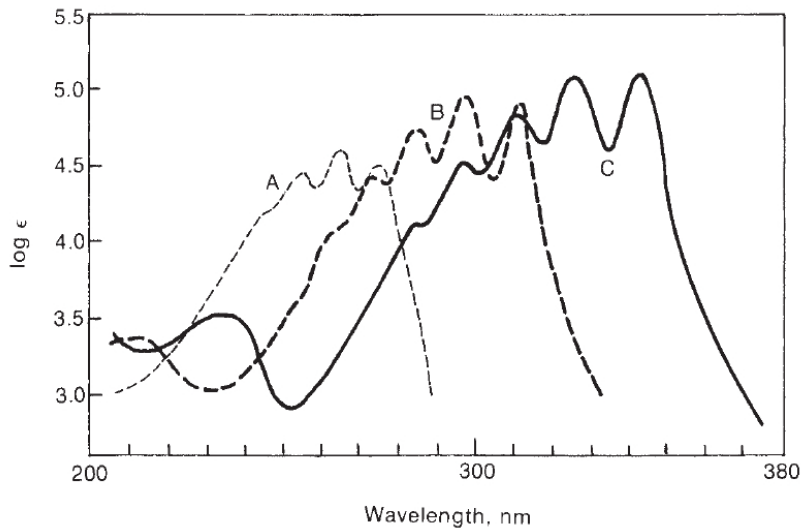
**Figure 4.5:** Ultraviolet Spectra of Dimethylpolyenes [53]

## 4.2 MOLECULAR DYNAMICS RESEARCH ON VIRUS

From the perspective of molecular dynamics, the structure of different categories of viruses are investigated. The research would reveal vulnerable segment in viruses and how UV exposure could lead to lethal effect on them. In this section, the explanation of inactivation mechanism of virus at a certain wavelength and exposure dose is given. According to the discussion in Section 4.1, this section would illustrate the probable internal transitions to different component of virus structure.

### 4.2.1 Definition and Properties of Viruses

There are a number of virus exist on earth, a virus is neither organism nor molecule, hence it is important to consider and define what is its nature. The definition of virus is to differentiate virus from bacteria, fungi, algae and protozoa according to their constituent and properties. Viruses could be defined with strictly intracellular and potentially pathogenic entities with an infectious phase, and the following features:

1) **Possessing only one type of nucleic acid**.
   The typical microorganisms include both deoxyribonucleic acid (DNA) and ribonucleic acid (RNA) nucleic acids. As is shown in Table 4.4, the type of nucleic acid is either DNA or RNA. However, evolving from microorganisms, the existence of some common features in viruses, in which case, viruses are considered as a special class of microorganisms.

**Table 4.4:** Organisms, Viruses and Cellular constituents [69]

|  | Organisms | Viruses | Genetic Material | Organelles endowed with genetic continuity |
|---|---|---|---|---|
| Types of nucleic acid | 2 | 1 | 1 | - |
| Multiplying as nucleic acid (Produced from nucleic acid only) | 0 | + | + | 0 |
| Growth and division | + | 0 | 0 | + |
| Presence of Lipmann system | + | 0 | 0 | 0/1 |
| Infectivity | + | + | 0 | 0 |

2) **Multiplying in the form of their genetic material**.
The reproduction integration of typical microorganisms contains ingredients nucleus, cytoplasm, cytoplasmic structures and cortex. When it comes to microorganism, the infecturn is microorganism itself. Considering the particularity of virus, the infecturn is its genetic material.

3) Unable to grow and to undergo binary fission.
The reproduction principle of microorganisms is the replication of genetic material. The virus multiplication process results in the de novo synthesis of viral proteins and genome, while the key factor of microorganisms multiplication is growth, which terminates in binary fission. The replication of genetic material is different from binary fission, viruses produced from nucleic acid only.

4) Devoid of a Lipmann system.
There is a system of enzymes in microorganism, in order to reach the goal of biology synthesis, potential energy is transformed to high energy bonds, which is called "Lipmann system" in microorganism. The lipmann system is absent from viruses, their energy source is the lipmann system of the host cell [55; 56].

According to above properties of viruses, the most significant component of viruses is the multiplication of genetic material for the synthesis of **viral proteins and genome**. In addition, the **host cell** as the energy source is supposed to be stressed.

## 4.2.2 Classification and Structure of Virus

Viruses are living organisms, they never live except when associated with their hosts. With in the same family, viruses could possibly infect a number of hosts, the physical and chemical properties of some viruses are illustrated in Table 4.5, the differences between viruses consist of **DNA or RNA viral nucleic acid, single-stranded or double-stranded nucleic acid, low or high molecular weight of viral nucleic acid**.

Table 4.5: The Physical and Chemical Properties of Viruses

| Virus | Host | Viral nucleic acid | Molecular weight of Viral nucleic acid | A | U or T | G | C | Molecular weight of virus | |
|---|---|---|---|---|---|---|---|---|---|
| MS2 | E.coli CR63 | ssRNA | $1*10^6$ | 23 | 25 | 27 | 25 | $3.6*10^6$ | [57] |
| R-17 | E.coli CR63 | ssRNA | $1.3*10^6$ | 23 | 25 | 26 | 25 | $4.2*10^6$ | [58] |
| fr | E.coli CR63 | ssRNA | $1.2*10^6$ | 24.3 | 23.7 | 27.1 | 24.9 | $4.2*10^6$ | [59] |
| fd | E.coli C | ssDNA | $1.3*10^6$ | 24.4 | 34.1 | 19.9 | 21.7 | $10.8*10^6$ | [59] |
| Vaccinia | Mouse L-60 | dsDNA | $150*10^6$ | 29.5 | 29.9 | 20.6 | 20.0 | $2000*10^6$ | [60] |
| Polio | Hela | ssRNA | $2*10^6$ | 30.5 | 24.8 | 25.5 | 19.2 | $7*10^6$ | [60] |
| EMC | Mouse L-60 | ssRNA | $2.1*10^6$ | 27.3 | 25.3 | 23.5 | 23.5 | $7*10^6$ | [61] |
| Herpes simplex | Hela | dsDNA | $60*10^6$ | 16 | 16 | 34 | 34 | - | [62] |
| Adenovirus | KB | dsDNA | $10*10^6$ | 22 | 21 | 27 | 29 | $200*10^6$ | [63] |

Besides viral nucleic acid, the influence of viral proteins cannot be ignored, which is closely correlated to viral nucleic acid. Capsid is composed of either protein or a lipid membrane and protein, and applied to package nucleic acid. Moreover, viruses are nucleoprotein particles, which are utilized to transfer certain genes between cells of a host and between hosts, viruses cannot live independently, so they would live in their host cell, mutual interactions take place accordingly. There are various viral capsids and encapsulated nucleic acids, according to the type of capsid, viruses are divided into non-enveloped and enveloped ones. The observation of virus depends on their size and complexity of virus capsids, small, non-enveloped, single-stranded, RNA plant viruses are conducive to observation, while enveloped viruses could prevent image observation at the beginning. Enveloped viruses as herpes simplex virus has symmetric nucleoprotein core, as for some virus such as rotaviruses, apart from nucleoprotein core, the virus are enveloped with outer protein instead of lipid shell [64].

This section would take Influenza A and Coronavirus as example, both of viruses are crown-like single-stranded RNA virus as Figure 4.6a and Figure 4.7a. The target virus utilized in inactivation experiments is Influenza A PR8 (A/Puerto Rico/8/1934), the typical structure is shown as Figure 4.6b, which is similar to the experimental virus. From external to internal structure, there are generally two main surface proteins, the hemagglutinin (HA) and the neuraminidase (NA) as spikes of envelope structure, an outer lipid membrane named envelope, matrix penetrate or beneath envelope, and proteins PB1, PB2, PA, NP joined with each RNA segment.
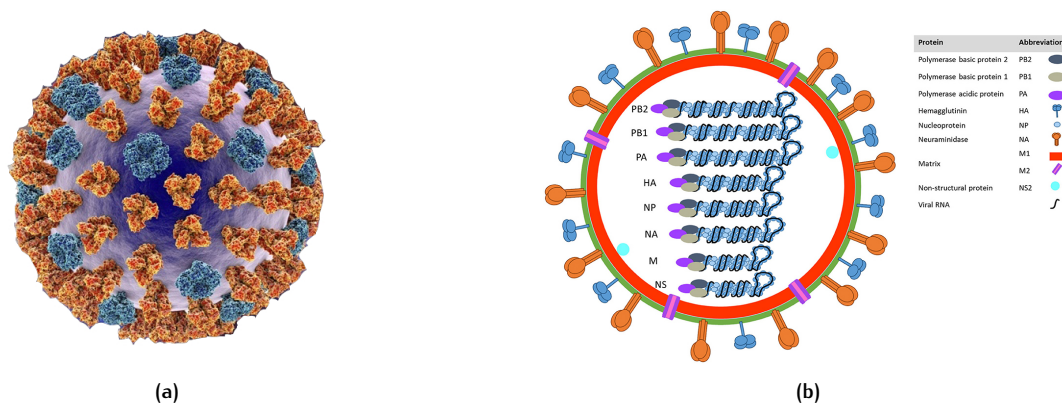


**Figure 4.6:** Model of (a) Influenza A Exterior. (b) Influenza A Virion Structure [67]

The outer envelope determines the binding and release of virus, HA receptor-binding character is the key factor of host range and influenza virus transmission [65]. According to antigenic properties, HA and NA are applied for virus classification. Theoretically, the components of virus consists of a negative sense RNA genome, encoding with eight RNA segments, the fourth segment of RNA codes for hemagglutinin, the eighth segment of RNA encodes NS1 protein, other proteins of corresponding RNA segments are shown in the figure [66]. Because of the presence of eight independent RNA segments in virus, infecting host cell with two or more viruses at the same time leads to the gene combination of parental viruses [67].

The SARS-COV-2 is another enveloped, single-stranded crown-like RNA virus as Figure 4.7b, with a single linear RNA segment. On the surface of the enveloped virus, glycoprotein serves as spikes. The nucleocapsid is composed of protein shell, envelope small membrane protein and membrane protein. The internal structure of Coronavirus includes nucleoprotein and genomic RNA. As it could be translated into a viral protein, it is considered to be a positive-sense virus. Since the virus is originated from animal reservoir, and there are genetic changes in virus, SARS-COV-2 could infect humans undoubtedly [68].
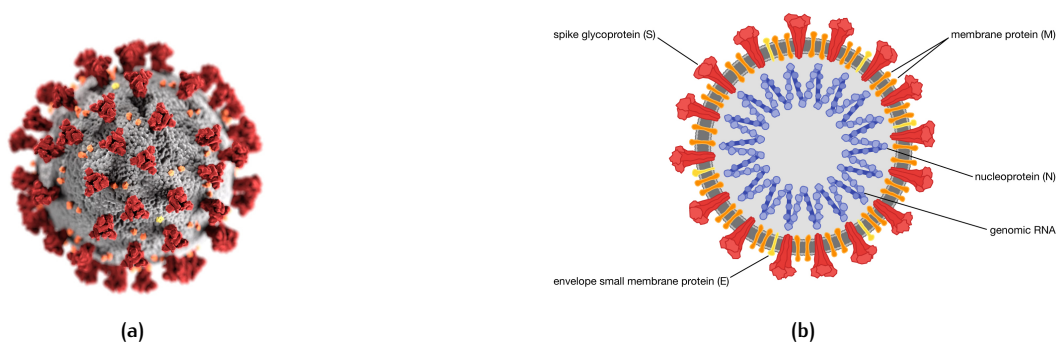


**Figure 4.7:** Model of (a) Coronavirus Exterior. (b) Coronavirus Structure [68]

Since then, the RNA segments and correspondent proteins are supposed to be paid attention to. Also, hemagglutinin and receptor binding mechanism of Influenza A results in the virus transmission, which indicates the influence of some protein of specific virus plays the key role on virus transmission. However, the structure, property and effect of protein varies a lot between different viruses, hence corresponding structure break and disinfection mechanism diverges accordingly. Moreover, structures of RNA segment are different between Influenza A virus and Coronavirus in above case, their molecular weight of viral nucleic acid are also inconsistent, in which case, the complexity of virus DNA or RNA is supposed to be taken into consideration of virus disinfection as well.

### 4.2.3 Inactivation Mechanism Research on the viral molecule

Previous sections introduce Absorption Spectroscopy, Molecular Electronic Transition, Virus Properties and core Genetic Material. The Absorption Spectroscopy would tell the molar absorptivity with corresponding wavelength, the absorbed energy could excite electrons from ground state to excited state, transitions from the highest occupied molecular orbital (HOMO) to lowest unoccupied molecular orbital (LUMO). In a specific virus particle, the genetic material, especially nucleic acids and viral proteins are vulnerable to UV exposure, leading to lethal structural break and replication failure. This section would illustrate the transformation and difference of virus structure result from UV exposure.

$$\frac{n}{n_0} = e^{-\sigma D} \tag{4.5}$$

Equation 4.5 indicates the relationship between virus titer and exposure parameter, n is the original titer of virus, and $n_0$ is titer after exposing to dose D, $\sigma$ represents the constant which is proportional to specific virus at particular wavelength, refers to a **cross-section**, and has dimension of $cm^2$ per photon. D is supposed to be explained with units of photons per $cm^2$ [69]. Therefore, exposure wavelength and exposure dose are the key factors of virus inactivation.

The cross-section is to measure the possibility of particle-particle interaction, which is electromagnetic absorption. Cross-section in terms of dimensions of the virus is applied to represent relative probability of a photon causing virus inactivation, absorption cross-section $\sigma$ is calculated as Equation 4.6, where $\alpha$ is **Absorption Coefficient**, n is the atomic number density [70].

$$\sigma = \alpha/n \tag{4.6}$$

Maini, Anil K states that at a given wavelength, absorption coefficient is determined by **Concentration and Molecular Cross-section** of chemical species in the tissue. For different tissues, the absorption spectrum varies because absorption depends on incident wavelength. Proteins have strong absorption in ultraviolet region of electromagnetic radiation, the protein absorption capability declines with the increase of wavelength, while haemoglobin becomes dominant absorber at increased wavelength. Overall, the Cross-section depends on constituents absorption, protein, oxyhemogobin and water result in the absorption of wavelength in ultraviolet, visible and infrared bands with various absorption coefficient. The concentration of constituents would influence absorption coefficient as well [71].

As is clarified in virus structure, proteins are not the unique genetic material, viral nucleic acid is of great significance as well. Whether viruses are DNA or RNA viral nucleic acid, single-stranded or double-stranded nucleic acid, low or high molecular weight of viral nucleic acid would influence the susceptibility to UV exposure. The cross-section as a measure of the probability of virus inactivation, which is measured and plotted as function of wavelength, representing action spectra for viruses as Figure 4.8 with similar shape. Within the range, there are two peak cross-section for each virus, one below 2300, the other one is around 2700, indicating the feature of UV inactivation probability as a function to wavelength.
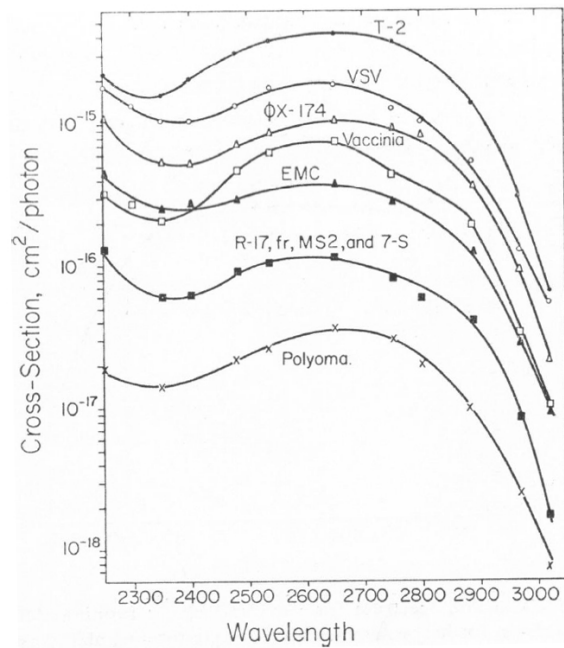
**Figure 4.8:** The UV action spectra for viral plaque-forming ability for viruses [69]

**Cross-section** $\sigma$ suggests the probability that a photon could result in virus inactivation, the measure of the possibility that a photon would be absorbed in a virus is **Absorption Cross-section** S, in which case, **Quantum Yield** $\phi$ can be calculated as Equation 4.7.

$$\phi = \frac{\sigma}{S} \tag{4.7}$$

$\phi$ is the quantity to evaluate **viral sensitivity to ultraviolet light** [69]. Some of the factors are related to the sensitivity are illustrated:

1) Stranded State on relative Quantum Yield

According to the statistics in Table 4.6, which indicates the relative quantum yield for single-stranded viruses and double-stranded viruses. As claimed by table, $\phi$ for single-stranded nucleic acids is at least ten times more sensitive to ultraviolet exposure than that of double-stranded nucleic acids. Virus fd is the DNA virus seems to be an exception with large quantum yield, while it could result from the difference between RNA and DNA viruses, dsRNA viruses are relatively 3 times more sensitive to UV than which of ssRNA viruses. Therefore, generally speaking, single-stranded viruses are susceptible to ultraviolet light than double-stranded viruses, RNA viruses are more vulnerable to ultraviolet exposure than DNA viruses.

**Table 4.6:** Relative Absorption Cross-section and Quantum Yield for Viruses [69]

| Virus | Viral nucleic acid | Viral absorption cross-section S ($cm^2/photon * 10^{14}$) | Viral inactivation cross section $\sigma$ ($cm^2/photon * 10^{16}$) | Relative quantum yield $\phi$ |
|---|---|---|---|---|
| MS2 (R-17, fr) | ssRNA | 8 | 1.1 | 14 |
| EMC | ssRNA | 13 | 3.5 | 27 |
| Polio | ssRNA | 15 | 3.5 | 23 |
| fd | ssDNA | 10 | 7.8 | 78 |
| Vaccinia | dsDNA | 980 | 6.5 | 0.7 |
| Herpes simplex | dsDNA | 380 | 4.6 | 1.2 |
| Adenovirus | dsDNA | 65 | 0.2 | 0.3 |

2) Stranded State on shape of Action Spectra

When individuals are vulnerable to infections, basic reproduction ratio represents the amount of cases that expected to appear as a result of individual infection [72]. As is illustrated in Table 4.7, ratio R is around 2.0 for double-stranded viruses, and approximately 1.0 for single-stranded viruses. The variance of ratio R could result from the Action Spectra shift, and could be explained with viral protein drives single-stranded nucleic acid become sensitive to ultraviolet exposure [69].

Table 4.7: Ratio R of the Inactivation Cross-section [69]

| Single-stranded Virus | Viral nucleic acid | R | Double-stranded Virus | Viral nucleic acid | R |
|---|---|---|---|---|---|
| MS2 | RNA | 0.9 | Vaccinia | DNA | 2.3 |
| R-17 | RNA | 0.9 | T-2 | DNA | 2.0 |
| EMC | RNA | 0.85 | Reovirus-3 | RNA | 0.3 |
| fd | DNA | 1.5 | Polyoma | DNA | 2.0 |

3) Role of Protein on viral sensitivity to UV

Viral protein absorbs most of photons especially in low wavelength range, hence the proteins of viruses are relatively more sensitive to ultraviolet exposure than nucleic acid [69]. Spectral Sensitivity of MS2 RNA damage measured with Polymerase chain reaction (PCR) is revealed as Figure 4.9, the RNA absorption of UV reaches the highest point at 260nm, and drops when decreasing to 240nm, while turning to increase with even lower wavelength. Therefore, there must be non-genomics damage existing below 240nm. Proteins are the potential better absorber of ultraviolet exposure at wavelengths below 240nm, and transfer energy to genome or extend damage to RNA in the case of MS2 genome [73]. The spectral sensitivity of MS2 reveals the probability that protein plays a significant role on virus inactivation. The mechanism of protein damage is much more complicated than what is stated at present, which would be discussed in the following section.
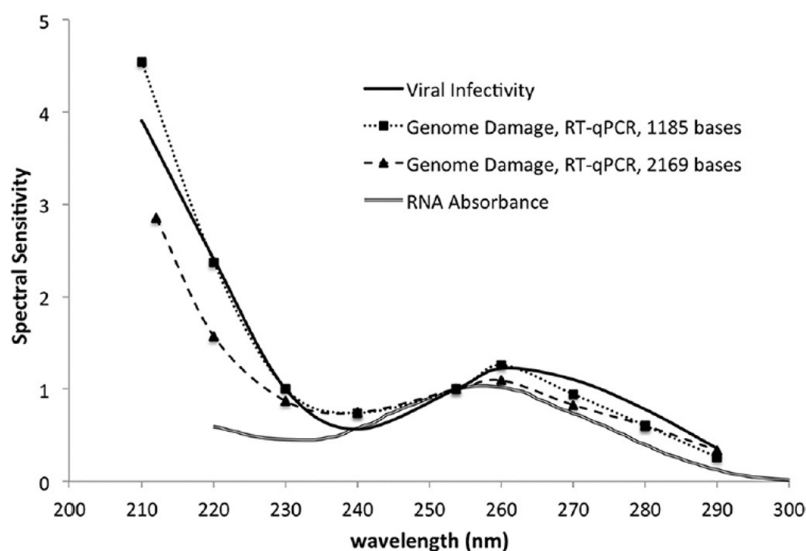


Figure 4.9: Spectral sensitivity of MS2 genome [73]

4) Host Cell Effects

Different from viruses in experiment condition for inactivation, viruses are living in host cells. The host cells are capable of modifying UV damage in infectious viruses, the mechanism is UV lesions repair by host cell enzymes [69], which would be further explained. As is indicated

that, the role of DNA repair capacity (DRC) is significant to genetic susceptibility, the relationship between three DNA repair genotypes and repair phenotype of ultraviolet-induced damage is on the way to be investigated [74].

Based on above viral sensitivity analysis, the factors could be divided into two categories, damage and repair. Ultraviolet exposure causes **photochemical damage** to viral nucleic acid and proteins, while host cell effects would repair UV damage to some extent. Some repair mechanisms would be illustrated, while remaining discussion places emphasis on ultraviolet damage to virus. For instance, Ultraviolet-induced photoproducts, cross-links and oxidation damages are miscellaneous DNA damage, which could be removed by nucleotide excision repair (NER), which is a particularly important DNA repair mechanism that removes DNA damage caused by ultraviolet light [75; 76]. Moreover, organisms have evolved with a number of repair mechanisms, including NER, base excison repair (BER) and mismatch repair (MMR) [77]. The following discussion would focus on the research on **the role of proteins, viral nucleic acid, and their mutual influence** on virus inactivation.

Beck Sara E. et al illustrated the UV wavelength-dependent damage to protein, taken Adenoviral proteins as example, the research is adopted to stress the variety and complexity of proteins in virus, and their sensitivity to UV exposure. There are different inside proteins, hexon, penton, fiber, minor capsid and core proteins. Also, Influenza A and Coronavirus have different proteins as mentioned in previous section, which reveals potential complicated virus inactivation mechanisms. As is shown in Figure 4.10, the highest sensitivity and greatest damage to viral proteins occur below 240nm, which could potentially explain proteins are better absorber of UV under 240nm. However, genre of proteins is too complex, resulting in tough differentiation. Figure 4.10 illustrates UV sensitivity of different protein relative to 254nm, at UV dose of $28mJ/cm^2$ emitted at 214nm of hexon and penton is around 4 times as much as that of core protein. Moreover, at $28mJ/cm^2$ or $38mJ/cm^2$, UV sensitivity of hexon and penton at 214nm is approximately 4 times as much as the same dose at 254nm [78].

Therefore, UV sensitivity of different proteins at the same wavelength varies, the UV sensitivity of the same protein at different wavelengths diverges as well, which could tell wavelength-dependent damage to proteins is too complicated to figure out because of too many protein genres even in one virus, UV sensitivity of proteins below 240nm are generally higher than that of proteins above 240nm, and has a tendency to increase below 240nm.
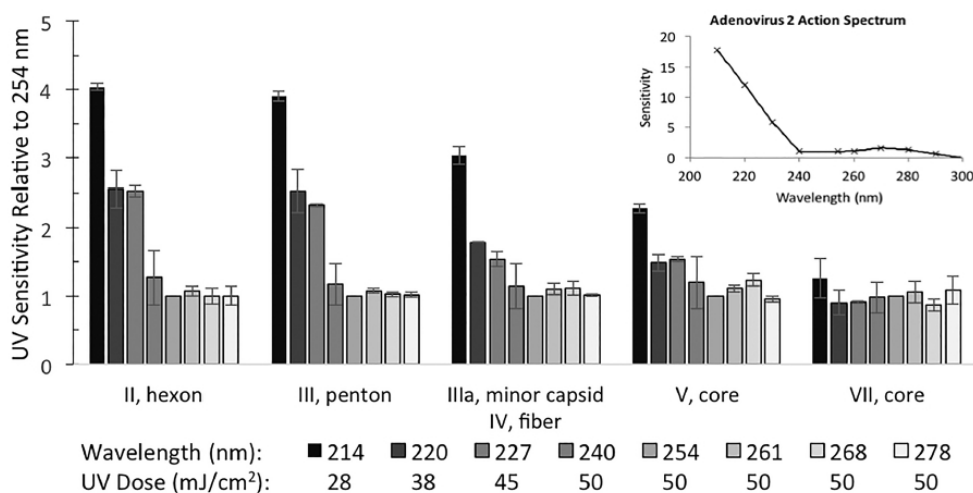


**Figure 4.10:** Sensitivities of HAdV2 proteins across the germicidal UV spectrum relative to their sensitivities at 254 nm in comparison to the HAdV2 action spectrum [78]

Sara E. Beck et al. suggest that RNA damage in MS2 as a function of germicidal curve spectrum could be applied to analyze UV-Induced Inactivation. MS2 coliphage is composed of a single-stranded RNA core with a protein capsid, in which case, the inactivation of MS2 definitely results from damage to proteins, damage to viral nucleic acid, or their mutual effect. According to Figure 4.9, Viral Infectivity curve reveals that the genome damage is the dominant factor leading to the UV inactivation of MS2 because of the similarity between infectivity curve and genome damage curve. Table 4.8 illustrates the statistics of UV wavelength, RNA damage and infectivity. The most efficient UV wavelength range as measured with RNA damage parameter is around 253.7nm and 260nm in the current research. Moreover, the table reveals the relationship between RNA damage and Infectivity, the rates of RNA damage reflects the loss of viral infectivity, the greater the RNA Damage, the greater the Viral Infectivity is [78]. It was analyzed that the vulnerability of MS2 RNA towards UV exposure is close to the susceptibility of MS2 coliphage itself to UV, in which case, **the dominant damage of MS2 is UV exposure damage to RNA structure**, leading to the infectivity of MS2 [73].

Table 4.8: Wavelength-specific MS2 RNA Damage (measured with the 2169 based region) [78]

| Wavelength $\lambda(nm)$ | RNA Damage k $(mJ/cm^2)$ | Infectivity $(mJ/cm^2)$ |
|---|---|---|
| 210 | 0.176 | 0.203 |
| 220 | 0.085 | 0.136 |
| 230 | 0.051 | 0.065 |
| 240 | 0.046 | 0.034 |
| 253.7 | 0.058 | 0.050 |
| 260 | 0.061 | 0.070 |
| 270 | 0.051 | 0.059 |
| 280 | 0.035 | 0.043 |
| 290 | 0.021 | 0.020 |

However, RNA absorbance of MS2 is divergent from the tendency of viral infectivity below 240nm while viral infectivity rises drastically, which reveals that UV exposure is absorbed by other viral structural, leading to high viral infectivity. The potential explanation is the UV energy absorbed by viral proteins are transferred to RNA structure, resulting in RNA damage and loss of viral infectivity [79]. The generated site-specific **RNA damage by protein absorption** results in **RNA-protein cross-links** or single-strand breaks [80]. MS2 is taken as an example to illustrate the role of viral nucleic acids, proteins in UV exposure inactivation. In order to explore the DNA/RNA damage due to UV absorption, emergence of cross-links is supposed to be put in the first place.



(a)  (b)
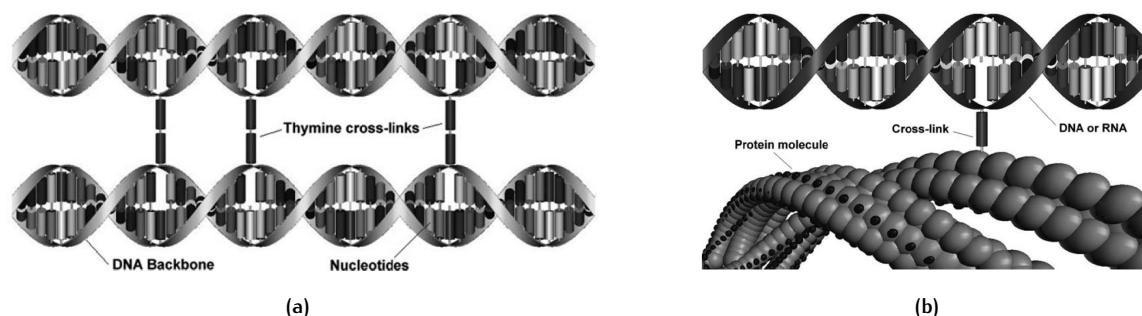
Figure 4.11: Cross-links between (a) thymine nucleotides of adjacent strands of DNA or uracil nucleotides of adjacent strands of RNA (b) the DNA (RNA) and the adjacent protein molecules, such as cell cytoplasm or the capsid [81]

### 4.2.4 NABs Absorption Spectrum

There are several categories of cross-links, between nucleic acids, or between nucleic acid and protein. Typically, Thymine, Cytosine, Adenine, and Guanine, four nucleic acid bases in Deoxyribonucleic acid (DNA). In Ribonucleic acid (RNA), Thymine is substituted with Uracil nucleic acid bases. Take DNA as example, cross-links could exist between nuclec acids, such as adjacent thymines or non-adjacent thymines as Figure 4.11a, or between DNA (RNA) structure and adjacent protein molecules in Figure 4.11b [81]. Study of protein association of DNA reveals protein-associated DNA is more vulnerable to UV exposure damage than isolated DNA [82]. Therefore, the influence of protein is hard to be ignored, however, there are various types of proteins exist in viruses, leading to complicated inactivation mechanism, the following discussion would put the inactivation mechanism of viral nucleic acid in the first place.
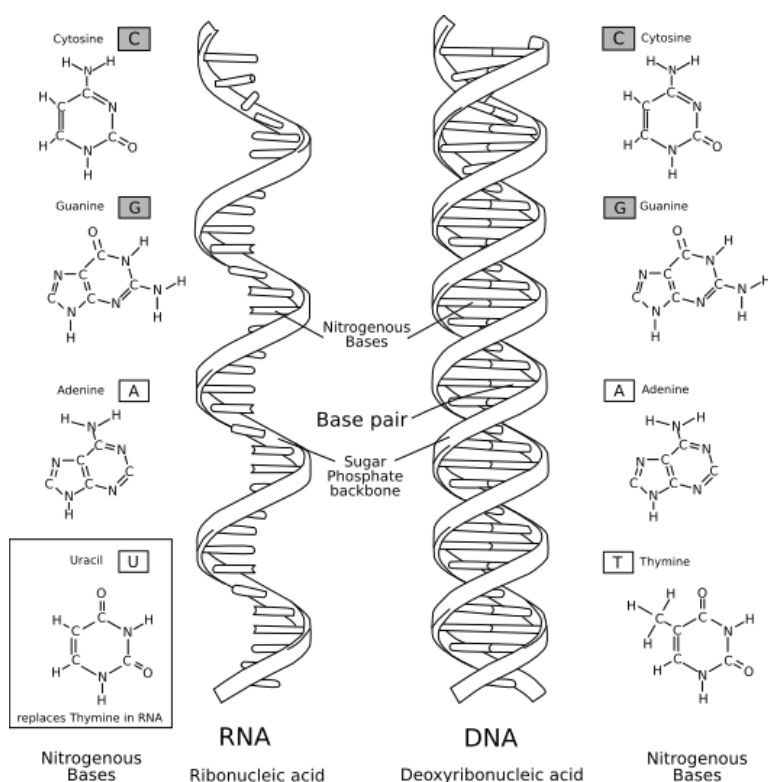


Figure 4.12: Structure of DNA/RNA and Nitrogenous Bases [83]

The consistent DNA or RNA structure in virus as shown in Figure 4.12 are responsible for storing genetic information, synthesizing proteins and reproduction. Based on the sugar phosphate backbone, Purines with double-ring structures include Adenine and Guanine in both DNA and RNA structure. Pyrimidines with single-ring structures consist of Cytosine and Thymine in DNA, while Uracil replaces Thymine in RNA [84].

As mentioned, cross-links could exist in viruses, which could result from UV wavelength inactivation. The **UV energy absorption** is the direct cause of intrastrand cyclobutyl-pyrimidine **dimers**, leading to genetic mutations or cell death [85; 86; 87]. In DNA, thymine dimers are the dominant dimers caused by UV exposure. As Figure 4.13, due to UV absorption, between adjacent nucleotides, cross-links between thymines and thymine dimers formed, so do non-adjacent nucleotides. Apart from thymine dimers, photo-products also include cytosine dimers formed in DNA, contributing to virus structural defects, incapable of reproduction and cell death [88].
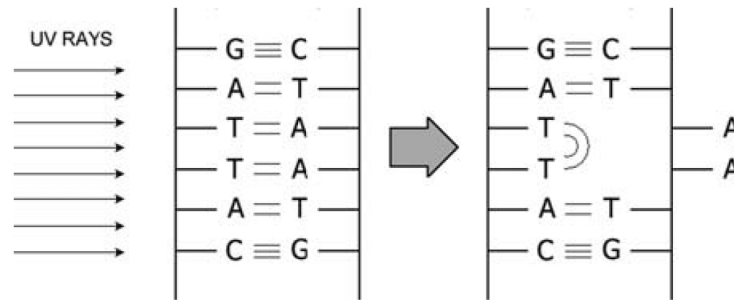
**Figure 4.13:** Thymine dimers caused by UV absorption in adjacent nucleotides [81]

When correlated with time, the formation of dominant uracil dimers in RNA of mengovirus remained steady while virus infectivity decreases drastically in Figure 4.14. Therefore, as a matter of fact, few cross-links are responsible for the inactivation of virus. In addition, the inactivation rate of each microorganism has own relationship with dimerization probability. At the beginning of exposure, uracil dimers formed, which is correlated with infectivity, forming covalent bonds between cysteine and the uracil in RNA. Formation of photoproducts due to structural modification of capsid proteins slower than formation of dimers, which could depends on the formation of covalent linkage between viral proteins [89].
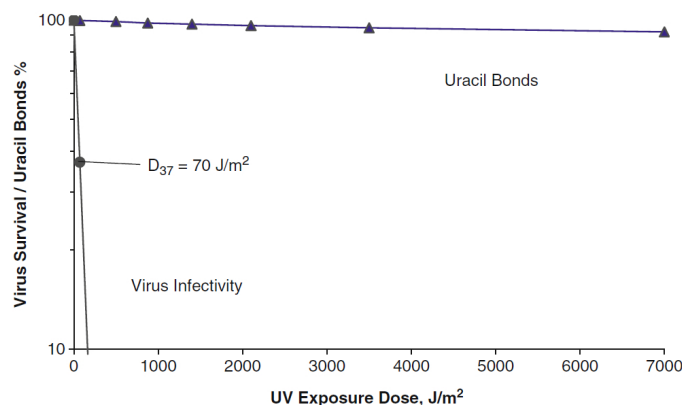


**Figure 4.14:** Effects of UV irradiation on Infectivity and on formation of Uracil Bonds in viral RNA [89]

From the perspective of absorption spectra, the spectra of DNA or RNA structure is the total of the solitary absorption band of each nucleotide, leading to the electronic transition of each molecule. When the absorbed UV energy satisfy the energy gap between molecular orbitals, the energy of electron is raised from ground state to excited state [90].

Microsystems as nucleic acid bases governed by $\pi$ electrons have absorption spectra resulting from $\pi \longrightarrow \pi^\star$ transitions in ultraviolet wavelength band, especially UV-C band and vacuum ultraviolet region from 100nm to 280nm. There are five nucleic acid bases, adenine, guanine, cytosine, thymine, and uracil, the optical absorption spectra measurement of sublimed films of five nucleic acid bases from 120nm to 400nm is shown as Figure 4.15. At room temperature, the measurements of optical absorption were implemented with spectrophotometer, dotted lines represent values obtained from direct reading, solid lines represent values corrected for light scattering but in similar shape [91].
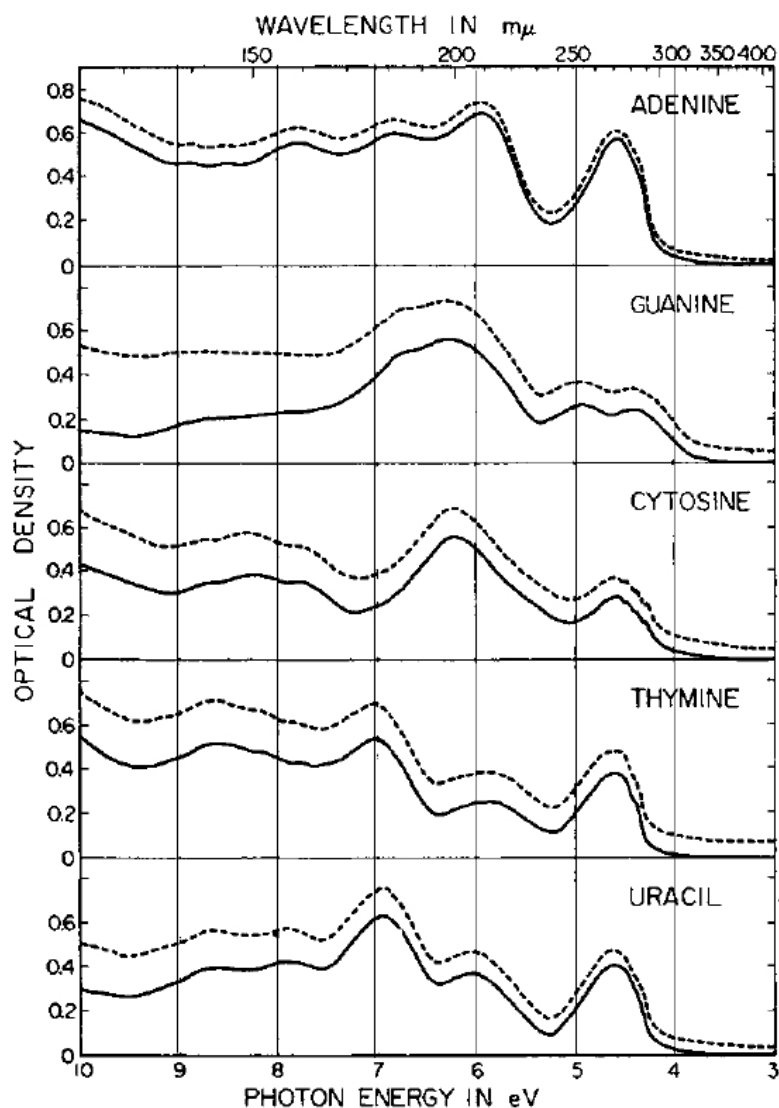
**Figure 4.15:** Absorption Spectrum of nucleic acid bases, dotted lines represent values obtained from direct reading, solid lines represent values corrected for light scattering [92]

Each absorption spectrum of five nucleic acid bases has its **absorptive capacity** and characteristic over specific electromagnetic wavelength range or peak wavelength as Table 4.9, the intensity of absorption, absorbance is described as optical intensity in Figure 4.15, which generally have peak absorbance in UV-C range, around 200nm and also below 200nm, thymine and uracil have peaks close to 265nm [92].

According to Table 4.9, generally, Quantum Yield of Pyrimidines as Cytosine, Thymine and Uracil is more than 10 times as much as that of Purines as Adenine and Guanine, and the UV absorption of Pyrimidines is more than 10 times of Purines [93]. The electronic configuration and available higher energy state of molecule at certain wavelength are responsible for the absorption capacity [94]. Section 4.1.2 illustrates Molecular Electronic Transition, in which case, only if the absorbed quantum of energy satisfy the difference of discrete energy states, these transitions have the probability to occur. Moreover, strong UV absorption wavelength region is related to the molecular structure,

Table 4.9: Positions of the Absorption Peaks and Quantum Yield of Nucleic Acid Bases [92]

| Nucleic Acid Bases | Absorption Wavelength Peaks $\lambda(nm)$ | Fluorescence Quantum Yield ($\times 10^4$) |
|---|---|---|
| Adenine | 269-272; 210; 182; 160; 145; 140 | 2.6 |
| Guanine | 282-289; 246-251; 198-200; 185; 155; 143 | 3.0 |
| Cytosine | 270-271; 199-203; 161; 150; 142 | 1.02 |
| Thymine | 265-270; 211; 176; 160; 152; 144 | 0.82 |
| Uracil | 264-268; 203-205; 178; 157; 144 | 0.45 |

usually contains double bonds. The Pyrimidines and Purines with ring structure manifests especially strong absorption.

### 4.2.5 Nucleic Acid Bases Dimerization

The photodynamics of dimerization is shown as Figure 4.16, there is a single-stranded sugar phosphate back-bone, exposure UV energy is absorbed by cyclobutane-type linkages(ring structures), the bonds between thymines and adenines break down, and double hydrogen bond forms between adjacent thymines. The principle damage to DNA is pyrimidine dimer, under the UV dose of $4.5 J/m^2$, 50000 pyrimidine dimers could generate per cell [95].
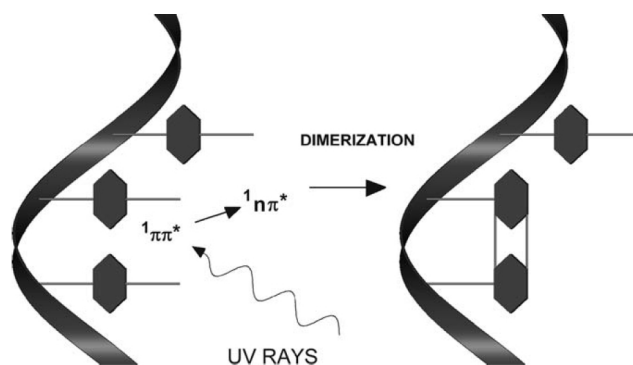


Figure 4.16: The photodynamics of dimerization [82]

UV exposure also gives rise to damage to nucleic acids in RNA, taking photo-dimerization of uracils as example, cyclobutane-like linkages after UV exposure is shown as Figure 4.17, the structure of sugar is not included because photodimerization dominantly takes place in remaining structure. Photo-dimerization results from UV damage mostly takes place with neibouring pyrimidines (sequentially bases YY = UU, CU, UC and UU) connecting with cyclobutane-type linkages [96].
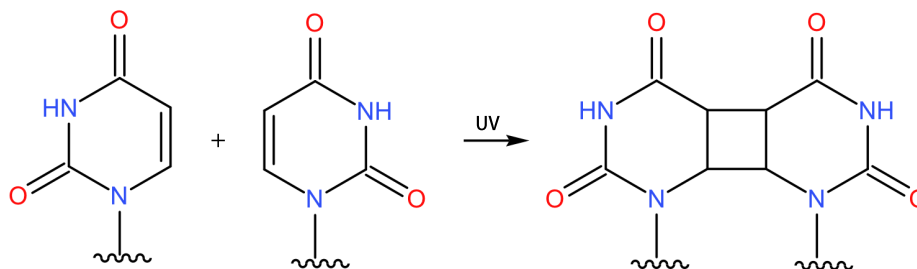


Figure 4.17: Cyclobutane dimerization product of two uracil bases initiated by UV absorption

The cross-links between uracil nuceotides and photo-dimerization between uracils give rise to the inactivation of RNA viruses [89]. The chemical model of photo-dimerization and cyclobutane-like linkages could also be observed through Figure 4.18, the transformation of cyclobutane-type linkages (ring structures) could be observed.
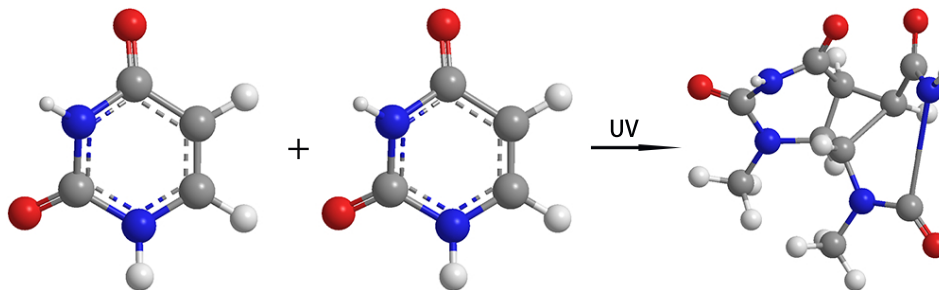


**Figure 4.18:** Photo Dimerization Chemical Model

As the experimental virus is single-stranded RNA virus, the research would focus on reactivity of dinucleotide in RNA. According to Figure 4.19, the frequency of sequence doublets is shown as a function of UV reactivity. The sequence in RNA could be covalently modified by UV exposure is a pyrimidine with a subsequent purine, and the histograms of less reactivity are AA, AU and UU.
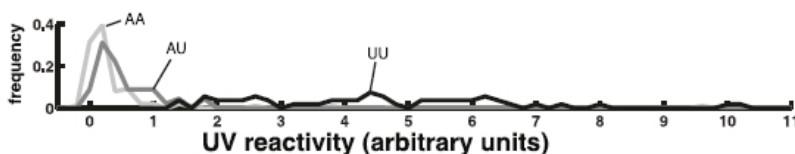


**Figure 4.19:** Histograms of UV reactivities at AA, AU, and UU sites from RNAs [96]

It could be observed from Figure 4.20 that the median and range of sequence doublets. Dinucleotides with great UV reactivity are among pyrimidines, such as UU, UC, CU and CC, and the one with highest UV reactivity is UU dinucleotide, most extreme data even beyond the interquartile range. The four doublets would be responsible for the UV-induced damage as **cyclobutane-type photo-dimers** in Figure 4.17. Alternatively, non-YY sequence may not lead to cyclobutane-type photo-dimers, which might due to transient contacts of base pairs [96].
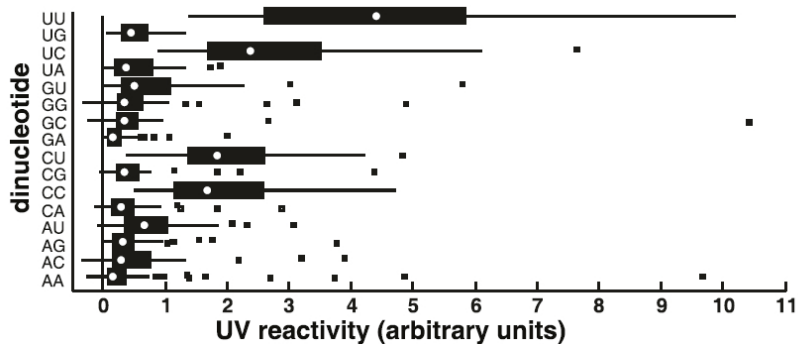


**Figure 4.20:** Box plot of reactivities across all dinucleotide types [96]

### 4.2.6 Internal Conversion Mechanism

Ultroviolet induced formation of **Cyclobutane Pyrimidine Dimers (CBPyr or Pyr<>PYr)** include Cyclobutane thymine dimer, Cyclobutane uracil dimer and Cyclobutane cytosine dimer by pairing of adjacent pyrimidine nucleobases sequentially. In between, thymine dimerization has been verified by **Femtosecond Spectroscopy** to that it could completely formed around 1 ps after UV exposure. In theory, an energy-degenerate structure between excited (S1) and the ground state (So), named Conical Intersection (CI) is the cause of ultrafast nonadiabatic photoreaction of thymine and cytosine dimers [97]. The energy transfer process of regarding molecule would be discussed.

From the perspective of molecular UV absorption and electronics transitions, the **ultrafast decay** of Nucleic Acid Bases (NABs) is based on Fluorescence decays and State Transition. The lifetime and transition of NABs excited state $S_{\pi\pi^\star}$ could be monitored by the Transient Absorption (TA) band Fluorescence Upconversion (FU).
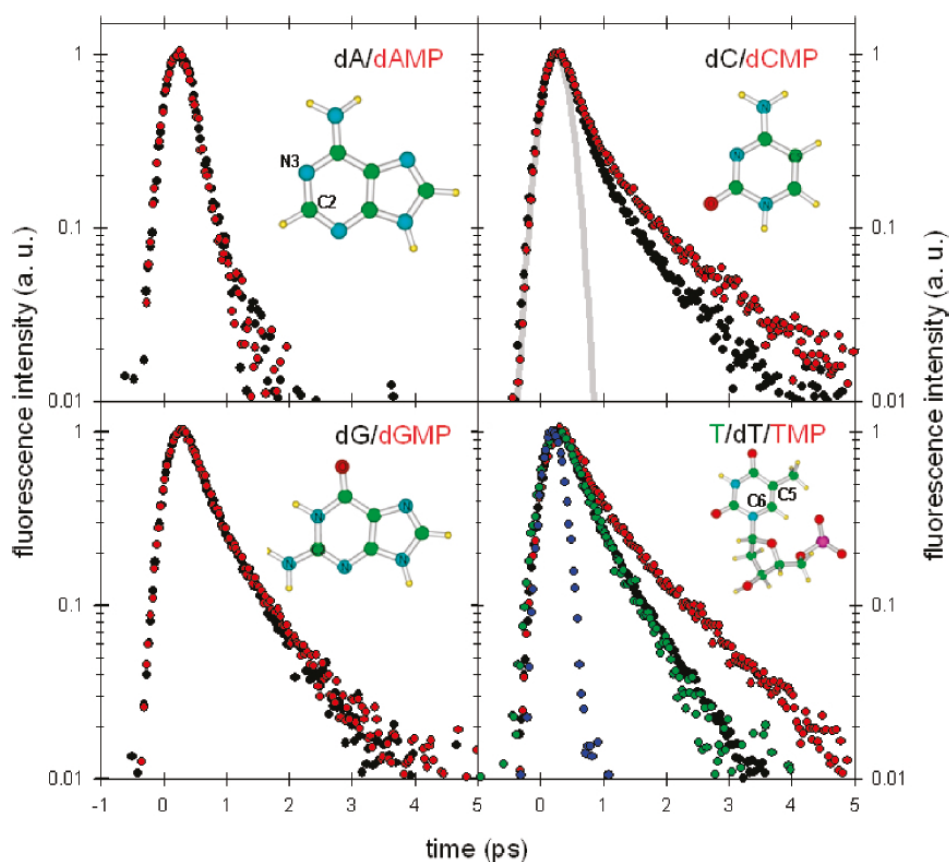


Figure 4.21: Fluorescence decays for the four nucleosides and nucleotides.The average lifetimes are 0.13/0.13 ps (dA/dAMP), 0.30/0.45 ps (dC/dCMP), 0.33/0.34 ps (dG/dGMP), 0.30/0.32/0.50 ps (T/dT/TMP), and <0.1 ps (U). [99]

**Internal Conversion** of general nucleoside induced Excited state decay takes place from excited state to electronic ground state in hundreds of femtoseconds [98]. The excited state decay is demonstrated as Figure 4.21, including fluorescence intensity of eight nuceosides and nucleotides. Nucleotide is composed of nuceoside and the phosphates, five nucleotides are denoted as (d)AMP, (d)GMP, (d)CMP, (d)TMP, and UMP, shown in red, while nucleosides shown in black. Particularly, thymine is shown in green, and uracil in blue. The study illustrates that the excited state decays of all NABs

are smaller than 1 ps. Overall, uracil owns the shortest decay time 0.1 ps, subsequently adenine decays in 0.13 ps, and guanine has the longest decay time 0.33 ps [99]. However, ález-Ramírez et al. proposes that some long-lived excimer decays to the ground states in more than 10 ps [100].

In addition, Figure 4.21 reveals the structure of adenine, cytosine, guanine, and thymidine monophosphate. As for purines, the twisting around C2 - N3 bond of Adenine induced the out-of-plane substituent bending in the reaction path. When it comes to pyrimidines, pyramidalization of C5, torsion of the C5 - C6 bond, as well as the out-of-plane movement of 5 substituent are involved in the internal conversion through **Conical Intersections** (CI) [99].

The existence of CI connection, which is a highly efficient Internal Conversion between excited state $S_{\pi\pi^*}$ and ground state $S_0$, leading to the ultrafast decay of the first singlet excited state $S_{\pi\pi^*}$. Specifically, there is a **Franck-Condon region** of uracil illustrated in Figure 4.22, which originates from initial flat structure, leading to the almost planar pseudo-minimum region. The particular reason for the ultrafast decay is the barrierless path connecting Franck-Condon region and Conical Intersection with ground state theoretically [101]. Afterwards, an out-of-plane deformation (pyramidalization) takes less than 100 fs to propel the structure to conical intersection in order to reach ground state. The internal conversion drives C5 in planar structure to perpendicular configuration [99].
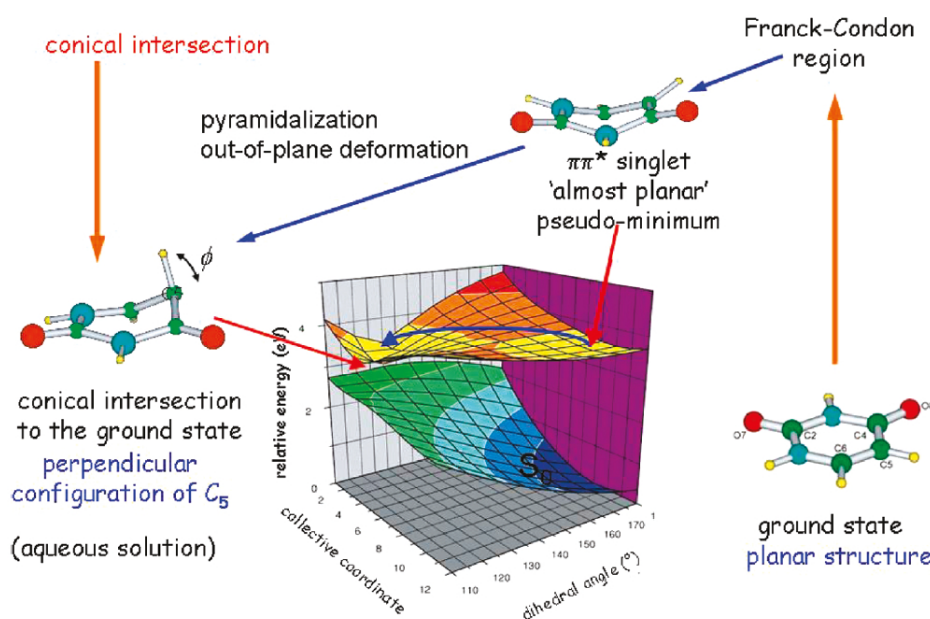


**Figure 4.22:** State evolution of uracil $S_{\pi\pi^*}$ excited-state dynamics in solution [99]

Apart from the ultrafast decay $S_{\pi\pi^*} \rightarrow S_0$, there is also a dark excited state $S_{n\pi^*}$ which has close energy level to $S_{\pi\pi^*}$, leading to $S_{\pi\pi^*} \rightarrow S_{n\pi^*}$ population transfer. Decay component of $S_{n\pi^*}$ measured with transient absorption is around 25 ps, which is highly dependent on environment, influencing the excited state dynamics of NABs [102]. For example, excited state lifetime of thymine in water is 0.39 ps, and drops to 0.24 ps in acetonitrile [103; 104].

The fluorescence decay of dGMP has been discovered to be strongly dependent on wavelength as reference to Figure 4.23, it takes longer decay time when wavelength shifts towards red. Out-of-plane deformation from plannar structure to flat planar pseudominimum region takes less than 100 fs to propel the structure to conical intersection. The theoretical excited state surface is almost flat as

a function of reaction coordinate toward CI, wavepacket dynamics movement from the same excited state energy potential level to ground state is shown to be wavelength dependent. Also, the excited state dynamics of other NABs depends on $S_{\pi\pi^*}$ energy surface between planar and non-planar structure [105].

As far as is been concerned, the ultrafast decay process of NABs excited state inactivation mechanism is indivisible related to wavelength, dark excited state, solvent (surrounding), potential energy surfaces and differences between NABs. Besides, recent researches reveal the characterization of a state of thymine and thymidine formed after 10 ps of excitation, named triplet state, which would be taken into subsequent discussion [106].



**Figure 4.23:** Wavepacket dynamics on excited-state potential energy surface [98]

In the triplet excited state of pyrimidine nucleobases (cytosine, uracil and thymine) pairs, the UV light induced CBPyrs has been learned through quantum-chemical CASPT2 studies. As mentioned, from the original monomer nucleobase excited state to the ground state photoproduct CBPyrs, mediated with nucleobases triplet state, photo-product formation is done through successive **Intersystem Crossing (ISC)** processes [107]. As shown in Figure 4.24, $C_5 - C_6$ and $C_{5'} - C_{6'}$ bonds laid parallelly in homodimer photo-products, which is attributed to barrier-less path from irradiated singlet state to CI structure (mention in Figure 4.22).



**Figure 4.24:** Structures and labeling of the DNA/RNA CBPyr homodimer photoproducts [97]

The bonds are elongated during efficient internal conversion process, connecting singlet excited state and ground state and leading to photoproduct formation. By different ISC mechanisms, the ultrafast singlet mediated internal conversion contributes to triplet state of nucleobases. By **triplet - triplet energy transfer (TET)**, CBPyer adducts formed on the basis of nucleobase photosensitization. The experimental and computational triplet excited state energy are illustrated in Table 4.10.

Table 4.10: Experimental and Theoretical Energies (eV) for Triplet Excited State (T1) of Pyrimidine Nucleobases [97]

|  | monomer | | dimer | monomer |
|---|---|---|---|---|
|  | $E_{VA}$ (eV) | $T_e$ | $T_e(T_1/S_0)_x$ | $Exp$ |
| cytosine | 3.66 | 2.98 | 2.70 | 3.50 |
| uracil | 3.8 | 3.15 | 2.47 | 3.65 |
| thymine | 3.59 | 2.87 | 2.36 | 3.60 |

Description of each parameter is shown as Table 4.11, $Exp$ corresponds to the value of $E_{VA}$ approximately, and the experimental triplet state energy is colsely to 3.5 - 3.65 eV [108; 109]. As for both singlet-triplet excitation energy and adiabatic transition $T_e$, the uracil owns the highest energy, 3.8 eV for $E_{VA}$, and 3.15 eV for $T_e$, following cytosine and thymine. Considering the complexity of biological environment, values of adiabatic band origin transitions are not representative enough.

Table 4.11: Experimental and Theoretical Parameter Description [97]

|  | Description |
|---|---|
| $E_{VA}$ | Vertical singlet-triplet excitation energy at the monomer ground-state Franck-Condon minimum |
| $T_e$ | Adiabatic So-T1 monomer minimum to minimum energy Electronic excitation band origin |
| $(T_1/S_0)_x$ | Adiabatic So-T1 homodimer minimum to minimum energy Lowest-energy singlet-triplet crossing |
| $Exp$ | Experimental monomer singlet-triplet band maxima, Gas-phase electron energy-loss spectroscopy |

Due to the excited state, excimer stabilization is undergone, following with formation of biradical **stepwise intermediate (SWI)**, a covalent bond between $C_6 - C_{6'}$ is formed between adjacent nuceobases. After the ISC process, SWI intermediate structure is considered as the most probable one to provoke the cyclobutane photoadduct formation. Within homodimers CC, UU and TT, thymine has the lowest energy 2.36 eV, following with uracil 2.47 eV and cytosine 2.70 eV. The structure SWI as Figure 4.25, is the connection between the state with minimum energy of CBPyr adduct and the ground state of monomers.

It could be figured out through Figure 4.24 that, C$=$N only exists in C <> C (CBC), while C$=$O exists in T <> T (CBT), U <> U (CBU) and C <> C (CBC). Since the spin density distributed on different bond atoms differ according to bond type, $\pi \longrightarrow \pi^\star$ character takes place in all cases of pyrimidine dimers, however, only $n \longrightarrow \pi^\star$ character shows its difference in CBC due to the existence of C$=$N [97; 110].
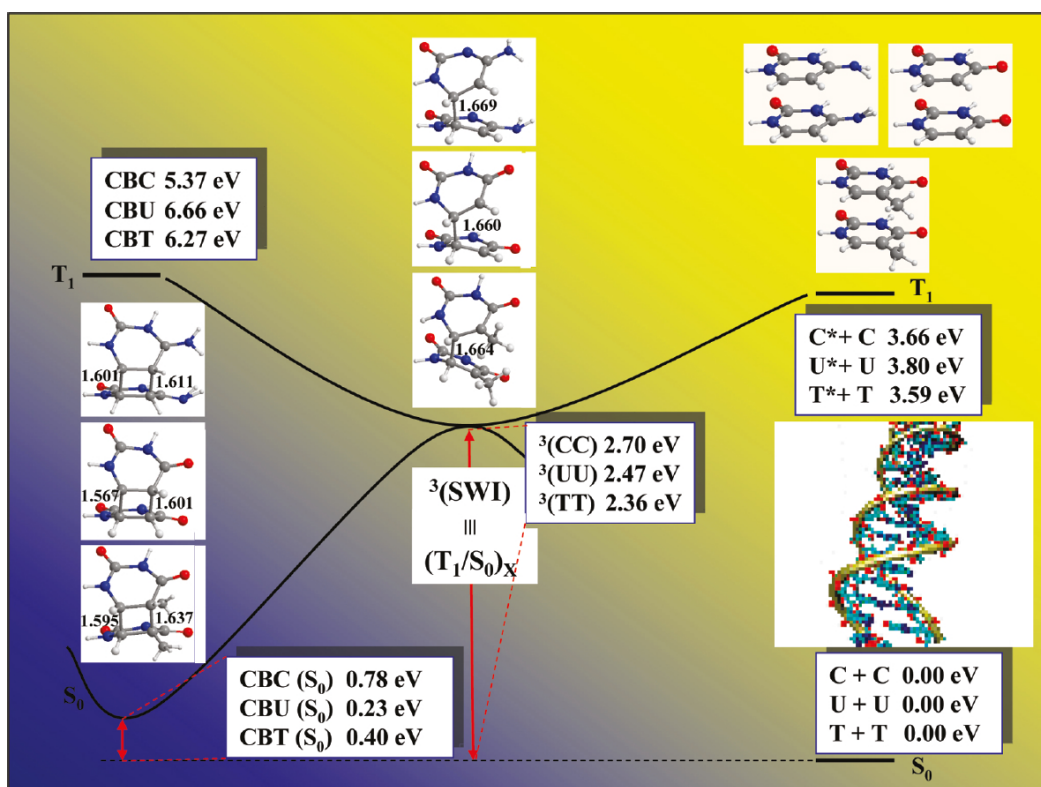
**Figure 4.25:** Scheme based on CASPT2 results of the triplet-mediated formation of CBPyr dimers [96]

To sum up, the molecular dynamics research on viruses figure out the property and stucture of viruses and UV exposure inactivation internal mechanism to the viral structures from the perspective of virus molecule at the beginning. During UV irradiation, ultraviolet energy is absorbed by viral proteins and viral nucleic acid bases (NABs), with different viral sensitivity to ultraviolet light. Regardless of viral damage maintenance, photochemical damage to viral proteins and viral NABs are vital damage to viruses. Since the complexity of viral proteins in numerous viruses, consistent viral NABs are chosen to be following research target.

Absorption Spectrum of NABs and Internal Conversion Mechanism of NABs Dimerization are discussed. The absorbed UV energy populates the NABs molecule, and ultrafast decay involved in internal conversion through conical intersection (CI) changes NABs molecule structure and drives the NABs to ground state with the lowest energy, accompanying with complicated energy states and transitions, such as triplet state and triplet - triplet energy transfer.

In terms of chemical bonding and electronic transition, different bond type may involve into corresponding transitions, driving electrons to orbitals with higher energy, leading to bonding weakening, absorption bands and transitions. The absorption spectrum and electronic energy transitions of nucleotides dimerization are intended to be investigated through molecular level simulation.

## 4.3 SIMULATION ON NUCLEOSIDES

Due to the theoretical and experimental research on UV Absorption Spectrum and Internal Conversion mechanism during dimerization between nucleosides. This section illustrates complementary simulations, including Absorption Spectrum of RNA nucleosides and inactivation process and mechanism of transition state. The simulation result would also be applied to explain the virus inactivation mechanism through UV energy absorbance and electronic energy transitions.

**Time-dependent density functional theory (TDDFT)** is a quantum mechanical theory used in the investigations of electronic dynamics of molecules in complicated systems [111; 112]. TDDFT is the tool to derive absorption spectrum in Gaussian, the calculation of excited state energy and frequency, leading to thermodynamic parameters of uracil. The calculation of excitation energy and oscillator intensity from ground state to excited state, transition broaden with Gaussian function and transition superimposition, resulting in UV-Vis Spectrum. On the other hand, Hybrid functions belong to exchange-correlation energy function in density function theory, contributing to ground state energy and frequency [113]. Moreover, **Transition state theory (TST)** is applied into interpretation of experimental rates of chemical reaction kinetics [114].

### 4.3.1 Absorption Spectrum Simulation

Since the experimental virus is single stranded RNA virus, Influenza A, the simulation of absorption spectrum is focused on four RNA nucleosides, Uracil, Adenine, Cytosine and Guanine, the structures of which are shown as Table 4.12, phosphates are not included in the structures.

Table 4.12: Stucture of nucleosides

| Uracil | Adenine | Cytosine | Guanine |
|--------|---------|----------|---------|
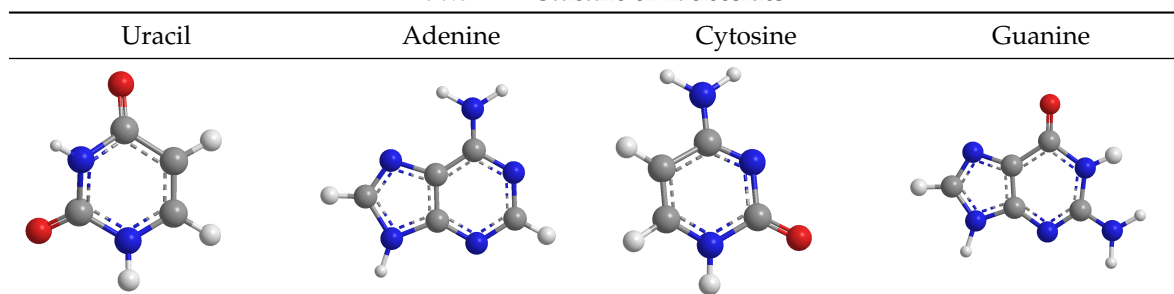


During general UV exposure, the nucleosides absorb UV energy, absorption of four nucleosides with different structure contributes to **Absorption Spectrum**, manifest in Figure 4.26 respectively. Absorbance within a range of UV wavelengths is measured as a function of time. The absorbance (ΔA) of Uracil indicates two zeniths within band 175 nm - 300 nm, one at 200 nm, the other one at 250 nm. And, the absorbance of uracil decreases when it is larger than 250 nm. When it comes to Adenine, with two ring structures and double-bonds, ΔA of Adenine is 1.5 times of uracil peak absorbance, where the optimal wavelength for UV absorption is 250nm.

Pyrimidines with single-ring structures consist of Cytosine and Uracil in RNA, which illustrates similar absorbance strength scale. Among four nucleosides, guanine reveals highest absorbance strength at the peak wavelength. It could be observed that Cytosine reaches peak wavelength at 225nm while 250nm for guanine. Within the experimental wavelength between 259nm and 284nm, on the basis of simulation result, the absorbance of four nucleosides drops with the increase of wavelength, corresponding to experimental tendency curve.

(a) Uracil Absorption Spectrum

(b) Adenine Absorption Spectrum

(c) Cytosine Absorption Spectrum

(d) Guanine Absorption Spectrum
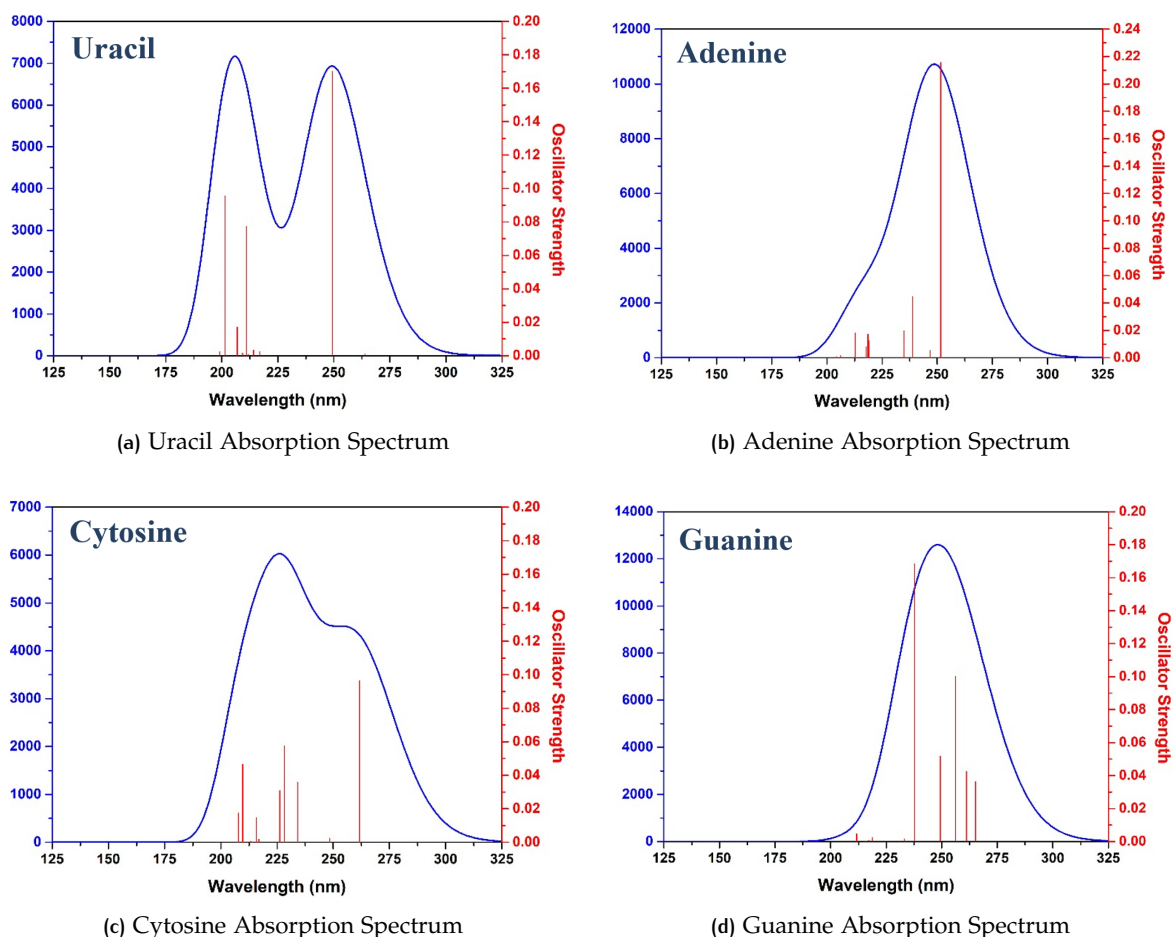
**Figure 4.26:** The absorption spectrums of four single nucleotides

### 4.3.2 Simulation on Uracil Transition

According to Section 4.2.6, both experimental and computational result illustrate uracil has the highest excited state energy, and the shortest ultrafast decay time. After the Absorption, an Internal Conversion occurs, electrons movement and electronics transitions takes place in between. Subsequently, the loss of energy and transition states contribute the structure variance of compound. Between four nucleosides, uracil with the shortest ultrafast decay time and comparatively medium absorbance is discussed in the following Transition State Theory, electronic energy and thermal correction calculation.

The rates of reactions are portrayed in transition state theory on the molecular scale. Collision of molecules results in the combination and formation of unstable, high energy structure. The molecules would transfer to new molecules or remain initial state when leaving from the high energy state. It is necessary to satisfy the required energy to reach the **activated transition state** in order to compose a product [115]. Therefore, it means reactant molecules collision do not form products directly because the formation of activated state is inevitable during the transition process.

Kinetic energy of colliding molecules are in possession of enough energy to activate complex to energetic state, which is represented by the standard Gibbs energy of activation, expressed with positive **molar Gibbs energy ($\Delta G^{\neq}$)**. In reference to Figure 4.27, molar Gibbs energy is the difference between the ground state of reactants and transition state of the reaction. In addition, the energy

difference between Activated Complex and Reactants is also labeled as **activation energy($E_a$)** in Figure 4.27 [116; 117; 118; 119].
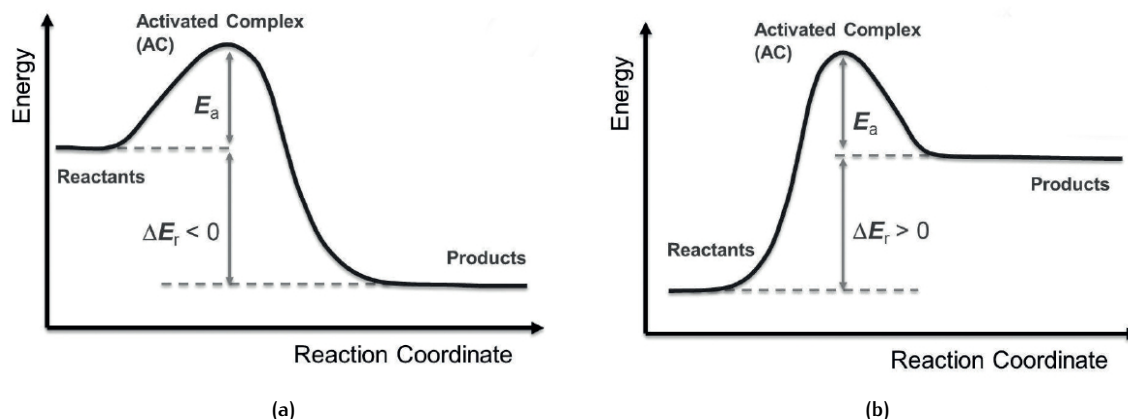


**Figure 4.27:** Potential energy profile or reaction coordinate diagram for exothermic

IRC Curve in traditional TST takes the property of saddle point into consideration, which is the peak internal energy point through the minimum energy route, revealing structural and energetic transition in the internal conversion system [120]. The reaction path would be described in the reaction simulation.

The TST theory is applied as the explanation of chemical process rate and the reaction correlation with temperature, medium and structure [121]. The activated state is energetic with potential energy while it is an unstable intermediate **Activated Complex (AC)**, the existence of transient state leads to the decomposition of AC and formation of products of reaction. The reaction rate is determined by the decomposition rate of AC [116]. The TST theory summarizes the two-stage chemical process as:

1. Formation of AC;

2. Decomposition of AC into the products of reaction;

as is described in reaction coordinate diagram. The reaction kinetics characterization of activation mechanism is completed with kinetic triplet, $E_a$, $A$ and $n$. $E_a$ is termed as activation energy, $A$ as activated complex and $n$ represents reaction type [122].

At the beginning, the states of transition process are illustrated in Table 4.13, the original uracil base is in ground state, the transition state of uracil nucleosides under ground state serves as the key transition state. In the end, a Cyclobutane uracil dimer formed.

**Table 4.13:** Inactivation Mechanism on Molecular Level

| Ground State Uracil | Transition state under Ground State | Cyclobutane uracil dimer |
| --- | --- | --- |
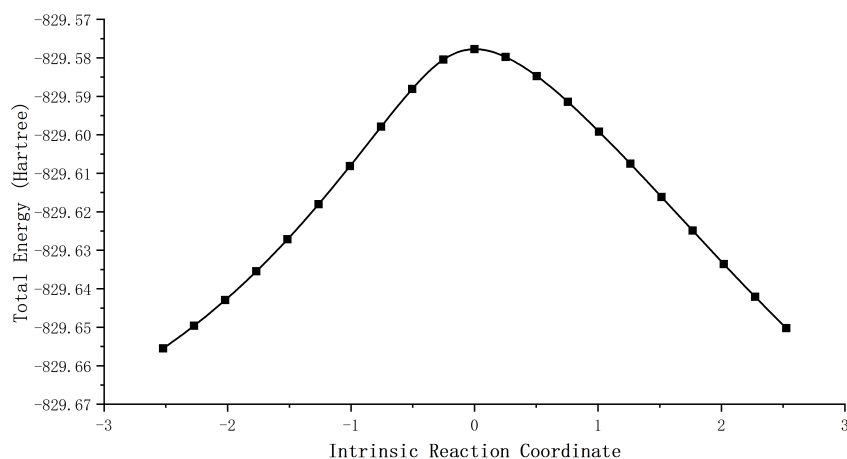
**Figure 4.28:** Total Energy of Reaction of ground state Uracils along IRC

Figure 4.28 reveals the total energy transition of uracil at the ground state, it complies with the typical transition state theory. The transition state, intermediate Activated Complex point could be observed during the reaction, corresponding to the transition state of uracil with the highest level of energy during reaction. At the same time, the transition state contributes to the decomposition of Activated Complex, causing the formation of product Cyclobutane uracil dimer.



(a)

(b)
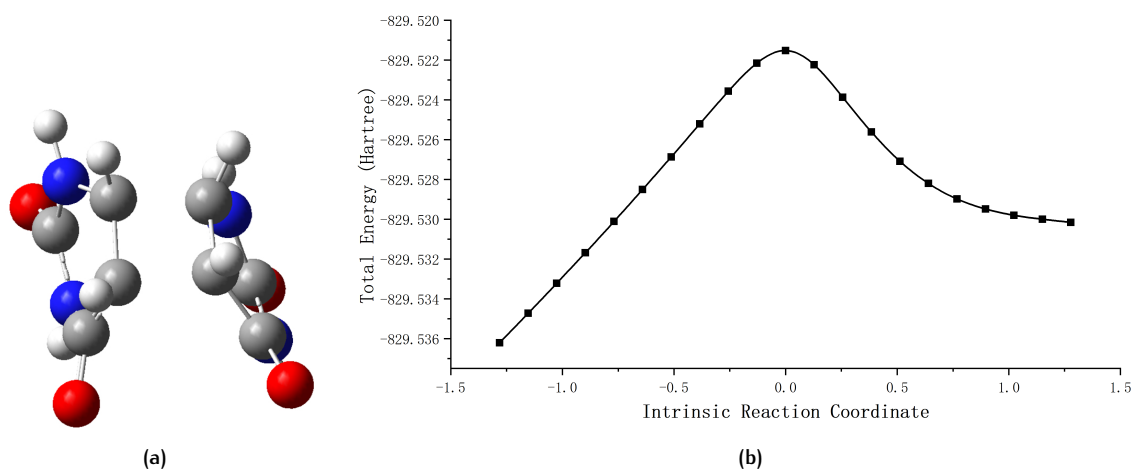
**Figure 4.29:** Excited State Uracil (a) Stucture of Transition State (b) Total Energy Transition of Reaction

Structure of uracils at the transition state is illustrated as Figure 4.29a, it is the transition state between reactant excited state uracils and product. Generally the reaction owns its formation and decomposition of Activated Complex (Transition State) shown as Figure 4.29b.

To sum up, the reaction simulation along IRC curve based on TST theory have proved that transition state is a necessary transient linkage between reactant and product, especially during the reaction from either ground state uracil or excited state uracil.

### 4.3.3  Electronic Energy and Thermal Correction

On the basis of Transition State Theory, deduction of reactant Gibbs free energy and reaction rate are derived from thermal simulation and calculation. Theoretically, reaction temperature T, reaction path degeneracy $\sigma$ and transmission coefficient $\kappa$, where $\kappa$ only matters when tunneling correction calculation is taken into consideration. As is discussed in last section, the process reaction rate is determined by factors as temperature, medium and structure. Taking temperature, medium and structure into consideration, according to TST Theory, the calculation of **reaction rate k** can be concluded as Equation 4.8.

$$k^{TST} = \sigma \frac{k_B T}{h} \left(\frac{RT}{P_0}\right)^{\Delta n} e^{-\Delta G^{0,\neq}/(k_B T)} \tag{4.8}$$

$$\sigma = \frac{\sigma_{rot,R}}{\sigma_{rot,TS}} \tag{4.9}$$

Reaction path degeneracy $\sigma$ could be derived from Equation 4.9. $\sigma_{rot,R}$ and $\sigma_{rot,TS}$ are rotational symmetry numbers of reactant and transition state respectively. $\left(\frac{RT}{P_0}\right)$ is the reverse of molar concentration, $\Delta n$ equals to 1 for gas phase bi-molecular, while $\Delta n$ equals to 0 for uni-molecular reactions. The $k_B T$ is the product of the Boltzmann's constant and thermodynamic temperature, which indicates energy on molecular scale, h is Planck's constant. The standard Gibbs energy of activation could also be obtained from Equation 4.10 [122; 123].

$$\Delta G^{0,\neq}(T)) = G^0_{TS}(T) - G^{Reactant}_0(T) \tag{4.10}$$

Applying ground state uracil as reactant, based on hybrid functions, the energy and frequency of ground state are calculated, as well as other script output, including four divisions Translation, Rotation, Vibration and Electron excitation. The divisions contribute to system Internal energy (U), Enthalpy (H), Entropy (S), Gibbs free energy (G), Constant Heat Capacity at constant Volume (CV), Constant Heat Capacity at constant Pressure (CP) and partition function (q). The script output of ground state are shown in Figure 4.30. Among the output parameters, the Gibbs free energy (G) has been paid attention to particularly because it is the key factor to calculate the reaction rate during transition, which is marked in figure.
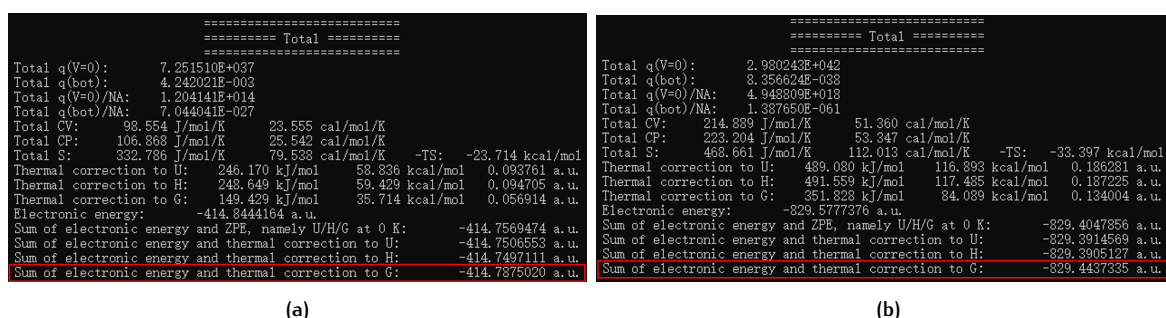


Figure 4.30: Thermal parameters of (a) Single-Uracil (b) Dual-Uracil under ground state

Corresponding Gibbs free energy values of ground state uracil have been listed in Table 4.14. Here is the reaction rate calculation of ground state uracil:

1. Prerequisite: Reaction with bi-molecular takes place in gas phase. Temperature = 298.15K. Reaction path degeneracy $\sigma = 1$. $P = 1 \quad bar$.

**Table 4.14:** Electronic Energy of Single-Uracil and Dual-Uracil under Ground State

| | Sum of Electronic Energy and Thermal Correction | | |
| --- | --- | --- | --- |
| | Single-Uracil | | Dual-Uracil Transition State |
| U | -414.7506553 a.u. | U | -829.3914569 a.u. |
| H | -414.7497111 a.u. | H | -829.3905127 a.u. |
| **G** | **-414.7875020 a.u.** | **G** | **-829.4437335 a.u.** |

2. Subtraction between two single-uracil reactant and dual-uracil transition state is $\Delta G^{\neq} = 344.6505461 \; kJ/mol$ (0.1312705 a.u.).

3. On the basis of TST theory Equation 4.8, reaction rate $k^{TST} = 6.419 \times 10^{-49} \; s^{-1}M^{-1}$ [124].
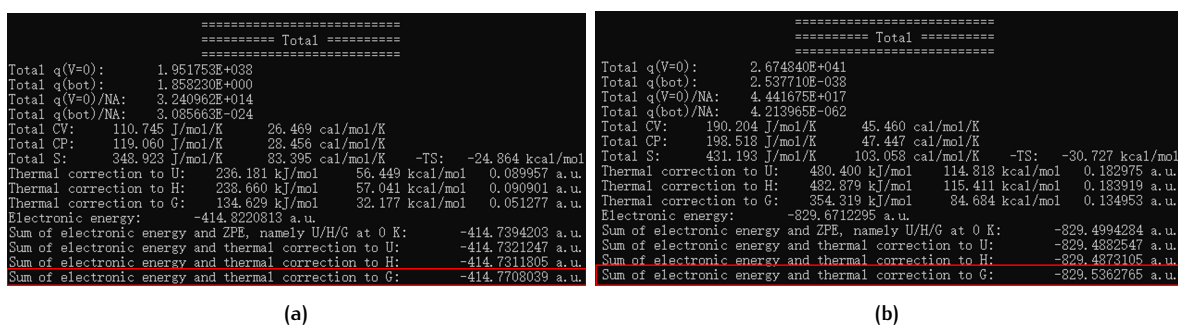
**Figure 4.31:** Thermal parameters of (a) Single-Uracil (b) Dual-Uracil under excited state

However, when excited state uracils serve as reactant, TDDFT was implemented for calculation, as well as transition script, reaction rate could be derived:

1. Prerequisite: Reaction with bi-molecular takes place in gas phase. Temperature = 298.15K. Reaction path degeneracy $\sigma = 1$. $P = 1bar$.

2. Subtraction between two excited state single-uracil reactant and dual-uracil transition state is $\Delta G^{\neq} = 13.9973196 \; kJ/mol$ ($5.3313 \times 10^{-3}$ a.u.).

3. On the basis of TST theory Equation 4.8, reaction rate $k^{TST} = 5.436 \times 10^{11} \; s^{-1}M^{-1}$ [124].

**Table 4.15:** Electronic Energy of Single-Uracil and Dual-Uracil under Excited State

| | Sum of Electronic Energy and Thermal Correction | | |
| --- | --- | --- | --- |
| | Single-Uracil | | Dual-Uracil Transition State |
| U | -414.7321247 a.u. | U | -829.4882547 a.u. |
| H | -414.7311805 a.u. | H | -829.4873105 a.u. |
| **G** | **-414.7708039 a.u.** | **G** | **-829.5362765 a.u.** |

$$t_{1/2} = \frac{1}{k[A]_0} \tag{4.11}$$

Some criteria utilizes $k^{TST} = 3.33 \times 10^{-3}$ as judgement of reaction rate. When $k^{TST}$ is larger than $3.33 \times 10^{-3}$, the reactions have the tendency to react faster, which is derived from half-life Equation 4.11, $[A]_0$ represents the initial concentration of reactants. When reaction temperature is 298.15K,

$[A]_0$ is 1M, assuming the reaction tendency criteria is 5 minutes, $k^{TST} = 3.33 \times 10^{-3}$. Under such circumstances, half life of ground state uracil takes $1.5579 \times 10^{48}$ s, which means the reaction could barely happen. However, half life of excited state uracil is calculated to be $1.8396 \times 10^{-12}$ s, around 1.84 ps, in which case, the transition of excited state uracil is a transient reaction [125].

Therefore, as claimed by uracil thermal simulation half-life calculation of bi-molecular reaction model, the transition of uracil under ground state takes more than thousand of years to happen, which could never happen. On the contrary, uracil transition is a transient reaction when excited state uracil is the reactant.

## 4.4 CONCLUSION

This chapter reveals the virus inactivation mechanism based on molecular dynamic research both from research on ultraviolet virus inactivation theory and molecular dynamic simulation specifically on nucleoside in viruses. The UV absorption by virus genetic material depends on viral sensitivity to UV exposure and photochemical reactions to viral materials, including viral NABs, viral proteins and mutual influence. Photochemical damage results in cross-links and cyclobutane-type photo-dimers. The absorbed UV energy of NABs could be measured with Absorption Spectrum. Subsequently, internal conversion takes place inside NBAs, NABs are populated and then ultrafast decay of excite state nucleosides degrades them to ground state through CI region. During the ultrafast decay, the chemical structure of carbon bonds varies, as well as the shape of nucleosides. According to Absorption Spectrum, UV wavelength with the highest highest viral sensitivity leads to particularly ultrafast decay.

At the same time, molecular dynamic research on nucleosides tell the Absorption Spectrum within UV-C range, beyond 250nm, four nucleosides reveal the highest absorption at the smallest wavelength. Taking uracil for example, on the basis of TST theory, the transition state tells the influence during reactions after exposure. When the uracil populates to excited state, molar Gibbs energy diminishes drastically, which causes higher reaction rate k (shorter half-life) than ground state uracil seriously.

The virus inactivation theory and molecular dynamic simulation manifest the potential suitable wavelength for virus inactivation, supporting the inactivation experiments, and explain the inactivation mechanism in accordance with photochemical reactions, internal conversion, electronic transitions, transition state theory and thermal correction.

# 5 | CONCLUSION AND FUTURE WORK

The current chapter would summarize thesis work in the previous chapters. Afterwards, some suggestions for future related work are put forward for discussion.

### 5.0.1 Conclusion

Since the outbreak of coronavirus, virus inactivation methodology has grown into a popular topic, numerous inactivation approaches have been taken into account. Although the inactivation methods vary a lot, their efficiency presents jagged as a fact, in which case, a quantitative inactivation platform is in need. The initial purpose of the thesis project is to construct a **UV-C LED Virus Inactivation Platform** for biomedical **Standard Virology Inactivation Experiments** in *Erasmus Medical Centre*. Arduino together with controllable CCSs take control of the driving current of each individual UV-C LED, hence each LED is in possession of high optical power resolution. In order to fulfill the quantitative requirement of exposure ultraviolet optical power , preparations have to be done for reasonable exposure dose of inactivation experiments:

1. Irradiance simulation is implemented before system design and assembly to ensure plausible exposure ultraviolet power at a certain diatance for inactivation.

2. LED light source characterization is done after system assembly for precise optical radiance power and wavelength measurements in *Signify* in order to measure quantitative UV radiance power of single-wavelength.

Because of the quantitative characterization and system modeling parameters, Design of Experiment is implemented for each virus sample in cell culture plate well. Moreover, the quantitative inactivation result can only be obtained when influential factors are excluded. Due to the key factors of DoE are **UV-C wavelength** and **Exposure Dose**, other potential factors are supposed to be ruled out through system design and reference experiments, such as cooling system design with on-board temperature monitor, and ozone reference experiment group.

The effectiveness of the inactivation platform was proved at the beginning experiment in Erasmus MC, the following difficulty was to delineate the upper bound and lower bound to observe reasonable **Inactivation Curve and Germicidal Curve**, which outline reduction rate trend as a function of exposure UV dose and UV-C wavelength respectively. The highest reduction rate at the largest exposure dose is expected to reach the upper bound of readout limitation as inactivation effectiveness evidence, however, the formation of plateau is supposed to be prevented for inactivation tendency observation. The following are approaches to attain plausible trendline:

1. Before experiments, literature review was aimed to discover viruses with similar virology structure to target experimental virus, their disinfection UV dose and experiment surroundings (surface disinfection, mask disinfection and etc.) as well.

2. Taking experience from literature review as reference, trial experiments were designed and implemented in Erasmus MC. Then, effective exposure dose range was uncovered, and the detective range could be narrowed accordingly during subsequent experiments.

3. After experiments, statistics were classified for different curves, and error bars were applied for data points in order to satisfy the smoothness of trendlines and prevent the influence of outliers at the same time.

The UV inactivation experiments have verify the effectiveness of inactivation of Influenza A. In addition, Inactivation Curve and Germicidal Curve reveal the performance of exposure dose and exposure wavelength respectively.

Moreover, the molecular dynamics research on inactivation mechanism through theoretical analysis and simulation intended to explain the viral sensitivity to ultraviolet light as a function of UV-C wavelength, especially for Nucleic Acid Bases. Inactivation theory was implemented by investigating the **Absorption Spectrum, Nucleic Acid Base Dimerization, and Electronic Transitions of Internal Conversion**.

1. Throughout the Absorption Spectrum research of five nucleic acid bases, peak absorption wavelength ranges are typically within UV-C band, pyrimidines Thymine (211 nm, 265 nm - 270 nm), Uracil (203 nm - 205 nm, 264 nm - 268 nm), Cytosine (199 nm - 203 nm, 270 nm - 271nm), and purines Adenine (210 nm, 269 nm - 272 nm), Guanine (246 nm and 251nm).

2. Photochemical products of dimerization take place between Nucleic acid bases, among all of them, UU (uracil doublets) has the highest UV reactivity. Photochemical reactions between pyrimidines lead to formation Cyclobutane Pyrimidine Dimers.

3. Under UV exposure, Internal Conversion occurs in nucleosides, absorbed UV energy results in the ultrafast decay (Fluorescence decays) via **Franck-Condon region and Conical Intersection**. Due to the energy absorption, the NAB transfers from the initial ground state (planar) to the electronically excited state (almost planar) through Franck-Condon region. Then, pyramidalization (out-of-plane deformation) takes place and leads to Conical Intersection, which finally causes the formation of ground state product (with perpendicular configuration).

4. The potential electronic energy transition depends on the bond type in corresponding nucleoside.

Molecular dynamics simulation was carried out towards Nucleic Acid Bases in RNA, quantum mechanical theory TDDFT calculates Absorption Spectrum and energy of state. The simulation is to illustrate absorption spectrum, transition state and electronic energy transfer, and is applied to support inactivation mechanism theory on purpose. Key insights are illustrated as follows:

1. The peak wavelength of RNA nucleosides, pyrimidines Uracil (200 nm, 250 nm), Cytosine (225 nm), and purines Adenine (250 nm), Guanine (250 nm).

2. Transition State Theory reveals the transition state during transformation, verified by IRC.

3. Taking Structure transformation, energy transition, Electronic Energy and Thermal Correction of RNA nucleoside Uracil into account, reaction rate of excited state uracil is derived to be shorter than that of ground state uracil, which reveals lower standard Gibbs energy of activation results in faster reaction process, and shorter half-life.

Both molecular dynamics theoretical analysis and simulation manifest the nucleoside absorption spectrum within UV-C band, which partially explain the peak inactivation wavelength in experiments. Within experimental band 259 nm - 284 nm, reduction tendency drops as a function of wavelength, which corresponds to the absorption spectrum tendency. In addition, within UV dose range, reduction increases as a function of dose until a plateau, which is consistent with the influence of absorbance strength. Higher exposure UV dose represents higher exposure UV energy, causing stronger potential absorbance. Verified transition state in simulation is the highest energy

state, which is most likely to be transferred from excited state (almost planar structure), leading to ultrafast decay and formation of dimer products. According to half-life calculation, fast reaction rate of excited state nucleoside results from lower standard Gibbs energy of activation, which is also the reason for ultrafast decay.

### 5.0.2 Future Work

The current platform and experiments are limited within UV-C band, in order to figure out the most efficient wavelength, Vacuum UV and UV-B wavelengths are supposed to be taken into account.

Characterization is now done with single UV-C LED when the LED is aligned with the center of detector. In a group, four LEDs illuminate at the same time during single-wavelength exposure, under the case that each LED view angle is 120 degree, a precise characterization could light four LEDs at the same time.

As a matter of fact, dried virus is placed at the center of cell culture plate well. Because of the quartz of LEDs, view angle is 120 degree, the UV exposure is not aligned directly to the virus. Once the light intensity of LED strengthened with the development of manufacture, dome shape quartz. In the light of Figure 5.1, the adopted quartz of LED affects the illumination area and intensity distribution. If the dried virus cover area is consistent, the adopted quartz and corresponding illumination area could adjust to the same scale.
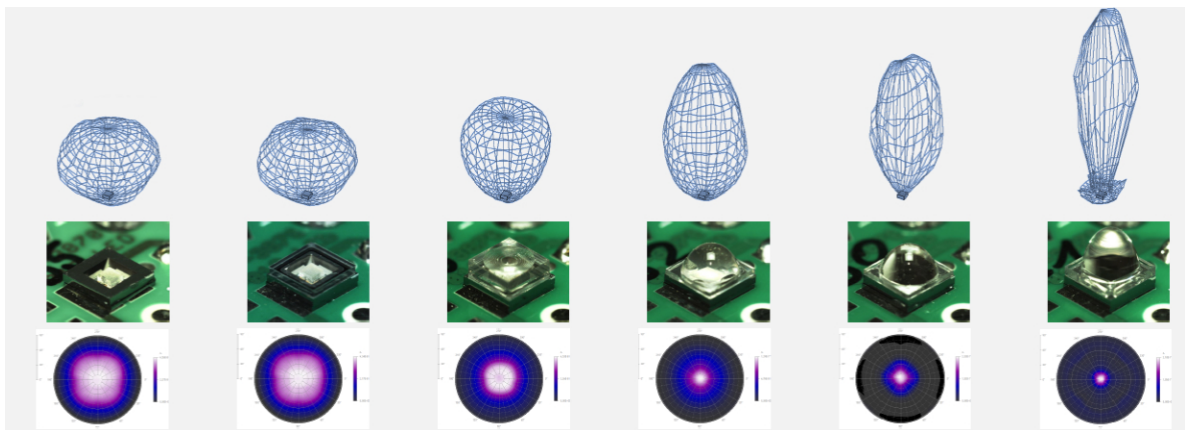


Figure 5.1: Measured Radiation Characterization

Different exposure time under the same UV exposure dose is probable to result in different inactivation reduction. DoE is designed for the proposal and could be attempted in the subsequent experiments.

Theoretical inactivation research is only in respect with nucleic acid base model in virus, while the complicated protein model is avoided to be concerned, the mutual effect between nucleic acid base and proteins as well. The subsequent research could also pay close attention to the role of protein in inactivation, especially the influence of protein below wavelength 240 nm.

# BIBLIOGRAPHY

[1] Biesert, L., and H. Suhartono. "Solvent/Detergent Treatment of Human Plasma-A Very Robust Method for Virus Inactivation. Validated Virus Safety of OCTAPLAS®." Vox sanguinis 74.S1 (1998): 207-212.

[2] Allison, Steven L., et al. "Oligomeric rearrangement of tick-borne encephalitis virus envelope proteins induced by an acidic pH." Journal of virology 69.2 (1995): 695-700.

[3] Thayer, Donald W., et al. "Radiation pasteurization of food." Council for Agricultural Science and Technology 7.1 (1996): 1-10.

[4] Syed, Deeba N., Farrukh Afaq, and Hasan Mukhtar. "Differential activation of signaling pathways by UVA and UVB radiation in normal human epidermal keratinocytes." Photochemistry and photobiology 88.5 (2012): 1184-1190.

[5] Arrasmith, William Wolfgang. Systems engineering and analysis of electro-optical and infrared systems. CRC Press, 2018.

[6] Gordon, Randy. "Skin cancer: an overview of epidemiology and risk factors." Seminars in oncology nursing. Vol. 29. No. 3. WB Saunders, 2013.

[7] Wentzel, Gregor, and Charlotte Houtermans. Quantum theory of fields. Courier Corporation, 2003.

[8] Kowalski, Wladyslaw. Ultraviolet germicidal irradiation handbook: UVGI for air and surface disinfection. Springer science  business media, 2010.

[9] Blanc, P. L., R. W. Tuveson, and M. L. Sargent. "Inactivation of carotenoid-producing and albino strains of Neurospora crassa by visible light, blacklight, and ultraviolet radiation." Journal of bacteriology 125.2 (1976): 616-625.

[10] Claus, Holger. "Ozone Generation by Ultraviolet Lamps." Photochemistry and Photobiology (2021).

[11] Schalk, Sven, et al. "UV-lamps for disinfection and advanced oxidation-lamp types, technologies and applications." IUVA news 8.1 (2005): 32-37.

[12] Sarigiannis, D. A., et al. "Exposure analysis of accidental release of mercury from compact fluorescent lamps (CFLs)." Science of the Total Environment 435 (2012): 306-315.

[13] Ketha, Hema, and Uttam Garg, eds. Toxicology Cases for the Clinical and Forensic Laboratory. Academic Press, 2020.

[14] Zhang, Jun-Ying, and Ian W. Boyd. "Lifetime investigation of excimer UV sources." Applied surface science 168.1-4 (2000): 296-299.

[15] Shur, Michael S., and Remis Gaska. "Deep-ultraviolet light-emitting diodes." IEEE Transactions on electron devices 57.1 (2009): 12-25.

[16] Fujioka, A., et al. "High-output-power 255/280/310 nm deep ultraviolet light-emitting diodes and their lifetime characteristics." Semiconductor Science and Technology 29.8 (2014): 084005.

[17] Sun, Ke-Xun, et al. "UV LED operation lifetime and radiation hardness qualification for space flights." Journal of Physics: Conference Series. Vol. 154. No. 1. IOP Publishing, 2009.

[18] Yoshikawa, Akira, et al. "Improve efficiency and long lifetime UVC LEDs with wavelengths between 230 and 237 nm." Applied Physics Express 13.2 (2020): 022001.

[19] Kirchman, David L. Processes in microbial ecology. Oxford University Press, 2018.

[20] Darnell, Miriam ER, et al. "Inactivation of the coronavirus that induces severe acute respiratory syndrome, SARS-CoV." Journal of virological methods 121.1 (2004): 85-91.

[21] Eickmann, Markus, et al. "Inactivation of Ebola virus and Middle East respiratory syndrome coronavirus in platelet concentrates and plasma by ultraviolet C light and methylene blue plus visible light, respectively." Transfusion 58.9 (2018): 2202-2207.

[22] Günther, Stephan, et al. "Management of accidental exposure to Ebola virus in the biosafety level 4 laboratory, Hamburg, Germany." The Journal of infectious diseases 204.suppl_3 (2011): S785-S790.

[23] Log and Percent Reductions in Microbiology and Antimicrobial Testing — Microchem Laboratory. https://microchemlab.com/information/log-and-percent-reductions-microbiology-and-antimicrobial-testing. Accessed 5 May 2021.

[24] Beck, Sara E., et al. "Evaluating UV-C LED disinfection performance and investigating potential dual-wavelength synergy." Water research 109 (2017): 207-216.

[25] Eickmann, Markus, et al. "Inactivation of three emerging viruses–severe acute respiratory syndrome coronavirus, Crimean–Congo haemorrhagic fever virus and Nipah virus–in platelet concentrates by ultraviolet C light and in plasma by methylene blue plus visible light." Vox sanguinis 115.3 (2020): 146-151.

[26] Terpstra, Fokke G., et al. "Potential and limitation of UVC irradiation for the inactivation of pathogens in platelet concentrates." Transfusion 48.2 (2008): 304-313.

[27] Cadnum, Jennifer L., et al. "Evaluation of ultraviolet-C Light for rapid decontamination of airport security bins in the era of SARS-CoV-2." Pathogens and Immunity 5.1 (2020): 133.

[28] Lede, Ivar, Karina Nolte, and René Kroes. "A Scalable Method for Ultraviolet C Disinfection of Surgical Facemasks Type IIR and Filtering Facepiece Particle Respirators 1 and 2." (2020).

[29] Liu, Jing, et al. "Role of Ozone in UV-C Disinfection, Demonstrated by Comparison between Wild-Type and Mutant Conidia of Aspergillus niger." Photochemistry and photobiology 90.3 (2014): 615-621.

[30] Quevedo-león, Roberto, et al. "Inactivation of Coronaviruses in food industry: The use of inorganic and organic disinfectants, ozone, and UV radiation." Scientia Agropecuaria 11.2 (2020): 257-266.

[31] Bohrerova, Zuzana, et al. "Comparative disinfection efficiency of pulsed and continuous-wave UV irradiation technologies." Water research 42.12 (2008): 2975-2982.

[32] Daryany, Mahmoud Karimi Azar, et al. "Study on continuous (254 nm) and pulsed UV (266 and 355 nm) lights on BVD virus inactivation and its effects on biological properties of fetal bovine serum." Journal of Photochemistry and Photobiology B: Biology 94.2 (2009): 120-124.

[33] Kowalkski, W. "Ultraviolet Germicidal Irradiation Handbook." (2009).

[34] Sagripanti, Jose-Luis, and C. David Lytle. "Sensitivity to ultraviolet radiation of Lassa, vaccinia, and Ebola viruses dried on surfaces." Archives of virology 156.3 (2011): 489-494.

[35] Yung, Kam Chuen, et al. "Thermal performance of high brightness LED array package on PCB." International Communications in Heat and Mass Transfer 37.9 (2010): 1266-1272.

[36] ISO 15858:2016 UV-C Devices — Safety information — Permissible human exposure, 2016.

[37] Emmert, Elizabeth AB. "Biosafety guidelines for handling microorganisms in the teaching laboratory: development and rationale." Journal of Microbiology Biology Education: JMBE 14.1 (2013): 78.

[38] Sommer, Regina, et al. "Inactivation of bacteriophages in water by means of non-ionizing (UV-253.7 nm) and ionizing (gamma) radiation: a comparative approach." Water Research 35.13 (2001): 3109-3116.

[39] Lytle, C. David, and Jose-Luis Sagripanti. "Predicted inactivation of viruses of relevance to biodefense by solar radiation." Journal of virology 79.22 (2005): 14244-14252.

[40] Blanchard, Emmeline L., et al. "Enveloped Virus Inactivation on Personal Protective Equipment by Exposure to Ozone." medRxiv (2020).

[41] Gong, Jia-You, et al. "For the inactivation of mold spores by UVC irradiation, with ozone acting as a promoter, TiO 2 nanoparticles may act better as a "sun block" than as a photocatalytic disinfectant." Photochemical Photobiological Sciences 13.9 (2014): 1305-1310.

[42] Tseng, Chunchieh, and Chihshan Li. "Inactivation of surface viruses by gaseous ozone." Journal of environmental health 70.10 (2008): 56-63.

[43] Hollas, J. Michael. Modern spectroscopy. John Wiley Sons, 2004.

[44] Harris, D., and M. Bertolucci. "An Introduction to Vibrational and Electronic Spectroscopy." (1978).

[45] Knee, J. L. "Spectra of Atoms and Molecules by Peter F. Bernath." AMERICAN JOURNAL OF PHYSICS 64 (1996): 93-93.

[46] Honsberg, C. B., and S. G. Bowden. "Photovoltaics education website." (2019).

[47] Skoog, Douglas A., F. James Holler, and Stanley R. Crouch. Principles of instrumental analysis. Cengage learning, 2017.

[48] Bouguer, Pierre. "Essai d'Optique sur la Gradation de la Lumière." (1922): 93-93.

[49] Silverstein, Robert M., and G. Clayton Bassler. "Spectrometric identification of organic compounds." Journal of Chemical Education 39.11 (1962): 546.

[50] Fleming, Ian. Frontier orbitals and organic chemical reactions. Wiley, 1977.

[51] Houk, Kendall N. "Frontier molecular orbital theory of cycloaddition reactions." Accounts of Chemical Research 8.11 (1975): 361-369.

[52] Pavia, Donald L., et al. Introduction to spectroscopy. Cengage learning, 2014.

[53] Scott, Alastair Ian. Interpretation of the Ultraviolet Spectra of Natural Products: International Series of Monographs on Organic Chemistry. Vol. 7. Elsevier, 2013.

[54] Nayler, P., and M. C. Whiting. "Researches on polyenes. Part III. The synthesis and light absorption of dimethylpolyenes." Journal of the Chemical Society (Resumed) (1955): 3037-3047.

[55] Lwoff, André. "The concept of virus." Microbiology 17.2 (1957): 239-253.

[56] Stadtman, E. R., G. David Novelli, and Fritz Lipmann. "Coenzyme A function in and acetyl transfer by the phosphotransacetylase system." Journal of Biological Chemistry 191.1 (1951): 365-376.

[57] Strauss Jr, James H., and Robert L. Sinsheimer. "Purification and properties of bacteriophage MS2 and of its ribonucleic acid." Journal of molecular biology 7.1 (1963): 43-54.

[58] ALFERT, M. and GESCHWIND, I. I., Proc. Natf Acad. Sci. U.S. 39. 991 (1953): 50-68

[59] Marvin, D. A., and H. Hoffmann-Berling. "Physical and chemical properties of two new small bacteriophages." Nature 197.4866 (1963): 517-518.

[60] Allison, A. C., and D. C. Burke. "The nucleic acid contents of viruses." Microbiology 27.2 (1962): 181-194.

[61] Martin, E. M., et al. "Studies on protein and nucleic acid metabolism in virus-infected mammalian cells. 1. Encephalomyocarditis virus in Krebs II mouse-ascites-tumour cells." Biochemical Journal 80.3 (1961): 585-597.

[62] Russell, W. C., and L. V. Crawford. "Some characteristics of the deoxyribonucleic acid from herpes simplex virus." Virology 21.3 (1963): 353-361.

[63] Hashimoto, Shuichi, Michael H. Pursley, and Maurice Green. "Nucleotide sequences and mapping of novel heterogenous 5-termini of adenovirus 2 early region 4 mRNA." Nucleic acids research 9.7 (1981): 1675-1690.

[64] Rossmann, Michael G., and John E. Johnson. "Icosahedral RNA virus structure." Annual review of biochemistry 58.1 (1989): 533-569.

[65] Xu, Rui, et al. "Structural characterization of the hemagglutinin receptor specificity from the 2009 H1N1 influenza pandemic." Journal of virology 86.2 (2012): 982-990.

[66] Palese, Peter, and Jerome L. Schulman. "Mapping of the influenza virus genome: identification of the hemagglutinin and the neuraminidase genes." Proceedings of the national academy of sciences 73.6 (1976): 2142-2146.

[67] Mancera Gracia, José Carlos, et al. "Influenza A Virus in Swine: Epidemiology, Challenges and Vaccination Strategies." Frontiers in Veterinary Science 7 (2020): 647.

[68] Dogra, Ayush, Bhawna Goyal, and Apoorav Maulik Sharma. "Corona virus: A novel outbreak." Biomedical and Pharmacology Journal 13.1 (2020): 05-10.

[69] Rauth, Andrew M. "The physical state of viral nucleic acid and the sensitivity of viruses to ultraviolet light." Biophysical Journal 5.3 (1965): 257-273.

[70] Samoc, Marek, Anna Samoc, and Paul A. Fleitz. Two-Photon Absorption Measurements: Establishing Reference Standards. AUSTRALIAN NATIONAL UNIV CANBERRA, 2007.

[71] Maini, Anil K. Lasers and optoelectronics: fundamentals, devices and applications. John Wiley Sons, 2013.

[72] Fraser, Christophe, et al. "Pandemic potential of a strain of influenza A (H1N1): early findings." science 324.5934 (2009): 1557-1561.

[73] Beck, Sara E., et al. "Comparison of UV-induced inactivation and RNA damage in MS2 phage across the germicidal UV spectrum." Applied and environmental microbiology 82.5 (2016): 1468-1474.

[74] Qiao, Yawei, et al. "Modulation of repair of ultraviolet damage in the host-cell reactivation assay by polymorphic XPC and XPD/ERCC2 genotypes." Carcinogenesis 23.2 (2002): 295-299.

[75] Qiao, Yawei, et al. "Modulation of repair of ultraviolet damage in the host-cell reactivation assay by polymorphic XPC and XPD/ERCC2 genotypes." Carcinogenesis 23.2 (2002): 295-299.

[76] Budden, Timothy, and Nikola A. Bowden. "The role of altered nucleotide excision repair and UVB-induced DNA damage in melanomagenesis." International Journal of Molecular Sciences 14.1 (2013): 1132-1151.

[77] Kimura, Seisuke, et al. "DNA repair in higher plants; photoreactivation is the major DNA repair pathway in non-proliferating cells while excision repair (nucleotide excision repair and base excision repair) is active in proliferating cells." Nucleic acids research 32.9 (2004): 2760-2767.

[78] Beck, Sara E., et al. "Wavelength-dependent damage to adenoviral proteins across the germicidal UV spectrum." Environmental science technology 52.1 (2018): 223-229.

[79] Wigginton, Krista Rule, et al. "UV Radiation Induces Genome-Mediated, Site-Specific Cleavage in Viral Proteins." ChemBioChem 13.6 (2012): 837-845.

[80] Gordon, Milton P. "Role of protein in the inactivation of viruses by ultraviolet radiation." Aging, Carcinogenesis, and Radiation Biology. Springer, Boston, MA, 1976. 105-122.

[81] Kowalski, Wladyslaw. "UVGI disinfection theory." Ultraviolet germicidal irradiation handbook. Springer, Berlin, Heidelberg, 2009. 17-50.

[82] Hegedüs, M., et al. "Validation of Phage T7 Biological Dosimeter by Quantitative Polymerase Chain Reaction Using Short and Long Segments of Phage T7 DNA¶." Photochemistry and photobiology 78.3 (2003): 213-219.

[83] Thies, Janice E. "Molecular approaches to studying the soil biota." Soil Microbiology, Ecology and Biochemistry. Elsevier, 2015. 151-185.

[84] Blanco, Gustavo, and Antonio Blanco. Medical biochemistry. Academic Press, 2017.

[85] Harm, Walter. "Biological effects of ultraviolet radiation." (1980).

[86] Koller, Lewis Richard. Ultraviolet radiation. Vol. 2. New York: Wiley, 1965.

[87] Kuluncsics, Z., et al. "Wavelength dependence of ultraviolet-induced DNA damage distribution: involvement of direct or indirect mechanisms and possible artefacts." Journal of Photochemistry and Photobiology B: Biology 49.1 (1999): 71-80.

[88] Masschelein, Willy J., and Rip G. Rice. Ultraviolet light in water and wastewater sanitation. CRC press, 2016.

[89] Miller, Richard L., and Peter GW Plagemann. "Effect of ultraviolet light on mengovirus: formation of uracil dimers, instability and degradation of capsid, and covalent linkage of protein to viral RNA." Journal of virology 13.3 (1974): 729-739.

[90] Hollaender, Alexander. "Radiation biology." Soil Science 82.2 (1956): 176.

[91] Yamada, Takenori, and Hideo Fukutome. "Vacuum ultraviolet absorption spectra of sublimed films of nucleic acid bases." Biopolymers: Original Research on Biomolecules 6.1 (1968): 43-54.

[92] D. Voet, W. B. Gratzer, R. A. Cox, and P. Doty, Biopolymers, 1, 103 (1063).

[93] Daniels, Malcolm, and William Hauswirth. "Fluorescence of the purine and pyrimidine bases of the nucleic acids in neutral aqueous solution at 300 K." Science 171.3972 (1971): 675-677.

[94] Smith, Kendric C., and Philip C. Hanawalt. Molecular photobiology: inactivation and recovery. Elsevier, 2013.

[95] Rothman, R. H., and R. B. Setlow. "An action spectrum for cell killing and pyrimidine dimer formation in Chinese hamster V-79 cells." Photochemistry and Photobiology 29.1 (1979): 57-61.

[96] Kladwang, Wipapat, Justine Hum, and Rhiju Das. "Ultraviolet shadowing of RNA can cause significant chemical damage in seconds." Scientific reports 2.1 (2012): 1-7.

[97] Climent, Teresa, et al. "Cyclobutane pyrimidine photodimerization of DNA/RNA nucleobases in the triplet state." The Journal of Physical Chemistry Letters 1.14 (2010): 2072-2076.

[98] Pecourt, Jean-Marc L., Jorge Peon, and Bern Kohler. "DNA excited-state dynamics: Ultrafast internal conversion and vibrational cooling in a series of nucleosides." Journal of the American Chemical Society 123.42 (2001): 10370-10378.

[99] Gustavsson, Thomas, Roberto Improta, and Dimitra Markovitsi. "DNA/RNA: building blocks of life under UV irradiation." The Journal of Physical Chemistry Letters 1.13 (2010): 2025-2030.

[100] González-Ramírez, Israel, et al. "On the photoproduction of DNA/RNA cyclobutane pyrimidine dimers." Theoretical Chemistry Accounts 128.4 (2011): 705-711.

[101] Serrano-Andres, Luis, and Manuela Merchan. "Are the five natural DNA/RNA base monomers a good choice from natural selection?: A photochemical perspective." Journal of Photochemistry and Photobiology C: Photochemistry Reviews 10.1 (2009): 21-32.

[102] Hare, Patrick M., Carlos E. Crespo-Hernandez, and Bern Kohler. "Solvent-dependent photophysics of 1-cyclohexyluracil: ultrafast branching in the initial bright state leads nonradiatively to the electronic ground state and a long-lived $1n^*$ state." The Journal of Physical Chemistry B 110.37 (2006): 18641-18650.

[103] Gustavsson, Thomas, et al. "Singlet excited-state behavior of uracil and thymine in aqueous solution: a combined experimental and computational study of 11 uracil derivatives." Journal of the American Chemical Society 128.2 (2006): 607-619.

[104] Gustavsson, Thomas, et al. "Singlet excited state dynamics of uracil and thymine derivatives: A femtosecond fluorescence upconversion study in acetonitrile." Chemical physics letters 429.4-6 (2006): 551-557.

[105] Miannay, Francois-Alexandre, et al. "Excited-state dynamics of dGMP measured by steady-state and femtosecond fluorescence spectroscopy." The Journal of Physical Chemistry A 114.9 (2010): 3256-3263.

[106] Hare, Patrick M., et al. "Time-resolved infrared spectroscopy of the lowest triplet state of thymine and thymidine." Chemical physics 347.1-3 (2008): 383-392.

[107] Kwok, Wai-Ming, Chensheng Ma, and David Lee Phillips. "A doorway state leads to photostability or triplet photodamage in thymine DNA." Journal of the American Chemical Society 130.15 (2008): 5131-5139.

[108] Etinski, Mihajlo, Timo Fleig, and Christel M. Marian. "Intersystem crossing and characterization of dark states in the pyrimidine nucleobases uracil, thymine, and 1-methylthymine." The Journal of Physical Chemistry A 113.43 (2009): 11809-11816.

[109] Abouaf, Robert, et al. "The triplet state of cytosine and its derivatives: Electron impact and quantum chemical study." The Journal of chemical physics 121.23 (2004): 11668-11674.

[110] Roca-Sanjuan, Daniel, et al. "DNA nucleobase properties and photoreactivity: Modeling environmental effects." Pure and Applied Chemistry 81.4 (2009): 743-754.

[111] Agostini, Federica, et al. "TDDFT and quantum-classical dynamics: A universal tool describing the dynamics of matter." Handbook of Materials Modeling: Methods: Theory and Modeling (2020): 75-121.

[112] Marques, Miguel, et al. Time-dependent density functional theory. Vol. 706. Springer Science Business Media, 2006.

[113] Janesko, Benjamin G., Thomas M. Henderson, and Gustavo E. Scuseria. "Screened hybrid density functionals for solid-state chemistry and physics." Physical Chemistry Chemical Physics 11.3 (2009): 443-454.

[114] Peters, Baron. Reaction rate theory and rare events. Elsevier, 2017.

[115] Dambrowitz, K. A., and S. M. Kuznicki. "Henry Eyring: A model life." Bulletin for the History of Chemistry 35.1 (2010): 46.

[116] Patra, B. B., and Biswajit Samantray. Engineering Chemistry I (for BPUT). Pearson Education India, 2010.

[117] Parker, Roger Hill. An Introduction to Chemical Metallurgy: International Series on Materials Science and Technology. Vol. 26. Elsevier, 2016.

[118] Book, Gold. "Compendium of chemical terminology." International Union of Pure and Applied Chemistry 528 (2014).

[119] Hinshelwood, C. N. "Proc R Soc London." Ser A. Vol. 113. 1926.

[120] Truhlar, Donald G., Bruce C. Garrett, and Stephen J. Klippenstein. "Current status of transition-state theory." The Journal of physical chemistry 100.31 (1996): 12771-12800.

[121] Petersson, George A. "Perspective on "The activated complex in chemical reactions"." Theoretical Chemistry Accounts. Springer, Berlin, Heidelberg, 2000. 190-195.

[122] Ptáček, Petr, František Šoukal, and Tomáš Opravil. "Introduction to the Transition state theory." Introducing the Effective Mass of Activated Complex and the Discussion on the Wave Function of this Instanton 27 (2018).

[123] Fernandez-Ramos, Antonio, et al. "Variational transition state theory with multidimensional tunneling." Reviews in computational chemistry 23 (2007): 125.

[124] Tian Lu, TSTcalculator, http://sobereva.com/310 (accessed 08, 21, 2021)

[125] Tian Lu, Bi-molecular Reactions, http://sobereva.com/506 (accessed 08, 21, 2021)

# PLATFORM MODULES AND ASSEMBLY
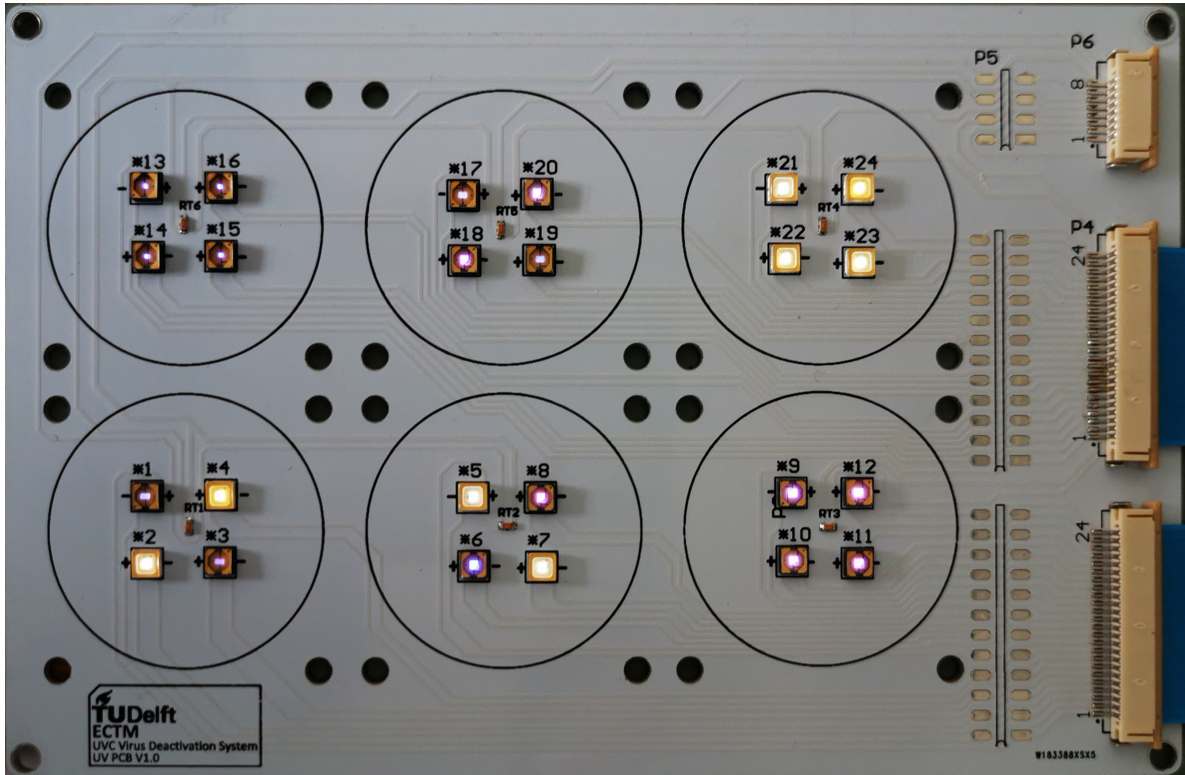


**Figure A.1:** LEDs illumination status of UV-C LED Array
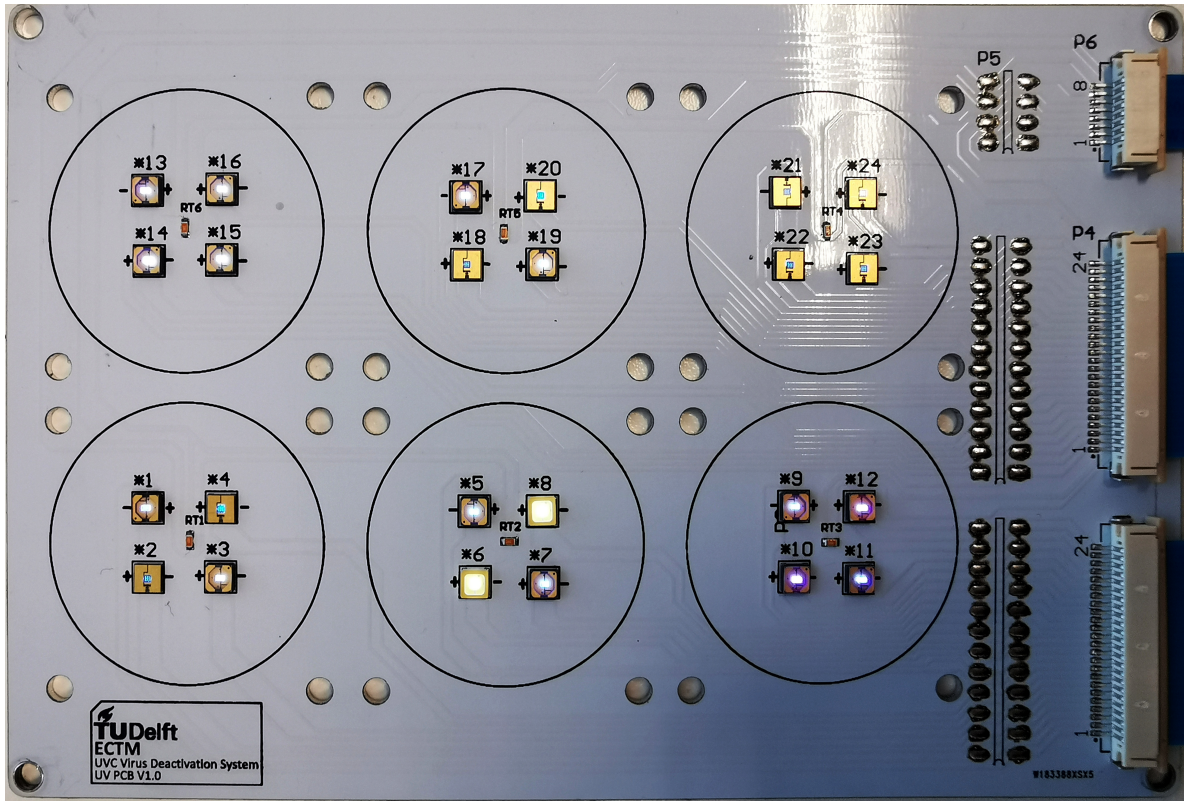
**Figure A.2:** LEDs illumination status of UV-C LED Array
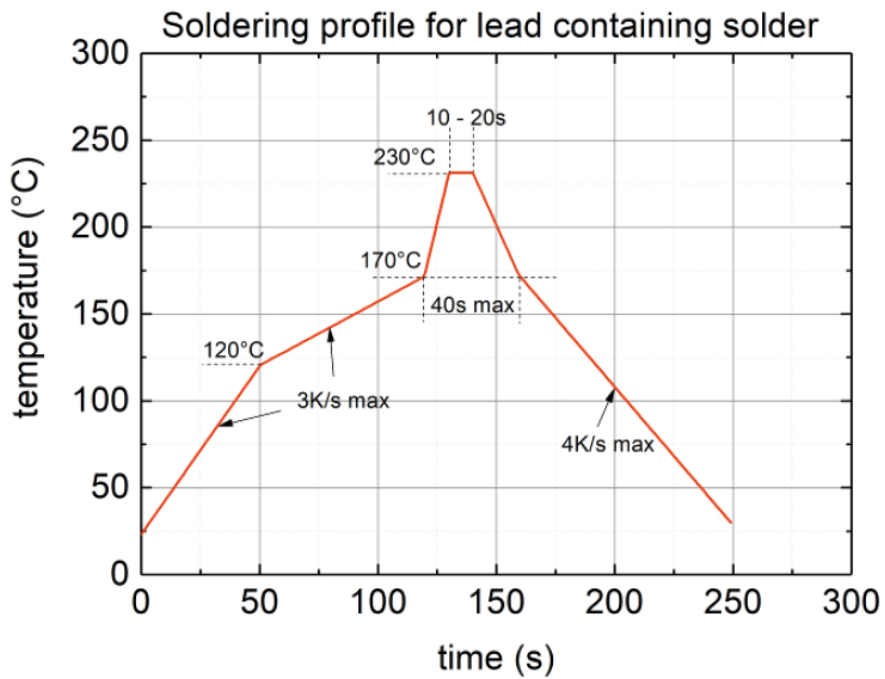


**Figure A.3:** Soldering profile for lead containing solder
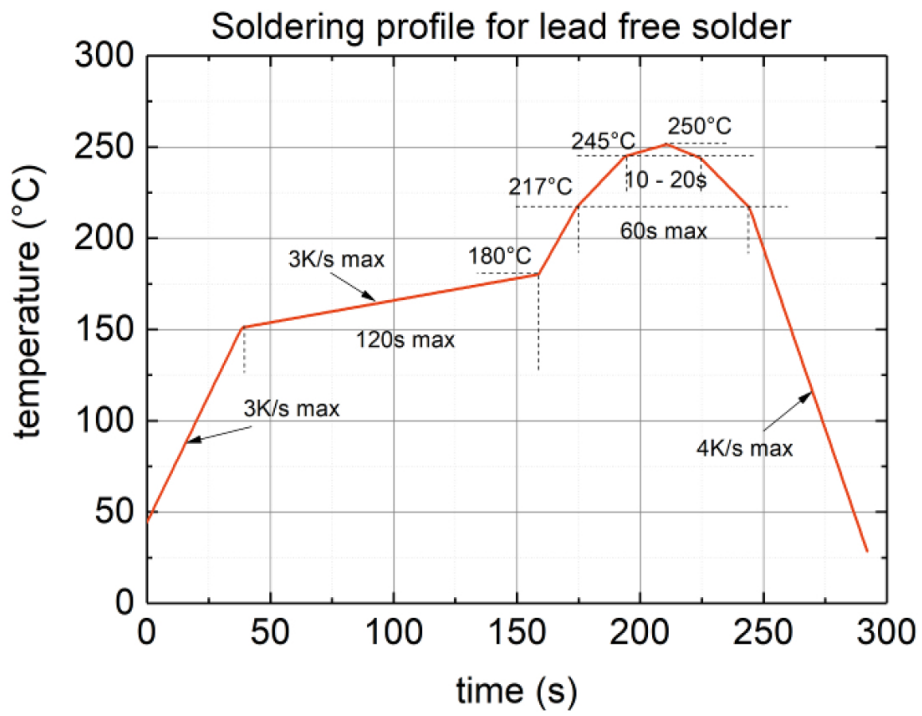
**Figure A.4:** Soldering profile for lead free solder
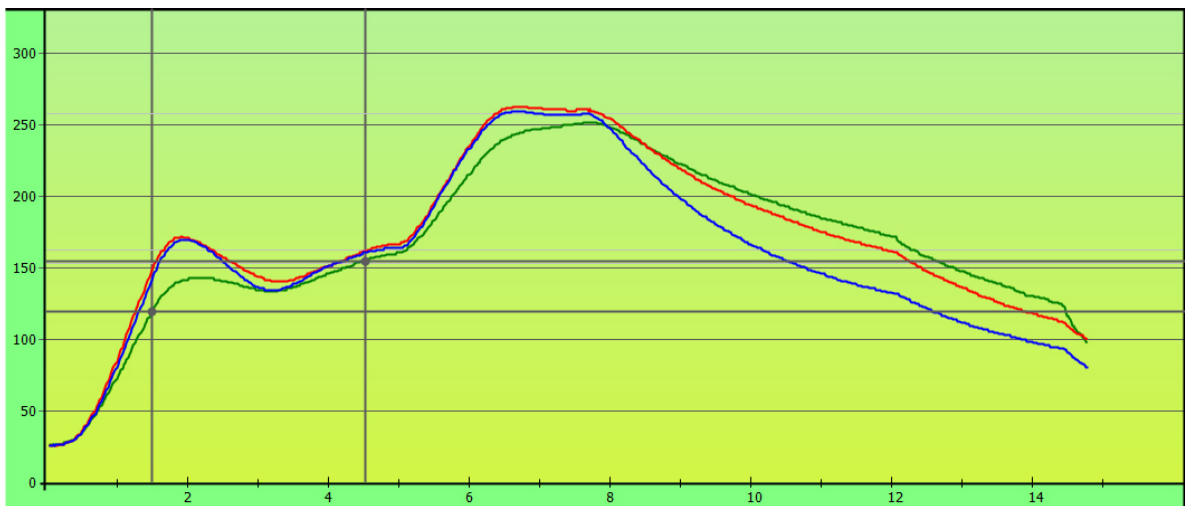


**Figure A.5:** Soldering profile for UV-C LED Array

# B | LED PCB FILE
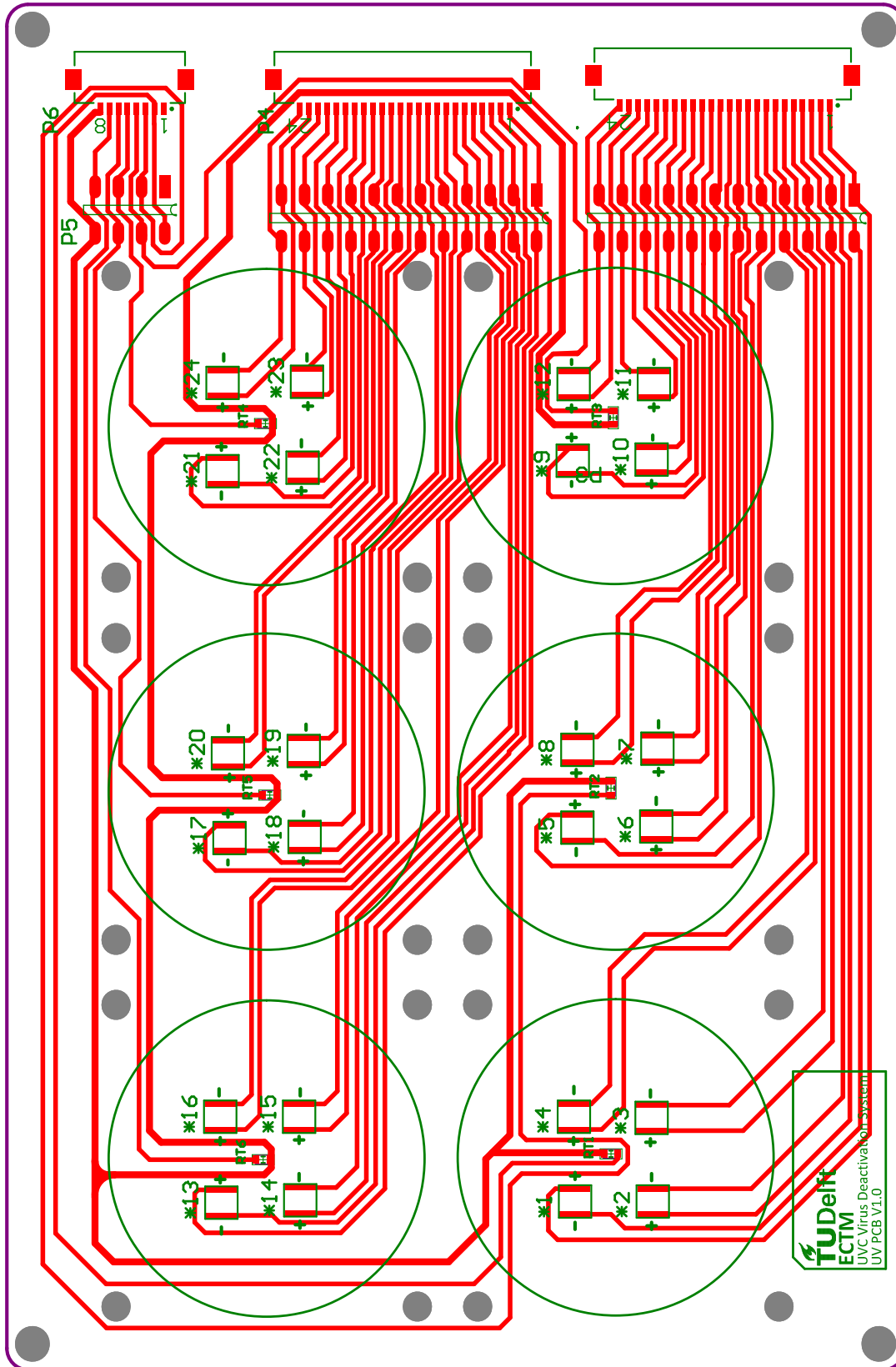
**Figure B.1:** PCB design file of *UVC Virus Inactivation Test Platform*

# C | EXPERIMENT DEVICE AND PROCESS
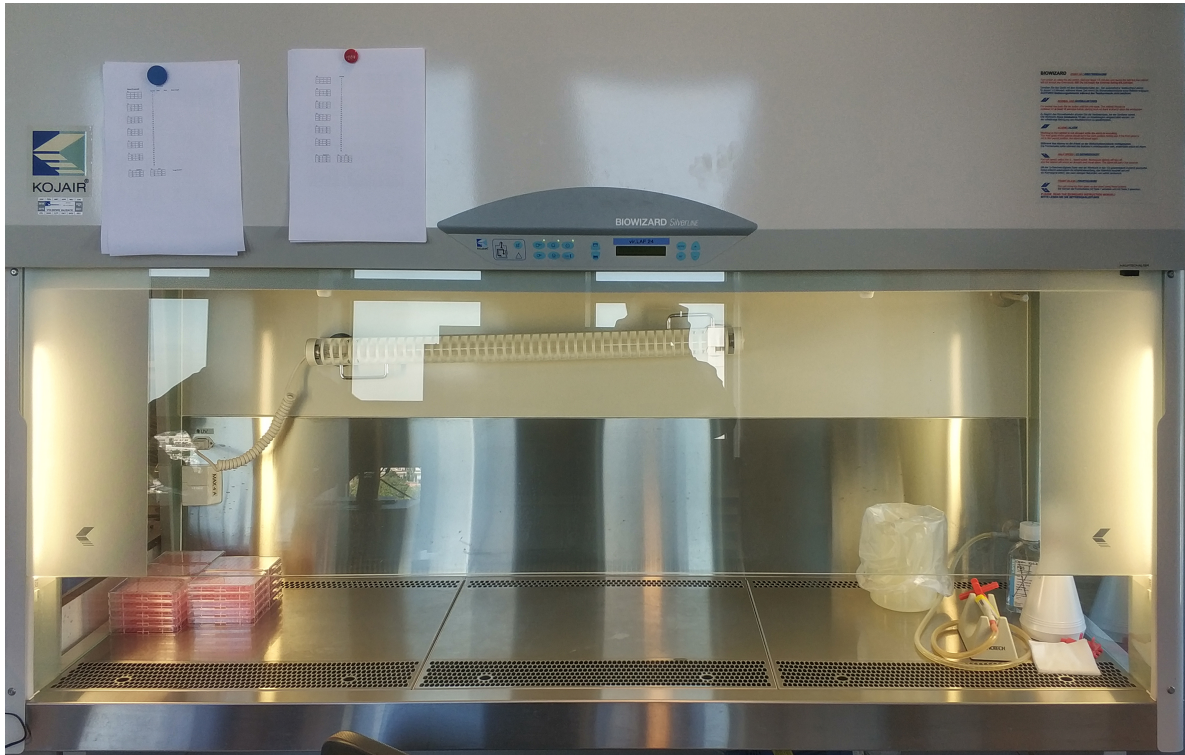


**Figure C.1:** Fume Hood for Inactivation

**Figure C.2:** Laboratory Incubator

**Figure C.3:** Back Titration Process